UNIVERSITEIT VAN PRETORIA
UNIVERSITY OF PRETORIA
YUNIBESITHI YA PRETORIA

# THERMODYNAMIC ANALYSIS OF A CIRCULATING FLUIDISED BED COMBUSTOR

by
Jeffrey Baloyi

*Submitted in partial fulfilment of the requirements for the degree*

Doctor of Philosophy in Mechanical Engineering

*in the*

Faculty of Engineering, Built Environment and Information Technology

University of Pretoria

2017

UNIVERSITEIT VAN PRETORIA
UNIVERSITY OF PRETORIA
YUNIBESITHI YA PRETORIA



# ABSTRACT

**Title: Thermodynamic Analysis of a Circulating Fluidised Bed Combustor**

**Author:** Jeffrey Baloyi

**Supervisors:** Prof Tunde Bello-Ochende and Prof Josua P. Meyer

**Department:** Mechanical and Aeronautical Engineering

**University:** University of Pretoria

**Degree:** Doctor of Philosophy (Mechanical Engineering)

The focus of the world is on the reduction of greenhouse gases, such as carbon dioxide, which contribute to the global warming currently experienced. Because most of the carbon dioxide emitted into the atmosphere is from fossil fuel combustion, alternative energy sources were developed and others are currently under study to see whether they will be good alternatives. One of these alternative sources of energy is the combustion of wood instead of coal. The advantages of wood are that it is a neutral carbon fuel source and that currently installed infrastructure used to combust coal can be retrofitted to combust wood or a mixture of wood and coal in an attempt to reduce the carbon dioxide emissions.

Spent nuclear fuel has to be cooled so that the decay heat generated does not melt the containment system, which could lead to the unintentional release of radioactive material to the surroundings. The heat transfer mechanisms involved in the cooling have historically been analysed by assuming that the fluid and solid phases are at local thermal equilibrium (LTE) in order to simplify the analysis.

The exergy destruction of the combustion of pine wood in an adiabatic combustor was investigated in this thesis using analytical and computational methods. The exergy destruction of the combustion process was analysed by means of the second law efficiency,

UNIVERSITEIT VAN PRETORIA
UNIVERSITY OF PRETORIA
YUNIBESITHI YA PRETORIA



which is the ratio of the maximum work that can be achieved by a Carnot engine extracting heat from the combustor, and the optimum work of the combustor. This was done for theoretical air combustion and various excess air combustions, with varied inlet temperatures of the incoming air. It was found that the second law efficiency reached an expected maximum for theoretical air combustion, and this held true for all varying air inlet temperatures. However, it was found that as the air inlet temperature was increased more and more, the maximum second law efficiency was the same for all excess air combustions, including the theoretical air combustion. It was also found that the results of the analytical and commercial computational fluid dynamics code compared well.

Another analysis was conducted of irreversibilities generated due to combustion in an adiabatic combustor burning wood. This was done for a reactant mixture varying from a rich to a lean mixture. A non-adiabatic non-premixed combustion model of a numerical code was used to simulate the combustion process where the solid fuel was modelled by using the ultimate analysis data. The entropy generation rates due to the combustion and frictional pressure drop processes were computed to eventually arrive at the irreversibilities generated. It was found that the entropy generation rate due to frictional pressure drop was negligible when compared with that due to combustion. It was also found that a minimum in irreversibilities generated was achieved when the air-fuel mass ratio was 4.9, which corresponded to an equivalent ratio of 1.64, which was lower than the respective air-fuel mass ratio and equivalent ratio for complete combustion with theoretical amount of air of 8.02 and 1.

Studieswere conducted to numerically analyse irreversibilities generated due to combustion in an adiabatic combustor burning wood. The first study analysed the effect of changing the incoming air temperature from 298 K to 400 K. The second study analysed the effect of

UNIVERSITEIT VAN PRETORIA
UNIVERSITY OF PRETORIA
YUNIBESITHI YA PRETORIA



changing the wall condition of the combustor from adiabatic to negative heat flux (that is heat leaving the system) for an incoming air temperature of 400 K. The irreversibilities generated in the combustor were calculated by computing the entropy generation rates due to the combustion, heat transfer and frictional pressure drop processes. For the first part of the study, it was found that for the minimum irreversibilities generated in the adiabatic combustor, the optimal air-fuel ratio (AF) corresponding to minimum irreversibilities slightly reduced from 4.9 to 4.8. In the second part of the study, it was found that by changing the wall condition from adiabatic to heat flux on the combustor, the AF corresponding to the minimum irreversibilities increased from 4.8 to 6. For the third part of the study, the combustor with a heat flux wall condition and a wall thickness simulated at an AF of 6, the sum of twice the wall thickness and the optimum diameter always added up to 0.32 m, resulting in the minimum irreversibilities.

An analytical model was developed to minimise the thermal resistance of an air-cooled porous matrix made up of solid spheres with internal heat generation. This was done under the assumption of LTE. It was found that the predicted optimum sphere diameter and the minimum thermal resistance were both robust in that they were independent of the heat generation rate of the solid spheres. Results from the analytical model were compared with those from a commercial numerical porous model using liquid water and air for the fluid phase, and wood and silica for the solid phase. The magnitudes of the minima of both the temperature difference and the thermal resistance seemed to be due to equal contribution from the thermal conduction heat transfer inside the solid spheres and heat transfer in the porous medium. Because the commercial numerical porous model modelled only the heat transfer occurring in the porous medium, it expectedly predicted half of the magnitudes of the minima of the temperature difference and thermal resistance of those by the analytical model.

UNIVERSITEIT VAN PRETORIA
UNIVERSITY OF PRETORIA
YUNIBESITHI YA PRETORIA



**Keywords**: second law efficiency, wood combustion, exergy, optimisation, irriversibilities, entropy generation rate, adiabatic combustor, wall heat flux, porous media, local thermal equilibrium, internal heat generation

# DEDICATION

I would like to dedicate this thesis to my family:

my wife, Amanda Gumbo,

our daughter, Masingita Baloyi,

and my parents, Joseph and Florah Baloyi.

UNIVERSITEIT VAN PRETORIA
UNIVERSITY OF PRETORIA
YUNIBESITHI YA PRETORIA



# ACKNOWLEDGEMENTS

I would like to express my deepest gratitude to my supervisors; firstly, Prof Bello-Ochende, for his constant and ever-present guidance, patience and encouragement during the course of this study; secondly, Prof Meyer, for his patience, resources he made available to us postgraduate students in the form of scholarships, office space, computers and software to do the research. Without all their support, I would not have been able to write this thesis.

I would also like to express my appreciation to the National Research Foundation (NRF), the University of Pretoria and the Council for Scientific and Industrial Research (CSIR), for financial support and for providing the infrastructure for the study.

I would like to express my appreciation to my fellow postgraduate students with whom I spent time during my studies for the enriching and encouraging environment they created; to mention just a few, Aggrey Mwesigye, Lloyd Ngo, Olabode Olakoyejo, Lanre Oboyopo, Noah Olugbenga, Yinka Adewumi, Francis Okafor, Saheed Adio, Gerard Muteba, Tshimanga Ntumba, Jean-Marc and Daniel Ewim.

I would like to express a special thank you and appreciation to my parents, Flora Baloyi and Joseph Baloyi, for their support and encouragement throughout my whole life, and for making sure that I got to this point in my life.

Lastly, I would like to give a special thank you to my wife, Amanda Gumbo, for all the support, encouragement, patience and understanding while I was busy with my studies.

UNIVERSITEIT VAN PRETORIA
UNIVERSITY OF PRETORIA
YUNIBESITHI YA PRETORIA



# TABLE OF CONTENTS

UNIVERSITEIT VAN PRETORIA
UNIVERSITY OF PRETORIA
YUNIBESITHI YA PRETORIA

UNIVERSITEIT VAN PRETORIA
UNIVERSITY OF PRETORIA
YUNIBESITHI YA PRETORIA





## LIST OF FIGURES

UNIVERSITEIT VAN PRETORIA
UNIVERSITY OF PRETORIA
YUNIBESITHI YA PRETORIA

UNIVERSITEIT VAN PRETORIA
UNIVERSITY OF PRETORIA
YUNIBESITHI YA PRETORIA

UNIVERSITEIT VAN PRETORIA
UNIVERSITY OF PRETORIA
YUNIBESITHI YA PRETORIA

UNIVERSITEIT VAN PRETORIA
UNIVERSITY OF PRETORIA
YUNIBESITHI YA PRETORIA

UNIVERSITEIT VAN PRETORIA
UNIVERSITY OF PRETORIA
YUNIBESITHI YA PRETORIA





## LIST OF TABLES

UNIVERSITEIT VAN PRETORIA
UNIVERSITY OF PRETORIA
YUNIBESITHI YA PRETORIA

# PUBLICATIONS RESULTING FROM THE STUDY

The following articles were published in peer-reviewed journals:

- Baloyi J, Bello-Ochende T, Meyer JP. Thermodynamic optimisation and computational analysis of irreversibilites in a small-scale wood-fired circulating fluidised bed adiabatic combustor. *Energy* 2014; 70: 653-663.
- Baloyi J, Bello-Ochende T, Meyer JP. Minimization of thermal resistance in an air cooled porous matrix made up of solid spheres with heat generation. *International Communications in Heat and Mass Transfer* 2012; 39 (7): 966- 970.

The following articles were published as part of peer-reviewed conference proceedings:

- Baloyi J, Bello-Ochende T, Meyer JP. "Wall heat flux influence on the thermodynamic optimisation of irreversibilities of a circulating fluidised bed combustor", 12th International Conference on Heat Transfer, Fluid Mechanics and Thermodynamics, 11-13 July 2016, Spain.
- Baloyi J, Bello-Ochende T, Meyer JP. "Optimum Diameter of a Circulating Fluidised Bed Combustor with Negative Wall Heat Flux", 11th International Conference on Heat Transfer, Fluid Mechanics and Thermodynamics, 20-23 July 2015, South Africa.
- Baloyi J, Bello-Ochende T, Meyer JP. "The analysis of exergy destruction of a wood fired adiabatic combustor", 5$^{th}$ International Conference on Applied Energy, 1-4 July 2013, South Africa.

UNIVERSITEIT VAN PRETORIA
UNIVERSITY OF PRETORIA
YUNIBESITHI YA PRETORIA



- Baloyi J, Bello-Ochende T, Meyer JP. "Optimum Geometry of Solid Porous Sphere with Heat Generation", 9th International Conference on Heat Transfer, Fluid Mechanics and Thermodynamics, 16-18 July 2012, Malta.

The following article was submitted to the *Energy Conversion and Management* journal:

- Baloyi J, Bello-Ochende T, Meyer JP. Thermodynamic optimisation of a wood fired combustor: the influence of wall heat flux, wall thickness and air inlet temperature, manuscript 2015.

UNIVERSITEIT VAN PRETORIA
UNIVERSITY OF PRETORIA
YUNIBESITHI YA PRETORIA



# NOMENCLATURE

*Abbreviation*

| | |
|---|---|
| CFD | computational fluid dynamics |
| HHV | higher heating value |
| LHV | hower heating value |

Symbols

| | | |
|---|---|---|
| $a$ | [$s^{-1}$] | velocity constant term |
| $A$ | [$mm^2$] | cross-sectional area |
| $AF$ | [-] | air-fuel mass ratio |
| $B_1$ | [-] | equation term |
| $B_3$ | [-] | equation term |
| $B_4$ | [-] | equation term |
| $B_6$ | [-] | equation term |
| Be | [-] | Bejan number |
| $\bar{c}$ | [kJ/kmol.K] | molar specific heat |
| $c$ | [kJ/kg.K] | specific heat |
| $c_p$ | [kJ/kg.K] | specific heat at constant pressure |
| $C$ | [-] | atomic carbon |
| $C_d$ | [-] | one of the mixture fraction variance transport equation constants |

UNIVERSITEIT VAN PRETORIA
UNIVERSITY OF PRETORIA
YUNIBESITHI YA PRETORIA



| | | |
|---|---|---|
| $C_g$ | [-] | one of the mixture fraction variance transport equation constants |
| $CO$ | [-] | carbon monoxide |
| $CO_2$ | [-] | carbon dioxide |
| $Cp$ | [kJ/kg.K] | sum of stoichiometric coefficient - weighted specific heat at constant pressure |
| $D$ | [mm] | diameter of the solid sphere; combustor diameter |
| $ER$ | [-] | equivalent ratio |
| $\overline{f}$ | [-] | mean mixture fraction |
| $\overline{f'^2}$ | [-] | mixture fraction variance |
| $f$ | [-] | mixture fraction |
| $\vec{F}$ | [-] | body force |
| $g$ | [m/s$^2$] | gravitational acceleration magnitude |
| $\vec{g}$ | [m/s$^2$] | gravitational acceleration |
| $G$ | [kg/s/m$^2$] | mixture mass flux |
| $\overline{h}$ | [kJ/kmol] | specific enthalpy |
| $\overline{h}^0$ | [kJ/kmol] | enthalpy of formation |
| $H$ | [-] | atomic hydrogen |
| $H$ | [mm] | height |
| $H$ | [kJ] | total enthalpy |
| $H_2$ | [-] | molecular hydrogen |
| $H_2O$ | [-] | water vapour |
| $\hat{i}$ | [-] | unit vector |

UNIVERSITEIT VAN PRETORIA
UNIVERSITY OF PRETORIA
YUNIBESITHI YA PRETORIA



| | | |
|---|---|---|
| $\dot{I}$ | [W] | irreversibility |
| $K$ | [$m^2$] | porous medium permeability |
| $K_f$ | [W/m.K] | fluid thermal conductivity |
| $k_m$ | [W/m.K] | porous medium thermal conductivity |
| $k_s$ | [W/m.K] | sphere thermal conductivity |
| $k$ | [-] | turbulent generation rate |
| $L$ | [m] | length of the porous medium; combustor height |
| $\dot{m}$ | [kg/s] | mass flow rate |
| $M$ | [kg/kmol] | molecular weight |
| $n$ | [-] | stoichiometric coefficient |
| $N$ | [-] | atomic nitrogen; entropy generation number |
| $N_2$ | [-] | molecular nitrogen |
| $O$ | [-] | atomic oxygen |
| $O_2$ | [-] | molecular oxygen |
| $P$ | [Pa] | pressure |
| $q$ | [W] | heat transfer rate |
| $q'''$ | [$W/m^3$] | heat source density |
| $q''_o$ | [$W/m^2$] | outer-wall heat flux |
| $q''_w$ | [$W/m^2$] | inner-wall heat flux |
| $Q$ | [W] | heat transferred |
| $R_T$ | [K/W] | thermal resistance |
| $\overline{R}$ | [kJ/kmol.K] | universal gas constant |
| $\bar{s}$ | [kJ/kmol.K] | specific entropy |

UNIVERSITEIT VAN PRETORIA
UNIVERSITY OF PRETORIA
YUNIBESITHI YA PRETORIA



| | | |
|---|---|---|
| $\bar{s}^{\circ}$ | [kJ/kmol.K] | absolute entropy |
| $\dot{S}_{gen}$ | [W/K] | entropy generation rate |
| $S_h$ | [-] | viscous dissipation energy source term |
| $S_m$ | [-] | solid phase to gas phase mass transfer source term |
| $t$ | [m] | combustor wall thickness |
| $T_{max}$ | [K] | maximum temperature at the centre of the sphere |
| $T_{min}$ | [K] | minimum temperature at the porous medium inlet |
| $T_{outlet}$ | [K] | temperature at the porous medium outlet |
| $T_{inlet}$ | [K] | temperature at the porous medium inlet |
| $T$ | [K] | temperature |
| $u$ | [m/s] | streamwise fluid velocity component |
| $u$ | [m/s] | speed |
| $\vec{v}$ | [m/s] | velocity |
| $\vec{v}$ | [m/s] | superficial fluid velocity vector |
| $W$ | [W] | work done |
| $x$ | [m] | streamwise position variable |
| $x$ | [-] | molar fraction |
| $X_1$ | [-] | equation term |
| $X_2$ | [-] | equation term |
| $X_3$ | [-] | equation term |
| $X_4$ | [-] | equation term |
| $X_5$ | [-] | equation term |

UNIVERSITEIT VAN PRETORIA
UNIVERSITY OF PRETORIA
YUNIBESITHI YA PRETORIA



| | | |
|---|---|---|
| $Y$ | [-] | mass fraction |
| $z$ | [-] | stoichiometric excess air multiplier |

*Greek symbols*

| | | |
|---|---|---|
| $\alpha$ | [$m^2/s$] | thermal diffusivity |
| $\beta$ | [-] | equation term |
| $\eta$ | [-] | second law efficiency |
| $\eta$ | [-] | dimensionless thermal resistance |
| $\varepsilon$ | [-] | void fraction |
| $\varepsilon$ | [-] | turbulent dissipation rate |
| $\gamma$ | [-] | solid/fluid thermal conductivity ratio |
| $\lambda$ | [-] | normalised second law efficiency |
| $\mu$ | [Pa.s] | molecular viscosity |
| $\mu_t$ | [Pa.s] | turbulent viscosity |
| $\phi$ | [-] | porosity |
| $\Psi$ | [-] | dimensionless sphere diameter |
| $\psi$ | [-] | normalised effective temperature difference with reference reservoir |
| $\theta$ | [-] | normalised maximum work done |
| $\rho$ | [$kg/m^3$] | density |
| $\sigma_t$ | [-] | one of the mixture fraction variance transport equation constants |
| $\bar{\bar{\tau}}$ | [-] | stress tensor |

UNIVERSITEIT VAN PRETORIA
UNIVERSITY OF PRETORIA
YUNIBESITHI YA PRETORIA



| | | |
|---|---|---|
| $\theta$ | [-] | dimensionless temperature |

*Subscript*

| | |
|---|---|
| 0 | superficial |
| af | adiabatic flame |
| Air | air |
| $char$ | char |
| $CO$ | carbon monoxide |
| $CO_2$ | carbon dioxide |
| Coarser | coarser grid |
| f | flame |
| $f$ | fuel |
| finer | finer grid |
| $g$ | gas |
| $gen, \min$ | minimum entropy generation rate |
| $gen(h)$ | entropy generation rate due to heat |
| $gen(p)$ | entropy generation rate due to frictional pressure drop |
| H | heat |
| H2O | water vapour |
| $H_2$ | molecular hydrogen |
| $h-t$ | heat transfer |

UNIVERSITEIT VAN PRETORIA
UNIVERSITY OF PRETORIA
YUNIBESITHI YA PRETORIA



| | |
|---|---|
| i | counting index |
| II | second law |
| l | maximum number of products |
| *m* | maximum number of reactants; mixture |
| *mf* | minimum fluidisation |
| max | maximum |
| min | minimum |
| $N_2$ | molecular nitrogen |
| $O_2$ | molecular oxygen |
| opt | optimum |
| p | product species |
| r | reactant species |
| *ref* | environment reference |
| *s* | solid species |
| *sd* | dense zone solid species |
| *se* | exit zone solid species |
| *t* | total of solid and gas |
| *th* | theoretical amount of air ratio |
| W | wall |

UNIVERSITEIT VAN PRETORIA
UNIVERSITY OF PRETORIA
YUNIBESITHI YA PRETORIA



# Chapter 1. INTRODUCTION

## 1.1 BACKGROUND AND MOTIVATION

The focus of the world is the reduction of greenhouse gases such as carbon dioxide. South Africa, together with most countries, has undertaken to reduce carbon dioxide emissions into the atmosphere by introducing the carbon tax system as a way of incentivising industrial emitters to reduce emissions. South Africa is not one of the top ten emitters of carbon dioxide in the world in absolute terms, but the country is one of the top emitters when measured on a per capita basis. South Africa currently generates about 93% of its electricity from coal combustion; however, the country plans to reduce this percentage to 46% by the year 2030 even though the electric power generated from coal will stay almost the same. Unfortunately, the carbon dioxide emitted, when the share of electricity generation from coal is reduced, will be more than the current levels because poor quality coal with between 45% to 60% ash content and lower heating values has been mined in the country for at least the last decade. This means that more coal has to be burnt to produce the same amount of electricity. To mitigate this problem, South Africa and the world have investigated alternative energy sources to see whether they will be good alternatives. One of the alternative sources of energy is the combustion of wood in place of coal because wood has a neutral carbon cycle. However, wood has lower calorific heat rates than coal. The investigation of better conditions under which to run combustion chambers burning wood is paramount if wood is to make a good alternative source of energy. A circulating fluidised bed combustion process is a unique process that has been used to generate energy with fuel which previously had been considered to be incombustible for current technologies. Fuels such as coal with a low calorific value and

UNIVERSITEIT VAN PRETORIA
UNIVERSITY OF PRETORIA
YUNIBESITHI YA PRETORIA



high ash content are not suitable for combustion in a conventional boiler; however they can be efficiently burned in a circulating fluidised bed combustion process. Biomass fuels such as wood and its wastes from the wood industry, as well as dried sewage and livestock waste, are some of the other fuels that are also combusted in a circulating fluidised bed combustor. The energy generated is in the form of heat, which can be used for steam in industrial processes or running a turbine for the generation of electricity.

Availability or exergy analysis of individual components or subsystems of a power plant can be complicated by the interdependencies between the various components. This takes away the opportunity to identify a component's optimum operating condition or dimensional parameters necessary for best overall performance of the power plant formed by the various components.

The air-fuel mass ratio (AF) is an important parameter in the combustion process, and one of the aspects of combustion that can be directly influenced by this parameter is whether the combustion process is complete or incomplete. For an incomplete combustion process, the combustion products mixture will contain unburnt fuel in the form of char and maybe volatile gases released from the devolatilisation of the solid fuel. There is negligible molecular oxygen in the combustion products mixture [1, 2, 3, 4]. In the case of complete combustion with excess air, there is molecular oxygen in the combustion mixture, but no fuel components will result from the devolatilisation process [1], assuming proper mixing occurred. Different AF ratios result in different exergies or availability of the energy released as measured by the average temperature of the combustion products.

The imperative to be energy efficient and not waste any available source of energy has led to the focus on energy recovery from discarded energy sources or from those used in an attempt to prevent environmental degradation. One of the current challenges to the environmental

UNIVERSITEIT VAN PRETORIA
UNIVERSITY OF PRETORIA
YUNIBESITHI YA PRETORIA



degradation is the storage of spent nuclear fuel. The storage of nuclear spent fuel or waste is complicated by the need to manage the decay heat generated by the fuel. The spent nuclear fuel has to be cooled so that the heat generated does not melt the containment system, which can lead to the unintentional release of radioactive material to the surroundings. A similar scenario takes place, although innocuous, when a pile of stones (heated as an energy storage mechanism) is cooled by a fluid flowing through gaps between the stones.

## 1.1. LITERATURE REVIEW

Combustion with theoretical air results in the highest possible adiabatic temperature that can be reached [1-4]. An increase in excess air percentage, which is accompanied by a decrease in adiabatic flame temperature, eventually results in a seizure of combustion at very high percentages of excess air. The adiabatic flame temperature of combustion with any excess air percentage can be increased by increasing the inlet temperatures of the incoming reactants. In complete combustion, the proportion of each combustion product can easily be predicted analytically through the stoichiometric equation [1, 2, 3, 4], whereas the incomplete combustion processes of solid fuels such as those found in circulating fluidised bed combustors are difficult to model. Chen et al. [5] found the optimum oxygen-fuel ratio for each fuel at which gasification is most efficient when they compared the gasification of raw biomass, torrefied biomass and coal using pure oxygen. Tran et al. [6] found that torrefaction of stump biomass resulted in increased heating values, but less reactive. Zhang et al. [7] found that the optimal proportion of oxygen used for pre-oxidation of 37% of the total oxygen supply greatly enhanced the gasification rate when they experimented on the gasification of caking coal in a pilot fluidised bed gasifier.

UNIVERSITEIT VAN PRETORIA
UNIVERSITY OF PRETORIA
YUNIBESITHI YA PRETORIA



Louis et al. [8] found that it was necessary to include the mixing, combustion and heat loss associated with non-adiabatic modelling in the model of an air-cooled syngas combustion chamber to accurately predict the NO formation in flames with heat loss when the model was compared with experimental data. Li and Zhong [9] found that with three experimental micro-tube combustors having the same outer diameter and combusting a methane-oxygen mixture, for the one with a stainless steel micro-tube, the heat loss due to radiation constituted about 70% of the total heat loss.

The effect of changes in excess air and of exhaust gas recirculation on exergy destruction was analysed by [10] for several fuels under various conditions. [11] used an exergy topological method to show that the exergy destroyed by the evaporator of a regenerative organic Rankine cycle was less than the exergy destroyed by the evaporator of an ordinary organic Rankine cycle. [12, 13] found that chemical looping reduced exergy destruction associated with the combustion process. [14] minimised the exergy destruction associated with the energy separation process of a vortex tube to optimise its dimensions. Exergy destruction analysis was used by [15] to study the earth's biosphere energy use through the conversion and usage of energy coming to the earth from the sun. Exergy destruction analysis was also used by [16] to reduce the heat transfer area of a complex refrigerant circuitry of condenser. [17] looked at avoidable and unavoidable exergy destructions and investment costs associated with the components of thermal systems. Methods were proposed by [18] that could be used to separate the exergy destruction of a component from the rest of the system. For the components of a power plant such as a combustion chamber, its exergy destruction could be analysed by treating the combustor as adiabatic and then isolating it from the rest of the power plant by coupling it to a reversible Carnot cycle power plant [2-4]. Elfasakhany et al. [19] found that the emissions of unburnt volatiles were due to fuel particle size and

UNIVERSITEIT VAN PRETORIA
UNIVERSITY OF PRETORIA
YUNIBESITHI YA PRETORIA



combustor configuration in the experimental and numerical studies they conducted of particles of pulverised wood in a combustion products mixture. Ziebik and Stanek [20] found that the exergy efficiency of a blast furnace process was high, but the compressing and preheating of the blast were found to be characterised by high exergy losses due to the associated combustion process. Ziebik and Stanek [21] also used exergy analysis to look at the thermal improvement of a blast furnace process through the increase of blast temperature and its oxygen enrichment. Nur Izyan and Shuhaimi [22] used exergy analysis to resolve a fossil fuel depletion problem on a crude oil distillation unit, which was due to high exergy losses on the first inlet furnace. Gupta and Reddy [23] conducted energy and exergy analyses on a combined-cycle power plant to find that the combustion chamber, gas turbines and heat recovery steam generators were the main sources of irreversibilities. The irreversibilities of proton exchange membrane fuel cells were analysed by Cihan, Hacihafizoglu and Kahveci [24] as a function of operating pressure, pressures of the electrodes, current density, etc. Ghazikhani et al. [25] used a double-pipe heat exchanger with counter-current flow to recover exergy by cooling the exhaust from a diesel engine, which increased with load and engine speed, and when the recovered exergy was utilised, the brake specific fuel consumption decreased drastically. When Chintala and Subramanian [26] used an exergy analysis method on a hydrogen-diesel engine, they found that the addition of molecular hydrogen resulted in an increase in the maximum available work and a reduction in irreversibility due to combustion. They also found that the addition of molecular hydrogen had no effect on the irreversibility due to friction and mixing, whereas the irreversibility due to unburnt fuel decreased due to the high temperature combustion. The cumulative irreversibility in the combustion chamber was found to decrease in an indirect injection diesel engine when

UNIVERSITEIT VAN PRETORIA
UNIVERSITY OF PRETORIA
YUNIBESITHI YA PRETORIA



Jafarmadar [27] increased the mass fraction of exhaust gas recirculation from 0% to 30% even though the exergy efficiency decreased.

Kunii and Levenspiel [28] found that once minimum fluidisation had been attained, the frictional pressure drop across a conduit for a fluidised system remained unchanged. Gupta and Reddy [29] developed a model that analysed the effect of pressure on the bed-to-wall heat transfer in a pressurised circulating fluidised bed riser, which agreed well with experiments and literature. Han et al. [30] found that pressurisation improved the capture of $CO_2$ when using CaO in a fluidised bed gasifier of sawdust. Coal fly-ash oxygen carriers were found by [31] to be effective in converting carbon dioxide into carbon monoxide when used in chemical looping combustion of synthesis gas.

Ting, Hung and Guo [32] found that at a certain range of the low Peclet number flow regime, minimal entropy was generated when they studied nanofluid with streamwise conduction in microchannels. Le Roux, Bello-Ochende and Meyer [33] used the technique of total entropy generation minimisation to find the optimum operating point of a turbine, and to optimise the geometric parameters of the recuperator and receiver of an open and direct solar thermal Brayton cycle. Mwesigye, Bello-Ochende and Meyer [34] found a minimum entropy generation rate for an optimum flow rate when they numerically investigated the entropy generation rate due to heat transfer and fluid friction in a parabolic trough receiver. Le Roux, Bello-Ochende and Meyer [35] used the dynamic trajectory optimisation method to find optimised geometric parameters, minimum irreversibility rates and maximum receiver surface temperatures for an open and direct solar thermal Brayton cycle.

Hua, Wu and Kumar [36] numerically analysed the effect of changing the wall conditions from adiabatic to heat loss through a wall on the combustion chambers burning a hydrogen-air mixture, as they varied from millimetre to micro-scale size. They discovered that the heat

UNIVERSITEIT VAN PRETORIA
UNIVERSITY OF PRETORIA
YUNIBESITHI YA PRETORIA



loss had the effect of quenching, even extinguishing, the combustion process inside the chamber as the chamber narrowed. Norton and Vlachos [37] numerically studied the effects of wall thickness and flow velocities on the combustion characteristics and flame stability in a premixed methane-air mixture micro-burner. They found two modes of flame blowout, one due to thick wall thermal conductivities and another due to low flow velocities. Feng, Liu and Li [38] numerically studied the combustion of an air-methane mixture inside a small tube with an axial temperature gradient at the wall. They found that the higher the wall temperature, the more stable the flame that can be realised for a given tube size.

Using the LTNE condition between the two phases, many researchers [39-44] created models in an attempt to solve the heat transfer problem for porous media and they showed that these models asymptoted into LTE models at special conditions. Concurrently, [45-52] compared the LTNE and LTE models for cases from metallic and non-metallic packed beds to microchannel heat sinks and annulus partially filled with porous media. They came up with criteria under which the LTE assumption was valid. Reddy and Narasimhan [53] numerically investigated a similar case where there was interplay between internal heat generation and externally driven natural convection inside a vertical porous annulus under steady-state conditions.

Whitaker [54] discusses constraints that must be satisfied when LTE is assumed. He suggests that these constraints must be satisfied when the following conditions are imposed: the solid and fluid phases' thermal diffusivities ratio must be equal, the thermal conductivities ratio must be equal, and the non-slip condition must hold. [55] and [56] developed LTE models for metallic foam porous channels and found that the LTE assumption was valid even if the solid thermal conductivity was markedly higher than that of the fluid. They developed an algorithm that did away with the need to conduct numerical calculations. Alazmi and Vafai [39]

UNIVERSITEIT VAN PRETORIA
UNIVERSITY OF PRETORIA
YUNIBESITHI YA PRETORIA



investigated the proper boundary condition to be used for a porous channel bounded by walls having a constant heat flux. They found that the Darcy number, porosity, solid-fluid thermal conductivity ratio and Reynolds number all had a significant effect on the results for the different boundary conditions tested, and this was when thermal dispersion and porosity variation were not considered. For a porous matrix with a stagnant fluid and a heat flux, Lage [58] showed that if the fluid and solid phases were in thermal equilibrium at the boundaries, they would then be in thermal equilibrium throughout the entire domain. Kou and Huang [57] investigated the effect of thermal boundary conditions applied to a vertical annular duct embedded in a porous medium. Teng and Zhao [59] developed a model that attempted to extend the applicability of Darcy's law beyond the laminar flow regime as defined by the microscopic Reynolds number of about 10. Optimisation of the performance and configuration of porous structures and systems were the subject of research [60-65] in which analytical models were developed.

## 1.2. JUSTIFICATION FOR THE STUDY

Not much work has been done to analyse the optimum operating conditions that would make the combustion of wood a viable alternative to coal combustion. This could be due to the cost of setting up experimental facilities to carry out studies to this effect. This study is confined to using numerical and analytical methodologies to arrive at a better understanding of phenomena involved in the circulating fluidised bed combustor, in particular the combustor component.

UNIVERSITEIT VAN PRETORIA
UNIVERSITY OF PRETORIA
YUNIBESITHI YA PRETORIA



## 1.3. AIM OF THE STUDY

The aim of the study is to analyse the optimum conditions under which the combustor component of a circulating fluidised bed combustor is to be operated, and to maximise the availability of the generated energy from the running of the system.

## 1.4. OBJECTIVES OF THE STUDY

The objectives of the study are as follows:

- to maximise the availability of the generated energy from the combustion process;
- to optimise the operating conditions of a combustor burning pitch pine wood;
- to optimise the diameter and wall thickness of a combustor burning pitch pine wood;
- to optimise the diameter of a discarded heat generating solid sphere that constitutes a porous medium used for heat recovery from the discarded solid spheres.

## 1.5. SCOPE OF THE STUDY

The study focuses on the steady-state operation of a circulating fluidised bed combustor, under fast fluidisation conditions. The nitrogen element in the air is assumed to be inert, there is no $NO_x$ included in the combustion modelling.

UNIVERSITEIT VAN PRETORIA
UNIVERSITY OF PRETORIA
YUNIBESITHI YA PRETORIA



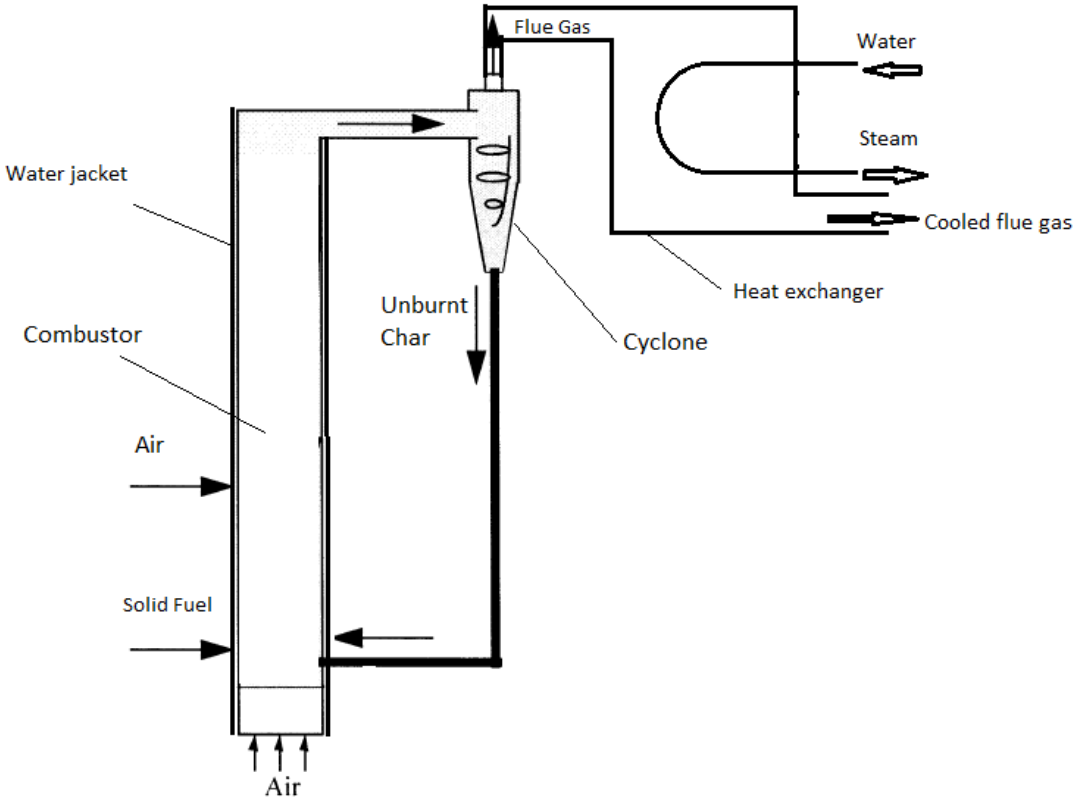


**Figure 1-1: Simplified sketch of a circulating fluidised bed combustor.**

The study is limited in particular to the combustor of the circulating fluidised bed combustor under various scenarios, as shown in Figure 1-1. The first scenario is a combustor with an adiabatic wall condition and maximum exergy generation. The second scenario is a combustor with an adiabatic wall condition and optimum air-fuel mass ratio resulting in minimum entropy generation. The third scenario is a combustor with a wall with heat leaving the system as expressed by a negative heat flux and optimum air-fuel mass ratio resulting in minimum entropy generation. The fourth scenario is a combustor with a wall with heat leaving the system as expressed by a negative heat flux and optimum diameter resulting in minimum entropy generation. The last aspect investigated is the energy recovery from the unburnt wood char collected from the cyclone. The extraction of heat from the char particles packed into the form of a porous medium made up of solid spheres with internal heat

UNIVERSITEIT VAN PRETORIA
UNIVERSITY OF PRETORIA
YUNIBESITHI YA PRETORIA



generation is investigated. Specifically, the optimum diameter of the solid spheres resulting in minimum thermal resistance to the extraction of heat through the flow of air or water through the porous medium is investigated.

## 1.6. ORGANISATION OF THE THESIS

The thesis is organised using the multiple manuscript format, which makes it easy to follow the investigated phenomena involved in a combustor of the circulating fluidised bed combustor. A description of the contents of each chapter is as follows:

- Chapter 2 briefly outlines the mathematical models used to investigate the selected phenomena involved in the circulating fluidised bed combustor.
- Chapter 3 presents the analysis of the theoretical maximum work that can be done by an adiabatic combustor on a Carnot cycle. The adiabatic combustor burns pitch pine wood as fuel with air being the oxidiser.
- Chapter 4 presents a study of a thermodynamic optimisation and analysis of the irreversibilities of an adiabatic circulation fluidised bed combustor burning pitch pine wood. The study specifically derives the optimum air-fuel mass ratio that will result in minimum irreversibilities from the combustor component of a circulating fluidised bed combustor. The study is done for a fixed geometry of the combustor.
- Chapter 5 takes the work presented in Chapter 4 further by considering the case when the wall condition on the wall changes from adiabatic to that of a heat flux with net heat leaving the combustor, and its effects on the optimum air-fuel mass ratio. The effect of a change on the air-fuel mass ratio by a change in air inlet temperature is also investigated. In addition, the optimum diameter and the change thereof in the

UNIVERSITEIT VAN PRETORIA
UNIVERSITY OF PRETORIA
YUNIBESITHI YA PRETORIA



optimum diameter when the combustor wall thickness is taken into consideration are also investigated.

- Chapter 6 looks at the case of the discarded unburnt char particle, still hot, in a general form of solid spheres with internal heat generation. The object is to find the optimum diameter of the solid spheres that will result in minimum thermal resistance when a fluid is passed through the porous medium formed by the packed solid spheres to recover heat.
- Chapter 7 presents conclusions that are drawn from the study and recommendations that can take forward the work done in the study.

UNIVERSITEIT VAN PRETORIA
UNIVERSITY OF PRETORIA
YUNIBESITHI YA PRETORIA



# Chapter 2. MATHEMATICAL MODELLING

## 2.1. INTRODUCTION

Because the study is conducted using mathematical modelling techniques, the two methods used in the study are described in brief below.

## 2.2. NUMERICAL MODELLING

### 2.2.1. Combustion numerical model

A numerical code, Ansys Fluent [68], which implements a finite volume method to discretise the three-dimensional domain was used. The steady-state continuity, momentum and energy equations that describe the governing laws prevailing in the fluid solid mixture flowing through the combustor are approximated by Reynolds-averaged Navier Stokes (RANS) equations described as follows:

**Conservation of mass and momentum**

The continuity equations for continuous phase (Eq. (2-1)), dispersed phase (Eq. (2-2) and Eq. (2-3)) and momentum Equation [68], as expressed by Eq. (2-4), are solved for under steady-state condition.

$$\nabla \cdot \left(\rho \vec{v}\right) = -s_m \tag{2-1}$$

$$\nabla \cdot \left(\rho \vec{v} \overline{f}\right) = \nabla \cdot \left(\frac{\mu_t}{\sigma_t} \nabla \overline{f}\right) + s_m \tag{2-2}$$

$$\nabla \cdot \left(\rho \vec{v} \overline{f'^2}\right) = \nabla \cdot \left(\frac{\mu_t}{\sigma_t} \nabla \overline{f'^2}\right) + C_g \mu_t \left(\nabla \overline{f}\right)^2 - C_d \rho \frac{\varepsilon}{k} \overline{f'^2} \tag{2-3}$$

$$\nabla \cdot \left(\rho \vec{v} \vec{v}\right) = -\nabla p + \nabla \cdot \left(\bar{\bar{\tau}}\right) + \rho \vec{g} + \vec{F} \tag{2-4}$$

The stress tensor [68] is given by Eq. (2-5):

$$\bar{\bar{\tau}} = \mu \left[\left(\nabla \vec{v} + \nabla \vec{v}^T\right) - \frac{2}{3} \nabla \cdot \vec{v} \hat{i}\right] \tag{2-5}$$

UNIVERSITEIT VAN PRETORIA
UNIVERSITY OF PRETORIA
YUNIBESITHI YA PRETORIA



$\mu$ is the molecular viscosity of the continuous phase, $\vec{F}$ is the interactive body forces between the dispersed and the continuous phases, $S_m$ is the source term accounting for the mass transfer from the solid phase to the gas phase and $\hat{i}$ is a unit vector. $\overline{f}$ and $\overline{f'^2}$ are the mixture fraction and its variance, and are computed by applying an assumed shape probability density function ($\beta$-function) when modelling the turbulence-chemistry interaction. Because the $\bar{f} = f - f'$ (where $f$ is the mixture fraction), the mean mixture fraction can be related to the air-fuel mass ratio (AF) by $f = ER/(ER + AF)$. $ER$ is the equivalent ratio.

The assumed shape probability density function ($\beta$-function) is given by Eq. (2-6).

$$p(f) = \frac{f^{\alpha-1}(1-f)^{\beta-1}}{\int f^{\alpha-1}(1-f)^{\beta-1} df} \qquad \textbf{(2-6)}$$

where $\alpha = \bar{f}\left[\bar{f}(1-\bar{f})/\overline{f}'^2 - 1\right]$ and $\beta = (1-\bar{f})\left[\bar{f}(1-\bar{f})/\overline{f}'^2 - 1\right]$.

Figure 4 shows the computed mean temperature as a function of mean mixture fraction inside the combustor, with a mean mixture fraction of 1 corresponding to 100% fuel with no air.

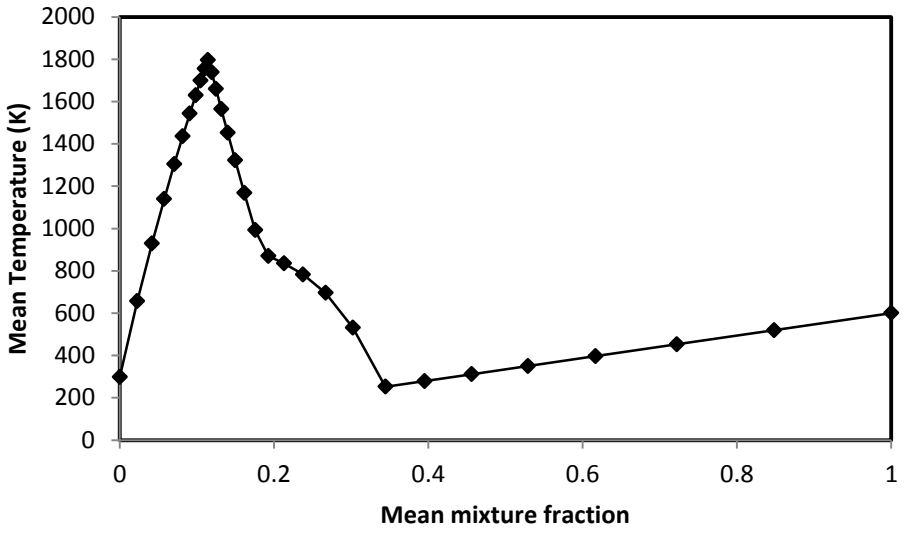


**Figure 2-1: The computed mean temperature distribution of the pitch pine wood combustion in air as a function of mean mixture fraction.**

**Turbulence modelling**

The chosen combustion model required the use of a turbulent model because the combustion model is a mixture model. To this end, the $k-\varepsilon$ turbulent model with enhanced wall function option is chosen for all simulations.

The turbulence closure model used to approximate turbulence is the standard $k-\varepsilon$ model.

UNIVERSITEIT VAN PRETORIA
UNIVERSITY OF PRETORIA
YUNIBESITHI YA PRETORIA



The turbulence energy $k$ is given by:

$$\frac{\partial}{\partial x_i}(\rho k u_i) = \frac{\partial}{\partial x_j}\left[\left(\mu + \frac{\mu_t}{\sigma_k}\right)\frac{\partial k}{\partial x_j}\right] + G_k + G_b - \rho\varepsilon - Y_M \quad \textbf{(2-7)}$$

and the turbulence dissipation rate $\varepsilon$ is given by:

$$\frac{\partial}{\partial x_i}(\rho \varepsilon u_i) = \frac{\partial}{\partial x_j}\left[\left(\mu + \frac{\mu_t}{\sigma_\varepsilon}\right)\frac{\partial \varepsilon}{\partial x_j}\right] + C_{1\varepsilon}\frac{\varepsilon}{k}\left(G_k + C_{3\varepsilon}G_b\right) - C_{2\varepsilon}\rho\frac{\varepsilon^2}{k} \quad \textbf{(2-8)}$$

$$\mu_t = \rho C_\mu \frac{k^2}{\varepsilon} \quad \textbf{(2-9)}$$

where:

$i$, $j$ and $k = 1,2,3$;

$G_k$ is the generation of turbulence kinetic energy due to mean velocity gradients;

$G_b$ is the generation of turbulence kinetic energy due to buoyancy;

$Y_M$ is the generation of turbulence kinetic energy due to fluctuating dilation in compressible turbulence to the overall dissipation rate;

$C_{1\varepsilon}$, $C_{2\varepsilon}$, and $C_{3\varepsilon}$ are constants;

$\sigma_k$ is the turbulent Prandtl number for the turbulence kinetic energy;

$\sigma_\varepsilon$ is the turbulent Prandtl number for the turbulence dissipation rate;

$\mu_t$ is the turbulent viscosity;

$C_\mu$ is a constant.

**Conservation of energy with combustion**

The energy for the non-premixed combustion model [68] is expressed by Eq. (2-10):

$$\nabla \cdot (\rho \vec{v} H) = \nabla \cdot \left(\frac{k_t}{c_p}\nabla H\right) + S_h \quad \textbf{(2-10)}$$

The total enthalpy $H$ is given by Eq. (2-11):

UNIVERSITEIT VAN PRETORIA
UNIVERSITY OF PRETORIA
YUNIBESITHI YA PRETORIA



$$H = \sum_{j=1}^{m} Y_j \left( \int_{T_{ref,j}}^{T} c_{p,j} dT + h_j^0 \left( T_{ref,j} \right) \right) \quad \textbf{(2-11)}$$

$Y_j$ is the mass fraction, $c_{p,j}$ is the specific heat and constant pressure and $h_j^0 \left( T_{ref,j} \right)$ is the enthalpy of formation of the $j^{th}$ species. $S_h$ is the source term due to viscous dissipation.

The P1 radiation model was chosen.

$$-\nabla . q_r = aG - 4an^2 \sigma T^4 \quad \textbf{(2-12)}$$

where:

$a$ is the absorption coefficient;

$G$ is the incident radiation;

$n$ is the refractive index of the medium;

$q_r$ is the radiation flux;

$T$ is the temperature;

$\sigma$ is the Stefan-Boltzmann constant.

Expression Eq. (2-12) can be directly substituted into the energy equation.

### 2.2.2. Porous media laminar flow model

The steady-state laminar flow model prevailing inside a porous medium is described as a set of equations as outlined below.

The continuity equation for the porous medium is given by:

$$\nabla . (\rho u) = 0 \quad \textbf{(2-13)}$$

The momentum equation is given by Darcy's law:

$$-\frac{dP}{dx} = \frac{\mu u}{K} \quad \textbf{(2-14)}$$

The energy equation is given by:

$$\rho C_p \vec{v} . \nabla T = k_m \nabla^2 T + q_m''' \quad \textbf{(2-15)}$$

where the porous medium thermal conductivity is given by:

UNIVERSITEIT VAN PRETORIA
UNIVERSITY OF PRETORIA
YUNIBESITHI YA PRETORIA


$$k_m = \phi k_f + (1-\phi)k_s \quad \textbf{(2-16)}$$

and the porous medium heat density is given by:

$$q'''_m = (1-\phi)q''' \quad \textbf{(2-17)}$$

## 2.3. THERMODYNAMIC MODELLING

The energy rate balance of a control volume at steady state with inlets and outlets, and heat flow through the wall boundary are represented by Eq. (2-18):

$$0 = \dot{q}_{CV} + \sum_{i=1}^{m} \dot{m}_i \left( h_i + \frac{V_i^2}{2} + g z_i \right) - \sum_{e=1}^{n} \dot{m}_e \left( h_e + \frac{V_e^2}{2} + g z_e \right) \quad \textbf{(2-18)}$$

where:

$g$ is the gravitational acceleration;

$h$ is the enthalpy;

$\dot{m}$ is the mass flow rate;

$\dot{q}_{Cv}$ is the control volume heat transfer rate;

$V$ is the flow speed;

$z$ is the height of the inlet ($i$) or exit ($e$) on the combustor.

The corresponding entropy rate balance at steady state is given by Eq. (2-19):

$$0 = \sum_{j=1}^{s} \frac{\dot{q}_j}{T_j} + \sum_{i=1}^{m} \dot{m}_i s_i - \sum_{e=1}^{n} \dot{m}_e s_e + \dot{S}_{gen} \quad \textbf{(2-19)}$$

where:

$s$ is th absolute entropy;

$\dot{S}_{gen}$ is the entropy generation rate;

UNIVERSITEIT VAN PRETORIA
UNIVERSITY OF PRETORIA
YUNIBESITHI YA PRETORIA



with the mass balance as represented by Eq. (2-20):

$$\sum_{i=1}^{m} \dot{m}_i = \sum_{e=1}^{n} \dot{m}_e \qquad \textbf{(2-20)}$$

Multiplying throughout Eq. (2-19) by $T_{ref}$ and then combining Eq. (2-18) with Eq. (2-19) give:

$$\dot{I} = \frac{\dot{m}_f}{M_f}\left(\sum_{i=1}^{m} n_{ri}\left(\bar{h} - T_{ref}\bar{s}\right)_{ri} - \sum_{i=1}^{l} n_{pi}\left(\bar{h} - T_{ref}\bar{s}\right)_{pi}\right) - \left(1 - \frac{T_{ref}}{T_w}\right)q''\pi DL \qquad \textbf{(2-21)}$$

where:

$D$ is the combustor diameter;

$\bar{h}$ is the specific enthalpy;

$\bar{s}$ is the specific entropy;

$\dot{I} = T_{ref}\dot{S}_{gen}$ is the rate of irreversibilities generated;

$\dot{m}_f$ is the fuel mass flow rate;

$M_f$ is the fuel molecular weight;

$n$ is the stoichiometric coefficient, which is computed as detailed in Appendix B;

$q''$ is the wall heat flux;

$T_{ref}$ is the environment reference temperature of 298 K; $T_w$ is the wall temperature.

# Chapter 3. ANALYSIS OF THEORETICAL MAXIMUM WORK THAT CAN BE DONE BY A WOOD-FIRED ADIABATIC COMBUSTOR

## 3.1. INTRODUCTION

Combustion with theoretical air is the ideal scenario at which combustion should take place because the adiabatic temperature that can be reached will be the highest possible [1-4]. However, it is physically impossible to achieve combustion with theoretical air, hence combustion always occurs with excess air. An increase in excess air percentage is accompanied by a decrease in adiabatic flame temperature, which will eventually result in seizure of combustion at very high percentages of excess air. The adiabatic flame temperature of combustion with any excess air percentage can be increased by increasing the inlet temperatures of the incoming reactants. The effect of exhaust gas recirculation on exergy destruction was analysed by [14] for several fuels under various conditions. The effect of changes in excess air was also analysed, as well as reactant temperature on exergy destruction. The exergy topological method was used by [15] to show that an evaporator of a regenerative organic Rankine cycle had lower exergy destruction than an evaporator of an ordinary organic Rankine cycle. The use of exhaust heat to improve the thermodynamic performance or an organic Rankine cycle was also employed by [66]. Chemical looping was shown by [12, 13] to reduce exergy destruction associated with the combustion process. Dimensions of a vortex tube were optimised by [10] by minimising the exergy destruction associated with the energy separation process of the system. [11] analysed the earth's

UNIVERSITEIT VAN PRETORIA
UNIVERSITY OF PRETORIA
YUNIBESITHI YA PRETORIA


biosphere energy use by looking at exergy destruction resulting from the conversion and usage of energy coming to the earth from the sun. The heat transfer area of a complex refrigerant circuitry of condenser coils was reduced as shown by [16] by using exergy destruction analysis. In the case of solid fuel such as wood [5], a special case arises where the increase in inlet temperature can effectively only be achieved for the incoming air. [17] looked at avoidable and unavoidable exergy destructions and investment costs associated with components of thermal systems. Availability analysis of individual components or subsystems of a power plant can be complicated by the interdependencies between the various components. This takes away the opportunity to identify a component's optimum operating condition or dimensional parameters necessary for best overall performance of the power plant formed by the various components. [18] proposes several methods that can be used to separate the exergy destruction of a component from the rest of the system of which it forms part. For the components of a power plant such as a combustion chamber, its exergy destruction was analysed by treating the combustor as adiabatic and then isolating it from the rest of the power plant by coupling it to a reversible Carnot cycle power plant [2-4]. The combustor's exergy destruction was then analysed by means of a second law efficiency, which was the ratio of the maximum work that could be done by a Carnot cycle extracting heat from the adiabatic combustor and the optimum work of the combustor obtained when the entropy generation term vanished. This method ensured that all the irreversibilities calculated were due to the combustion process alone. To this end, the exergy destruction of a pine wood-fired adiabatic combustor was analysed by means of second law efficiency of a Carnot cycle power plant.

UNIVERSITEIT VAN PRETORIA
UNIVERSITY OF PRETORIA
YUNIBESITHI YA PRETORIA


## 3.2. ADIABATIC COMBUSTOR

### 3.2.1. Fuel properties

The fuel that was combusted in the adiabatic combustor was pitch pine wood. The properties of pitch pine were adapted from [67]. Pitch pine ultimate analysis data is given in Table 3-1.

**Table 3-1 Pitch pine ultimate analysis data (adapted from [67]).**

| Element | Value |
|---|---|
| C | 59.0 (%) |
| H | 7.2 (%) |
| O | 32.7 (%) |
| Ash | 1.13 (%) |
| HHV | 24220 (kJ/kg) |
| LHV | 16091.2 (kJ/kg) |
| Molecular weight | 98 (kg/kmol) |

The empirical formula of the fuel was formulated from the ultimate analysis data by simply dividing the weighted percentage of each element by its corresponding molecular weight as given by a method adopted from [67] to arrive at an empirical formula given by Eq. (3-1):

$$C_{4.9}H_{7.2}O_2 \quad \textbf{(3-1)}$$

The computation is demonstrated in Appendix A.

### 3.2.2. Combustion process

The adiabatic combustor as illustrated in Figure 3-1 was assumed to operate under steady-state thermomechanical-chemical equilibrium (TMCE) conditions. This means that all

UNIVERSITEIT VAN PRETORIA
UNIVERSITY OF PRETORIA
YUNIBESITHI YA PRETORIA


properties are evaluated at steady-state and equilibrium conditions. The combustion of the wood fuel occurred at standard atmospheric pressure in the presence of air, which was approximated on molar basis as constituted by 79% nitrogen and 21% oxygen, and only complete combustion of the fuel was considered.

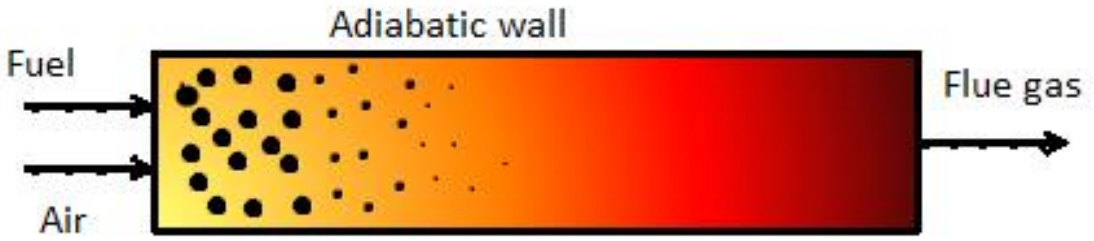


**Figure 3-1: Sketch of an adiabatic combustor.**

The combustion analysis was based on 1 kmol of fuel oxidised by air at an arbitrary excess percentage, that is additional air to theoretical air needed for complete combustion. The reason for the excess air is that combustion can only take place when there is more than the theoretical amount of air present. The general stoichiometric equation of the combustion process undergone by the pitch pine in the presence of air at arbitrary excess level is given by Eq. (3-2):

$$(C_{4.9}H_{7.2}O_2)+(z)n_{Air}(O_2+3.76N_2)\rightarrow n_{H_2O}H_2O+n_{CO_2}CO_2+n_{N_2}N_2+n_{O_2}O_2 \qquad \textbf{(3-2)}$$

where symbols $n_{Air}$, $n_{H_2O}$, $n_{CO_2}$, $n_{N_2}$, $n_{O_2}$ and *z* represent stoichiometric coefficients, and 3.76 is the ratio of the molar fraction of molecular nitrogen to that of molecular oxygen. The stoichiometric coefficient z specifically represents the excess multiple of the theoretical air. For instance, for stoichiometric combustion, that is combustion with theoretical air, *z = 1*.

The general energy equation in an adiabatic combustor operated under TMCE and steady-

UNIVERSITEIT VAN PRETORIA
UNIVERSITY OF PRETORIA
YUNIBESITHI YA PRETORIA



state conditions with kinetic and potential energies assumed to be negligible, as adopted from [1-4], is given by Eq. (3-3):

$$\sum_{i=1}^{l} n_{pi}\left(\Delta\bar{h}\right)_i = \bar{h}^{\circ}_{rp} + \sum_{i=1}^{m} n_{ri}\left(\Delta\bar{h}\right)_i \qquad \textbf{(3-3)}$$

where $\bar{h}^{\circ}_{rp}$ is the solid fuel specific enthalpy of combustion, $n$ is a species stoichiometric coefficient and $\Delta\bar{h} = \bar{h}\left(T, p_{ref}\right) - \bar{h}\left(T_{ref}, p_{ref}\right)$ is a species change in specific enthalpy when the temperature increases from a reference value of $T_{ref} = 298\ K$ to a temperature $T$. Subscripts $p$ and $r$ stand for products and reactants respectively. Pitch pine wood, like other solid fuels, does not have heat formation data tabulated anywhere. However, information which is available is the higher heating value (HHV) or lower heating value (LHV), which is just the magnitude of the specific enthalpy of combustion, $\bar{h}^{\circ}_{rp}$. In the current analysis, the magnitude of the specific enthalpy of combustion was equated to the lower heating value. From Eq. (3-3), the sum of the specific enthalpies of the gaseous species exiting the adiabatic combustor can be computed, from which the outlet flame temperature $T_{af}$ can be interpolated from thermodynamic data tables like those found in [1] and [2].

## 3.3. CFD MODEL

The CFD model used in the study was a non-premixed combustion model implemented in ANSYS Fluent 14 [68]. The ‘single mixture fraction’ option was selected. The model allowed for the use of the ultimate analysis data as found in Table 3-1 for the combustion calculation because the composition and fractions of devolatilised constituents from the solid fuel were not known. The adiabatic combustor was modelled as a 3000 mm long, 100 mm in diameter cylinder, as illustrated in Figure 3-2.

UNIVERSITEIT VAN PRETORIA
UNIVERSITY OF PRETORIA
YUNIBESITHI YA PRETORIA


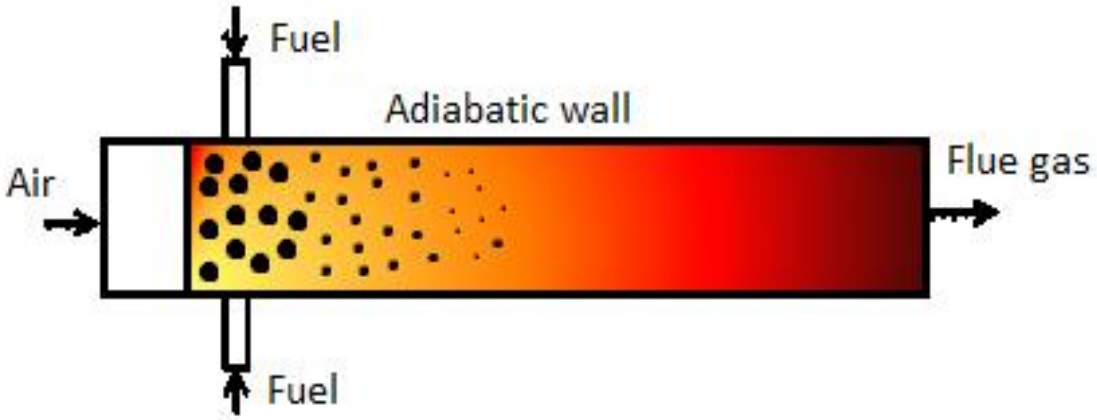


**Figure 3-2: Sketch of a CFD adiabatic combustor.**

There were four fuel inlets each with a 25 mm diameter opening and a length of 100 mm. They were positioned perpendicular to the axial direction of the cylinder. The fuel inlets were placed 50 mm from the inlet of the cylinder, and each fuel inlet was at a 90° offset from its adjacent neighbour. Upstream of the inlet of the cylinder was a 150 mm long cylinder whose inlet was used as the air inlet. The whole domain was meshed using 414 803 polyhedral cells. The k-ε turbulent model was used because the gas flow was relatively straight with no turns and twists, and the cylinder wall was adiabatic. Identical mass flow rate at each fuel inlet was varied to match the right air-fuel mass ratios of the different air excess percentages, while the inlet temperature was set at the pine wood fuel devolatilisation temperature of 600 K [67]. The mass flow rate at the air inlet was fixed for all air excess percentages at a value of 0.34808 kg/s. The inlet temperature on the air inlet was varied from 298 K to 1500 K for each air excess percentage. A pressure-based solver was used with a presto! scheme for pressure and second-order upwind scheme for momentum, continuity, energy and turbulence terms. The outputs of the cases were the adiabatic flame temperature and the molar fractions of the combustion products, namely: $CO_2$, $N_2$, $O_2$ and $H_2O$. However, for calculations of the

UNIVERSITEIT VAN PRETORIA
UNIVERSITY OF PRETORIA
YUNIBESITHI YA PRETORIA



thermodynamic performance of the adiabatic combustor, the molar fractions of the four combustion products needed to be converted into stoichiometric coefficients. Each molar fraction was related to all four stoichiometric coefficients by the expression $x_{pi} = n_{pi} \Big/ \sum_{i=1}^{l} n_{pi}$.

The results were four equations, namely a set of homogeneous equations [69-72], which have infinite numbers of solutions. The infinite number of solutions impasse was resolved by choosing or setting the value of one of the stoichiometric coefficients as part of the desired solution. The stoichiometric coefficient whose value was set was $n_{N_2}$, which was set to the same value as determined by the analytical method in Section 3.2. From this, the set of homogeneous equations was solved to obtain the remaining three stoichiometric coefficients. The computation of the stoichiometric coefficients is outlined in more detail in Appendix B.

## 3.4. THE CARNOT CYCLE SECOND LAW EFFICIENCY MODEL

The exergy per kmol of fuel of an adiabatic combustor which exchanges heat with a reference temperature reservoir at Tref is given by Eq. (3-4), as represented by the optimum work per kmol of fuel [3] that can be done by the combustion products exiting the combustor when the entropy generation term vanishes.

$$W_{opt} = \sum_{i=1}^{m} n_{ri}\left(\bar{h} - T_{ref}\bar{s}\right)_{ri} - \sum_{i=1}^{l} n_{pi}\left(\bar{h} - T_{ref}\bar{s}\right)_{pi} \qquad \textbf{(3-4)}$$

The specific entropy is defined as $\bar{s}_{pi} = \bar{s}^{\circ}_{pi}(T) - \bar{R}\ln(px_{pi}/p_{ref})$, where $p = p_{ref}$, and $x_{pi} = n_{pi} \Big/ \sum_{i=1}^{l} n_{pi}$ is the molar fraction of each combustion product species. The same expressions apply for reactants. The specific entropy of the solid fuel is computed by defining [1] it as $\bar{s} = \bar{c}\ln\left(T_{ref}/273\right)$, where $\bar{c}$ is the specific heat of the solid fuel [1]. The specific

UNIVERSITEIT VAN PRETORIA
UNIVERSITY OF PRETORIA
YUNIBESITHI YA PRETORIA


enthalpies $\bar{h}(T)$ were computed and interpolated at their respective temperatures $T$ where they were read off the thermodynamic tables [1, 2] for each constituent gas species. The optimum work is the maximum possible theoretical work that can be done by the adiabatic combustor. However, to properly analyse how much of this optimum work can possibly be accessed, the adiabatic combustor was coupled to a reversible Carnot cycle power plant [4], as illustrated in Figure 3-3.

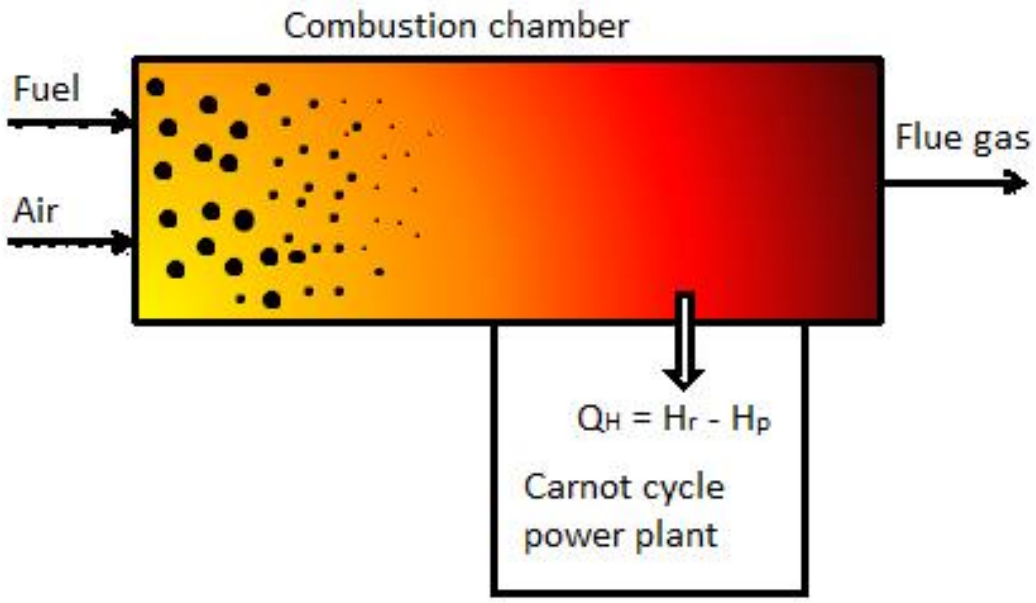


**Figure 3-3: Sketch of an adiabatic combustor coupled to a reversible Carnot cycle power plant.**

This coupling ensured that all irreversibilities in the system were due to the combustion process alone, as represented in Eq. (3-4). In general, the work done per kmol of fuel by the Carnot cycle power plant is given by Eq. (3-5):

UNIVERSITEIT VAN PRETORIA
UNIVERSITY OF PRETORIA
YUNIBESITHI YA PRETORIA


$$W = Q_H\left(1-\frac{T_{ref}}{T_f}\right) \quad \textbf{(3-5)}$$

where $W$ is the work done per kmol of fuel by the power plant, $Q_H$ is the heat that could have been extracted per kmol of fuel from a combustor, and $T_f$ is the flame temperature at which $Q_H$ was transferred and the temperature at which the combustion products would be exiting the combustor. $Q_H$ is simply the difference between the enthalpies of reactants and products, as expressed by Eq. (3-6):

$$Q_H = H_r\left(T_r, p_{ref}\right) - H_p\left(T_f, p_{ref}\right) \quad \textbf{(3-6)}$$

However, for an adiabatic combustor, the sum of specific enthalpies of reactants is the same as the sum of specific enthalpies of products exiting it. Therefore, $H_r\left(T_r, p_{ref}\right) = H_p\left(T_{af}, p_{ref}\right)$. Eq. (3-6) becomes $Q_H = H_p\left(T_{af}, p_{ref}\right) - H_p\left(T_f, p_{ref}\right)$. The specific heat at constant pressure, $\bar{c}_p$, for all products of combustion, is assumed to be constant with respect to temperature. With this assumption in mind, the specific enthalpies can be represented as functions of temperature, resulting in Eq. (3-7):

$$Q_H = \sum_{i=1}^{n}\left(n\bar{c}_p\right)_{pi}\left(T_{af} - T_f\right) = C_p\left(T_{af} - T_f\right) \quad \textbf{(3-7)}$$

where $C_p = \sum_{i=1}^{n}\left(n\bar{c}_p\right)_{pi}$. Eq. (3-7) is substituted into Eq. (3-5), and then differentiated from the work done per kmol of fuel with respect to $T_f$ to arrive at the maximum work that can be done by a Carnot cycle power plant, as given by Eq. (3-8):

$$W_{\max} = C_p T_{af}\left[1-\left(\frac{T_{ref}}{T_{af}}\right)^{1/2}\right]^2 \quad \textbf{(3-8)}$$

The maximum work done occurred for an optimum effective flame temperature, as given by Eq. (3-9):

UNIVERSITEIT VAN PRETORIA
UNIVERSITY OF PRETORIA
YUNIBESITHI YA PRETORIA



$$T_{f,opt} = \left(T_{ref} T_{af}\right)^{1/2} \quad \textbf{(3-9)}$$

$W_{max}$ can be written as a function of $T_{f,opt}$ by substituting Eq. (3-9) into Eq. (3-8), resulting in Eq. (3-10):

$$W_{\max} = C_p T_{ref} \left( \frac{T_{f,opt}}{T_{ref}} - 1 \right)^2 \quad \textbf{(3-10)}$$

The second law efficiency of the Carnot cycle power plant is computed by taking the ratio of the maximum work, as given by Eq. (3-8), to the optimum work, as given by Eq. (3-4), and is expressed by Eq. (3-11):

$$\eta_{II} = \frac{W_{\max}}{W_{opt}} \quad \textbf{(3-11)}$$

As mentioned in Section 3.1, combustion with theoretical air will result in the highest adiabatic flame temperature, which would correspond to the biggest maximum work done per kmol of fuel. Yet this kind of combustion is physically unachievable. For this reason, the thermodynamic performance at 0% excess air is used as the standard by which thermodynamic performance at any arbitrary air excess percentage is measured. Therefore, Eq. (3-10) is normalised by its special case of 0% excess air to give Eq. (3-12):

$$\theta = \frac{W_{\max}}{W_{\max.o\%}} = \left( \frac{T_{f,opt} - T_{ref}}{T_{f,opt,0\%} - T_{ref}} \right)^2 = \psi^2 \quad \textbf{(3-12)}$$

where $\psi = \left(T_{f,opt} - T_{ref}\right) / \left(T_{f,opt,0\%} - T_{ref}\right)$. Likewise, the second law efficiency, as given by Eq. (3-11), is also normalised with respect to the special case of 0% excess air and results in Eq. (3-13):

$$\lambda = \frac{\eta_{II}}{\eta_{II,0\%}} \quad \textbf{(3-13)}$$

UNIVERSITEIT VAN PRETORIA
UNIVERSITY OF PRETORIA
YUNIBESITHI YA PRETORIA


## 3.5. RESULTS AND DISCUSSION

Table 3-2 lists the stoichiometric coefficients for selected air excess percentages, together with fuel-to-air ratios in molar and mass bases. The fuel-to-air ratios represent the amount of air required to combust 1 kg or 1 kmol of fuel.

**Table 3-2: Stoichiometric analyses at selected air excess percentages for pitch pine wood complete combustion.**

| Air excess | 0% | 0%-CFD | 20% | 20%-CFD | 40% | 40% -CFD |
|---|---|---|---|---|---|---|
| $n_{Air}$ | 5.7 | 5.7 | 5.7 | 5.7 | 5.7 | 5.7 |
| $n_{H_2O}$ | 3.6 | 3.493 | 3.6 | 3.502 | 3.6 | 3.503 |
| $n_{CO_2}$ | 4.9 | 4.808 | 4.9 | 4.819 | 4.9 | 4.817 |
| $n_{N_2}$ | 21.432 | 21.432 | 25.718 | 25.718 | 30.0 | 30.0 |
| $n_{O_2}$ | 0 | 0.185 | 1.14 | 1.310 | 2.28 | 2.448 |
| Z | 1 | 1 | 1.2 | 1.2 | 1.4 | 1.4 |
| $\overline{AF}$ | 27.132 | 27.132 | 32.558 | 32.558 | 37.985 | 37.985 |
| $AF$ | 8.021 | 8.021 | 9.625 | 9.625 | 11.229 | 11.229 |

With the stoichiometric coefficient of $N_2$ fixed to the same value predicted by the analytical method, it can be seen from Table 3-2 that results from CFD underpredict the stoichiometric coefficients of the other combustion products species, except for those of $O_2$ where they are overpredicted. CFD also predicted that there will be $O_2$ in the combustion products mix for 0% excess air.

UNIVERSITEIT VAN PRETORIA
UNIVERSITY OF PRETORIA
YUNIBESITHI YA PRETORIA


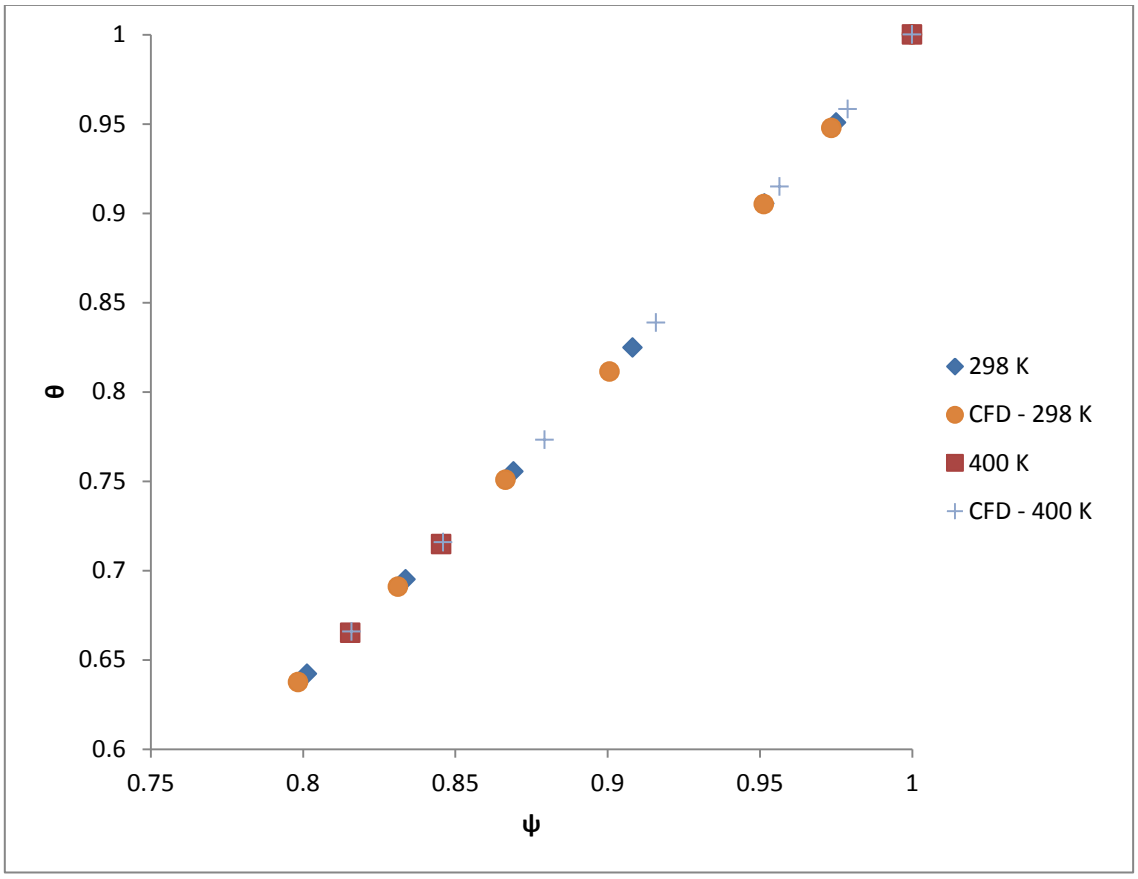


**Figure 3-4**: **Plot of normalised work that can be done by a Carnot cycle power plant for varying air excess percentages at varying air inlet temperatures.**

The normalised work that can be done by the Carnot cycle power plant, as given by Eq. (3-12), for air excess percentages varying from 0% to 50%, is computed and plotted in a graph, as illustrated in Figure 3-4. This is done for air inlet temperatures varying from 298 K to 1 500 K. Figure 3-4 shows that they all fall on the same parabolic line as predicted by Eq. (3-12). From the same figure, it can also be seen that the data from CFD falls exactly on the same parabolic line.

UNIVERSITEIT VAN PRETORIA
UNIVERSITY OF PRETORIA
YUNIBESITHI YA PRETORIA


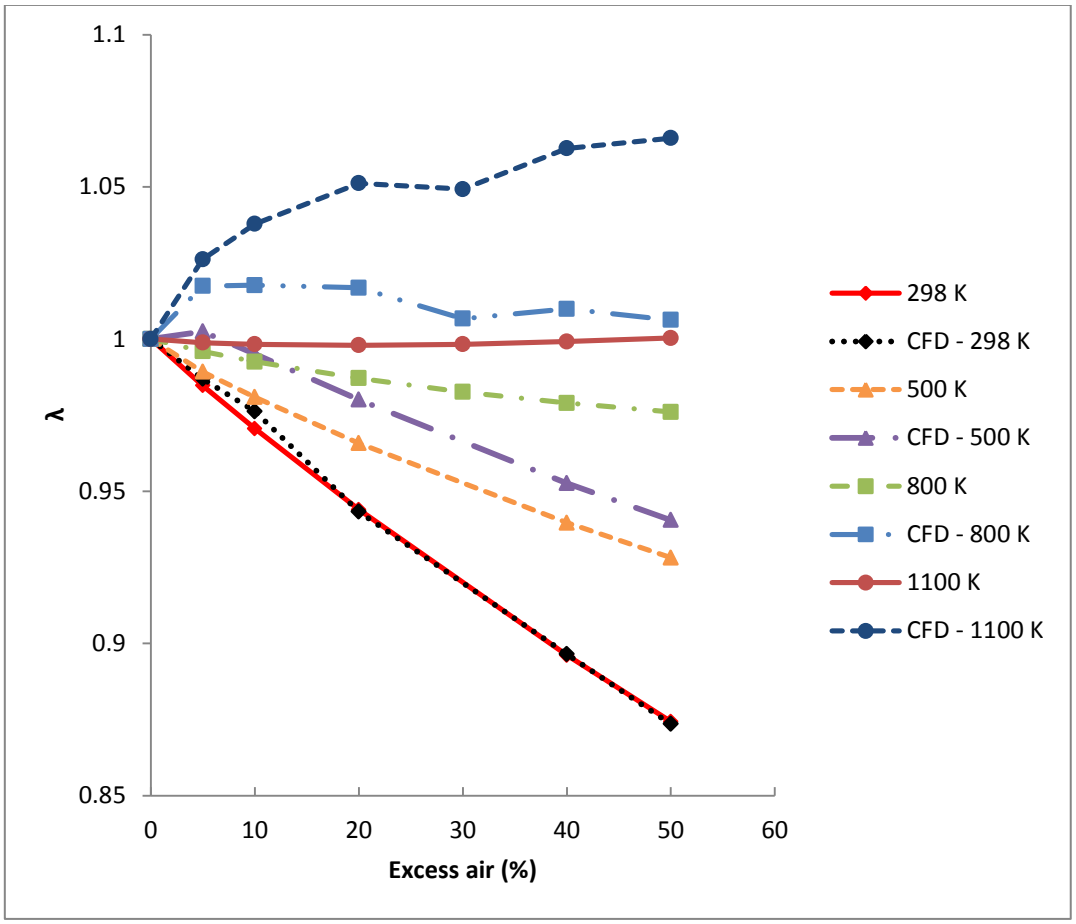


**Figure 3-5**: **Plot of normalised second law efficiency of Carnot cycle power plant for varying air excess percentages at varying air inlet temperatures.**

The normalised second law efficiency of the Carnot cycle power plant for varying excess air percentages at varying air inlet temperatures, as expressed by Eq. (3-13), was plotted, as illustrated in Figure 3-5. The figure shows the drop in efficiency as the excess air is increased from 0% to 50%. However, this drop in efficiency reduces as the air inlet temperature is increased from the reference temperature of 298 K. For the analytical case when the incoming air temperature reached a value of 1 100 K, the efficiency for air excess percentages above 0% exceeded unity. This could be due to the fact that the excess air passing through the adiabatic combustor was changed less than the air used in the combustion

UNIVERSITEIT VAN PRETORIA
UNIVERSITY OF PRETORIA
YUNIBESITHI YA PRETORIA


process because of the smaller difference between the incoming air temperature and the final adiabatic flame temperature. Hence the smaller increase in entropy production for combustion with air excess more than for combustion with 0% excess air. The peaking in efficiency at 5% excess air instead of 0% excess air is due to the deficit in the observed second law efficiency at 0% excess air CFD results. This is due to air in the combustion products (as represented by the presence of $O_2$ in the combustion products mix listed in Table 3-2 for 0% combustion), which reduced the adiabatic flame temperature. Because the maximum work that can be performed by the Carnot cycle power plant is computed solely using the adiabatic flame temperature, the work done computed is lower than expected. As mentioned before, the second law efficiencies of all excess air combustion of the CFD simulations are normalised with respect to the second law efficiency at 0% excess air combustion. Therefore, Figure 3-5 shows plots for CFD simulations which appear to have a better thermodynamic performance than at 0% excess air combustion.

UNIVERSITEIT VAN PRETORIA
UNIVERSITY OF PRETORIA
YUNIBESITHI YA PRETORIA


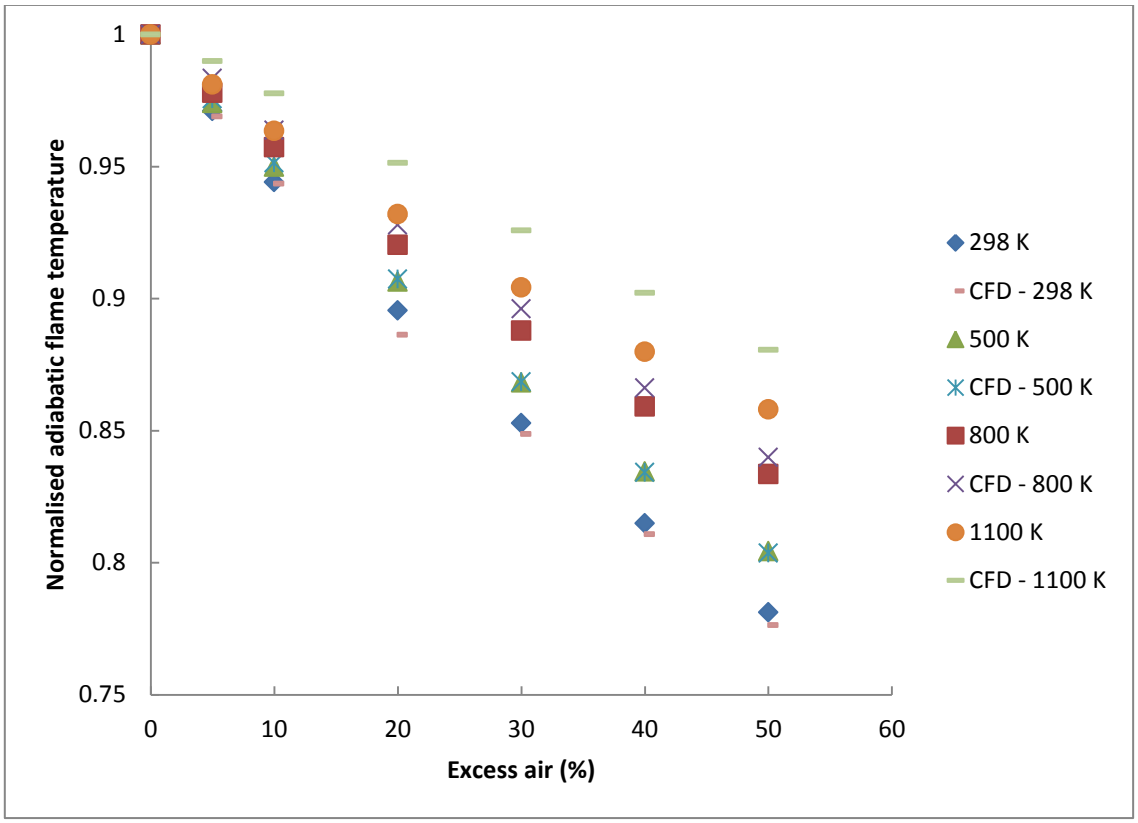


**Figure 3-6: Plot of normalised adiabatic flame temperatures for varying air excess percentages at varying air inlet temperatures.**

The adiabatic flame temperatures achieved at varying air excess percentages at varying air inlet temperatures are computed for the analytical method and CFD simulations. They are normalised with respect to the values at 0% excess air and were plotted in Figure 3-6. The absolute values of the adiabatic flame temperatures were also plotted in Figure 3-7.

UNIVERSITEIT VAN PRETORIA
UNIVERSITY OF PRETORIA
YUNIBESITHI YA PRETORIA


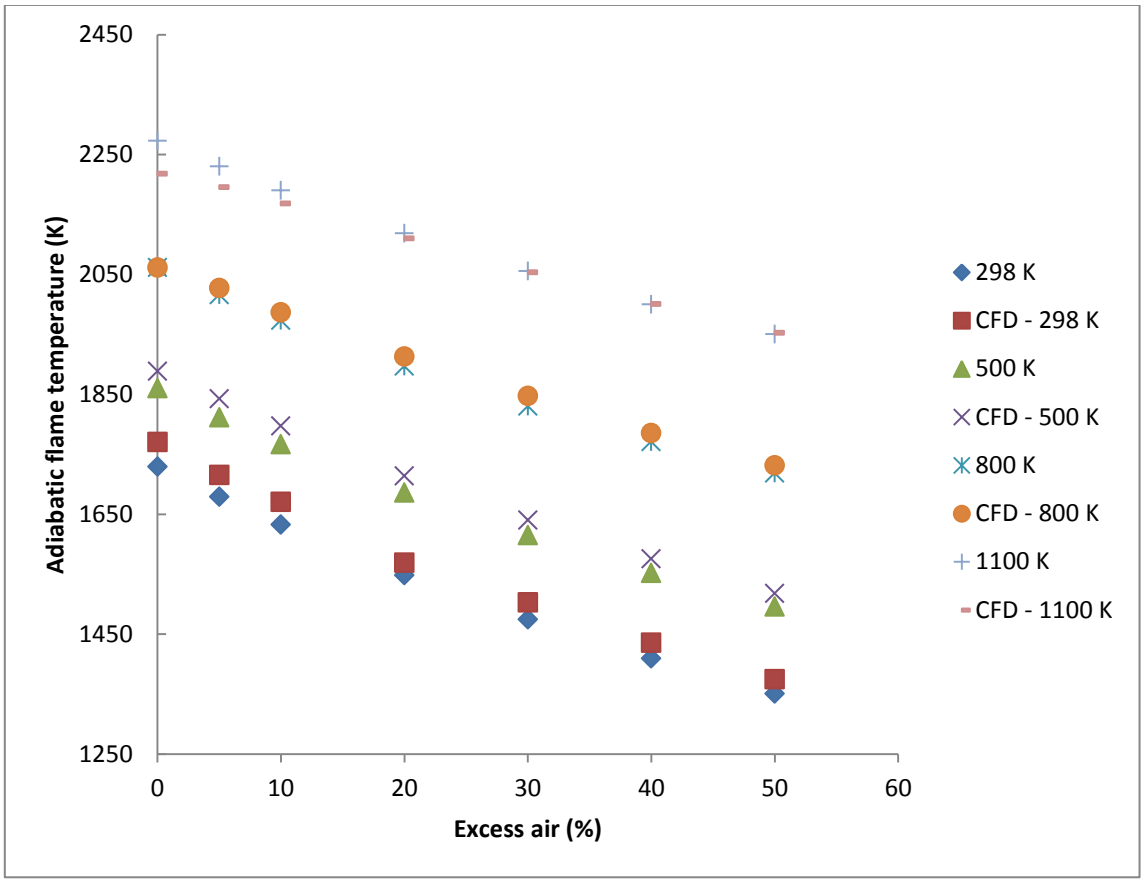


**Figure 3-7: Plot of adiabatic flame temperatures for varying air excess percentages at varying air inlet temperatures.**

## 3.6. CONCLUSION

The second law efficiency of a pine wood-fired adiabatic combustor was found to drop as the air excess percentage of air was increased from that needed for theoretical combustion. However, the efficiency was found to increase as the incoming air temperature was increased from the reference value of 298 K. This phenomenon was observed to continue until the efficiency exceeded that of theoretical combustion for incoming air temperature of 1 100 K and greater. This observed phenomenon was even more pronounced for CFD results.

UNIVERSITEIT VAN PRETORIA
UNIVERSITY OF PRETORIA
YUNIBESITHI YA PRETORIA


# Chapter 4. THERMODYNAMIC OPTIMISATION AND COMPUTATIONAL ANALYSIS OF IRREVERSIBILITES IN A SMALL-SCALE WOOD-FIRED CIRCULATING FLUIDISED BED ADIABATIC COMBUSTOR

## 4.1. INTRODUCTION

Incomplete combustion processes of solid fuels such as those found in circulating fluidised bed combustors are difficult to model as compared with complete combustion [73]. The reason is that for complete combustion, the proportion of each combustion product can easily be predicted analytically through the stoichiometric equation [73, 2, 3, 4], whereas this cannot be the case for incomplete combustion. This makes it hard to predict the performance of a combustion unit as measured against desired output. The air-fuel mass ratio (AF) can be selected such that combustion occurs, but for incomplete combustion, the proportions of the combustion products cannot be predicted analytically, as mentioned earlier. For an incomplete combustion process, the combustion products mixture will contain unburnt fuel in the form of char and maybe volatile gases released from the devolatilisation of the solid fuel. There is negligible molecular oxygen in the combustion products mixture [73, 2, 3, 4]. In the case of complete combustion with excess air, there will be molecular oxygen in the combustion mixture, but there will not be any fuel components that resulted from the devolatilisation process [1], assuming proper mixing occurred. Because the combustor is adiabatic, the total enthalpy across it does not change, but entropy increases [73]. A way to

alleviate this predicament is to conduct experiments or run numerical simulations that predict the proportion of each combustion product. Elfasakhany et al. [19] undertook experimental and numerical studies to find reasons for the emissions of unburnt volatiles and particles of pulverised wood in combustion products mixture, and they found that the emissions were sensitive to fuel particle size and combustor configuration. Different AF ratios will result in different exergies or availability of the energy released as measured by means of a combustion products average temperature. Chen et al. [5] compared the gasification of raw biomass, torrefied biomass and coal using pure oxygen, and found that there was an optimum oxygen-fuel ratio for each fuel at which gasification was most efficient. Tran et al. [6] found that torrefaction of stump biomass resulted in increased heating values and grindability of the fuel when compared with untreated biomass, but terrofaction made the treated fuel less reactive. Zhang et al. [7] experimented on the gasification of caking coal in a pilot fluidised bed gasifier, where they found that the optimal proportion of oxygen used for pre-oxidation of 37% of the total oxygen supply greatly enhanced the gasification rate. The availability of the energy released from the combustion process can be quantified through the computation of an entropy generation rate as given by Bejan [4]. Le Roux, Bello-Ochende and Meyer [33] used the technique of total entropy generation minimisation to find the optimum operating point of a turbine, and to optimise the geometric parameters of a recuperator and receiver of an open and direct solar thermal Brayton cycle. Mwesigye, Bello-Ochende and Meyer [34] numerically investigated the entropy generation rate due to heat transfer and fluid friction in a parabolic trough receiver. They found that a minimum entropy generation rate existed for every combination of concentration ratio and inlet temperature, which corresponded to an

UNIVERSITEIT VAN PRETORIA
UNIVERSITY OF PRETORIA
YUNIBESITHI YA PRETORIA


optimum flow rate. Le Roux, Bello-Ochende and Meyer [35] used the dynamic trajectory optimisation method to find optimised geometric parameters, minimum irreversibility rates and maximum receiver surface temperatures for an open and direct solar thermal Brayton cycle. For an adiabatic circulating fluidised bed combustor, the entropy generation rate is due to frictional pressure loss across the combustor and the combustion process. The frictional pressure drop across a conduit for a fluidised system as given by Kunii and Levenspiel [28] remains the same once minimum fluidisation has been attained. Gupta and Reddy [29] analysed the effect of pressure on the bed-to-wall heat transfer in a pressurised circulating fluidised bed riser by modifying a cluster renewal model developed for atmospheric circulating fluidised bed riser columns. The model they developed agreed well with experimental results and literature. Han et al. [30] found that pressurisation improved the capture of $CO_2$ when using CaO in a fluidised bed gasifier of sawdust. Aisyah, Ashman and Kwong [31] found that coal fly-ash oxygen carriers were effective in converting carbon dioxide into carbon monoxide when used in chemical looping combustion of synthesis gas. Aghbalou, Badia and Illa [74] conducted an exergetic optimisation of a solar collector and thermal storage system where they used a phase change material. The optimisation resulted in an analytical model that compared well with experimental data they generated a priori. Kousksou et al. [75] conducted a second law analysis of latent thermal storage for a solar system where they studied the behaviour of phase change material in the form of its melting temperature. Exergy analysis of phase change materials was also conducted by Li et al. [76], in which they developed a mathematical model for the thermal storage of energy from a solar collector system. They developed the model based on the finite-time thermodynamics

UNIVERSITEIT VAN PRETORIA
UNIVERSITY OF PRETORIA
YUNIBESITHI YA PRETORIA


method. A review of exergy-based performance evaluation of phase change materials latent heat thermal storage systems was conducted by Jegadheeswaran, Pohekar and Kousksou [77], in which they looked at the influence of design parameters and operating conditions on optimisation of the thermal storage systems. Brandvoll and Bolland [78] used exergy analysis on results from simulations to show that a chemical looping combustion process had lower irreversibilities than a conventional combustion process with air. Srinivas et al. [79] conducted energy and exergy analyses of pressurised and atmospheric circulating fluidised bed char combustion units, in which they identified the pressure ratio and maximum value of the gas turbine inlet temperature as the parameters that had a dominant impact on the combined cycle plant performance. The exergy efficiency of a blast furnace process was found to have high exergy efficiency, but the compressing and preheating of the blast was found to be characterised by high exergy losses due to the associated combustion process in a study conducted by Ziebik and Stanek [20]. Ziebik and Stanek [21] also looked at the thermal improvement of a blast furnace process through the increase of blast temperature and its oxygen enrichment. They did this through energy and exergy analyses. Nur Izyan and Shuhaimi [22] used exergy analysis on a crude oil distillation unit to find strategies to reduce the fossil fuel depletion problem. They found that the first inlet furnace had the highest exergy loss and that the best strategies were to reduce the heat loss from the furnace stack and an overall cleaning schedule of crude preheat train. Gupta and Reddy [23] conducted energy and exergy analyses on a combined-cycle power plant all in the aim of modernising the plant. They found that the combustion chamber, gas turbines and heat recovery steam generators were the main sources of irreversibilities. The irreversibilities of proton exchange membrane

UNIVERSITEIT VAN PRETORIA
UNIVERSITY OF PRETORIA
YUNIBESITHI YA PRETORIA


fuel cells were analysed by Cihan et al. [24] as a function of operating pressure, pressures of the electrodes, current density, etc. Bapat, Majali and Ravindranath [80] did an exergetic evaluation of two quintuple effect evaporators with and without heat recovery, and found that an increase in exhaust inlet temperature resulted in deterioration in exergetic performance of the evaporator with heat recovery and the quality of the end product. Ghazikhani et al. [25] used a double-pipe heat exchanger with counter-current flow to recover exergy by cooling the exhaust from a diesel engine. They found that the recovered exergy increased with increasing load and engine speed. They also found that when they used the recovered exergy, the brake specific fuel consumption decreased markedly. Ghazikhani et al. [81] investigated the improvement in performance and reduction in emissions due to ethanol additives in a two-stroke SI engine. They found that there was a reduction in brake specific fuel consumption and there was a reduction in pollutants emitted, with a 35% reduction in CO emission being the highest. In a related paper, Gazikhani, Hatami and Safari [82] found that for 5% added ethanol into the fuel, the second law efficiency was higher for 2 500 and 3 000 revolutions per minute settings. Chintala and Subramanian [26] used an exergy analysis on a hydrogen-diesel engine to determine the maximum available work and irreversibility due to mixing, combustion, unburnt fuel and friction. They found that the maximum available work increased with $H_2$ addition because of the reduction in irreversibility due to combustion. They also found that the addition of $H_2$ had no effect on the irreversibility due to friction and mixing, whereas the irreversibility caused by unburnt fuel decreased because of the high temperature combustion that resulted with the addition of $H_2$. Jafarmadar [27] found that even though the exergy efficiency decreased when he increased the mass fraction of exhaust gas

recirculation in an indirect injection diesel engine from 0% to 30%, the cumulative irreversibility in the combustion chamber decreased. Ting, Hung and Guo [32] investigated the entropy generated by nanofluid with streamwise conduction in microchannels. They found that there existed minimal entropy generation at a certain range of the low Peclet number flow regime. The need to combat the rise in CO and $CO_2$ emissions from coal combustion has put pressure on utilities and governments of countries where the main source of electricity is from coal combustion. Substitutes for coal combustion that can result in lower emissions of CO and CO2 are some of the mitigation solutions under consideration at the moment. These substitutes can be a complete replacement of coal with wood as a source of heat in a boiler or a blending of wood with coal. However, combustors usually do not completely burn the solid fuel, especially circulating fluidised combustors. In order to investigate the viability of wood as a source of heat in a typical combustor setting, the analysis of irreversibilities generated during the combustion of pitch pine in an adiabatic circulating fluidised bed combustor was conducted as the air-fuel mass ratio was varied to achieve a reactant mixture varying from a rich mixture to a lean mixture. This was achieved by fixing the fuel mass flow rate at one value, but the air mass flow rate was reduced or increased.

## 4.2. MATHEMATICAL MODEL

The study was of an adiabatic combustor burning pitch pine wood as illustrated in Figure 4-1. The adiabatic combustor consisted of a cylinder with an adiabatic wall, inlets for the solid fuel and primary air inlet for the air used to devolatilise the solid fuel and secondary air inlets if needed to complete the combustion of the fuel. The different states of complete/incomplete

UNIVERSITEIT VAN PRETORIA
UNIVERSITY OF PRETORIA
YUNIBESITHI YA PRETORIA


combustion were attained by changing the mass flow rate of the incoming oxidising air, thereby varying the AF. The chemical formula of the solid fuel as computed in [73] is given by $C_{4.9}H_{7.2}O_2$.

The lower heating value of the fuel from [73] was given as 1 6091.2 kJ/kg and the molecular weight of the fuel was calculated as 98 kg/kmol. The specific heat at constant pressure was also given as 1.680 kJ/kg.K.

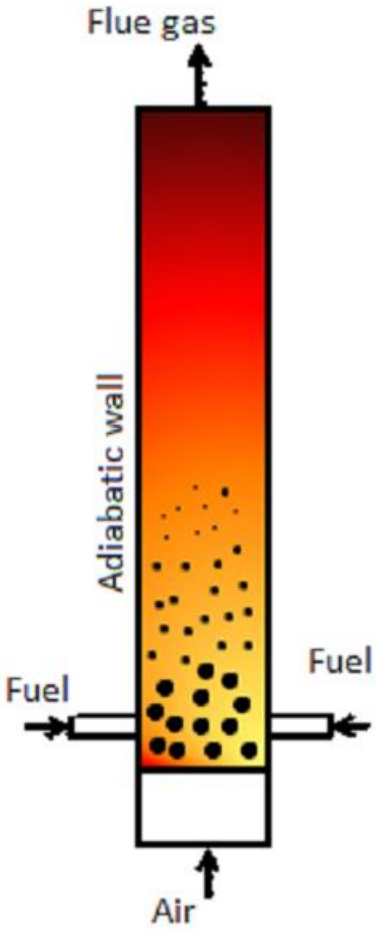


**Figure 4-1: Schematic of an adiabatic combustor (adopted from [73]).**

The availability of the energy released from the combustion process was analysed for scenarios on both sides of the theoretical air complete combustion point, i.e. the incomplete

combustion with air deficiency and complete combustion with excess air. Complete combustion of pitch pine wood occurs at an AF of 8.02, as was determined in [73]. The availability was analysed as a function of AF.

### 4.2.1. Exergy analysis

The irreversibility generation rate that results from the combustion and frictional pressure drop processes taking place in an adiabatic combustor is given by Eq. (4-1):

$$\dot{I} = \frac{\dot{m}_f}{M_f}\left(\sum_{i=1}^{m} n_{ri}\left(\bar{h} - T_{ref}\bar{s}\right)_{ri} - \sum_{i=1}^{l} n_{pi}\left(\bar{h} - T_{ref}\bar{s}\right)_{pi}\right) \quad \textbf{(4-1)}$$

Because the enthalpy terms cancel out in Eq. (4-1), the irreversibility generation rate can also be defined by Eq. (4-2):

$$\dot{I} = T_{ref}\dot{S}_{gen} \quad \textbf{(4-2)}$$

where $\dot{S}_{gen}$ is the entropy generation rate. The specific entropy is given by Eq. (4-3):

$$\bar{s}_{pi} = \bar{s}^{\circ}_{pi}(T) - \bar{R}\ln(Px_{pi}/P_{ref}) \quad \textbf{(4-3)}$$

The static pressure in the combustor is the same as the reference static pressure, i.e. $P = P_{ref}$, and the molar fraction of each product species, $x_{pi}$, is given by Eq. (4-4):

$$x_{pi} = n_{pi}\Big/\sum_{i=1}^{l} n_{pi} \quad \textbf{(4-4)}$$

$n_{pi}$ is the stoichiometric coefficient of combustion product species *i*. The same expressions apply for reactants. $\bar{h}$ is the specific enthalpy, $\bar{s}^{\circ}_{pi}$ is the absolute entropy, $\bar{R}$ is the universal gas constant, $p$ is the static pressure, $P_{ref}$ is the reference static pressure of the environment and $T_{ref}$ is the reference temperature of the environment. The specific entropy of the solid fuel is computed by defining [1], as given by Eq. (4-5):

$$\bar{s} = \bar{c}\ln\left(T_f/298\right) \quad \textbf{(4-5)}$$

UNIVERSITEIT VAN PRETORIA
UNIVERSITY OF PRETORIA
YUNIBESITHI YA PRETORIA



$\bar{c}$ is the molar specific heat of the solid fuel.

The entropy generation rate $\dot{S}_{gen}$ is due to the combustion and the pressure drop phenomena. Generally, the entropy generation rate term is not defined in detail in terms of its constituents. Section 4.2.1.1. gives the detailed expressions of the entropy generation rate term constituents.

#### *4.2.1.1. Entropy generation rate*

Entropy generation rate is a term that can be used to quantify the inefficiencies of thermodynamic systems as they convert energy from one form to another. Complete elimination of this term is not possible for real systems; however, its minimisation can result in maximisation of the exergy available from these systems and hence improved efficiencies. The entropy generation rate term due to combustion is defined [4] in terms of the change in entropy of the system due to reactions. On the other hand, the entropy generation rate due to frictional pressure drop is defined in terms of the pressure drop of the system [4]. Each of the two terms is defined and derived, in turn, as presented below.

### 4.2.1.2. Friction pressure drop entropy generation rate

The friction pressure drop entropy generation rate term is made up of the contribution due to the air-fuel mixture as it flows through the riser. The contribution due to the air-fuel mixture flow is given by Eq. (4-6):

$$\dot{S}_{gen(p)} = \frac{\dot{m}_t \Delta P}{\rho_m T_m} \qquad \textbf{(4-6)}$$

UNIVERSITEIT VAN PRETORIA
UNIVERSITY OF PRETORIA
YUNIBESITHI YA PRETORIA



$\Delta P$ is the pressure drop across the combustor, $\dot{m}_t$ is the total air and fuel mass flow rate, $\rho_m$ is the mixture density, $T_m$ is the mixture temperature. The pressure drop across the riser due to the air-fuel mixture [28] is given by Eq. (4-7):

$$\Delta P = L_{mf}\left(1-\varepsilon_{mf}\right)\left(\rho_f - \rho_g\right)g \qquad \textbf{(4-7)}$$

$\varepsilon_{mf}$ is the minimum fluidisation solid volume fraction, $\rho_f$ is the char density, $\rho_g$ is the gaseous density, $L_{mf}$ is the minimum fluidisation height and $g$ is acceleration due to gravity. The pressure drop can also be expressed in terms of the total height of the riser by using an expression found in [28] for an air-solid mixture undergoing fast fluidisation inside a vertical column, as given by Eq. (4-8):

$$L_{mf}\left(1-\varepsilon_{mf}\right) = \frac{\varepsilon_{sd}-\varepsilon_{se}}{a} + H_t\varepsilon_{sd} - H_f\left(\varepsilon_{sd}-\varepsilon_s^*\right) \qquad \textbf{(4-8)}$$

$\varepsilon_{sd}$ is the solid volume fraction in the bed region of the riser, $\varepsilon_{se}$ is the solid volume fraction at the exit of the riser, $a$ is an empirical velocity term, $H_t$ is the total height of the riser, $H_f$ is the freeboard height and $\varepsilon_s^*$ is the minimum value that $\varepsilon_{se}$ can assume. Kunii and Levenspiel [28] also give an expression for $H_f$, as given by Eq. (4-9):

$$H_f = \left[\ln\left(\varepsilon_{sd}-\varepsilon_s^*\right) - \ln\left(\varepsilon_{se}-\varepsilon_s^*\right)\right]/a \qquad \textbf{(4-9)}$$

When Eq. (4-7), Eq. (4-8) and Eq. (4- 9) are substituted into Eq. (4-6), the pressure drop is eliminated and this results in an expression as given by Eq. (4-10):

$$\dot{S}_{gen(p)} = \frac{\dot{m}_t\left(\rho_f-\rho_g\right)g\left[\frac{\varepsilon_{sd}-\varepsilon_{se}}{a} + H_t\varepsilon_{sd} + \ln\left(\frac{\varepsilon_{se}-\varepsilon_s^*}{\varepsilon_{sd}-\varepsilon_s^*}\right)\left(\frac{\varepsilon_{sd}-\varepsilon_s^*}{a}\right)\right]}{\left(\varepsilon_{se}\rho_f + \left(1-\varepsilon_{se}\right)\rho_g\right)T_m} \qquad \textbf{(4-10)}$$

The mixture density is computed, as expressed by Eq. (4-11):

$$\rho_m = \varepsilon_{se}\rho_f + \left(1-\varepsilon_{se}\right)\rho_g \qquad \textbf{(4-11)}$$

UNIVERSITEIT VAN PRETORIA
UNIVERSITY OF PRETORIA
YUNIBESITHI YA PRETORIA



The empirical velocity term $a$ can be expressed in terms of the fuel mass flow rate and the AF. Firstly, the empirical velocity term is given by $a = 10/u_0$, where $u_0$ is the superficial velocity. But the superficial velocity is given as $u_0 = (1-\varepsilon_{sd})u_g$, where $u_g$ is the gas velocity. The gas velocity, in turn, is expressed as Eq. (4-12):

$$u_g = \dot{m}_g / \rho_g A \qquad \textbf{(4-12)}$$

Given the fact that the total mass flow rate is expressed by Eq. 4-(13), and that the air-fuel mass ratio is expressed as $AF = \dot{m}_g / \dot{m}_f$, the superficial velocity can be written as expressed by Eq. (4-14):

$$\dot{m}_t = \dot{m}_g + \dot{m}_f \qquad \textbf{(4-13)}$$

$$u_0 = (1-\varepsilon_{sd})\frac{\dot{m}_f AF}{\rho_g A} \qquad \textbf{(4-14)}$$

Hence the empirical velocity term can be expressed in terms of the fuel mass flow rate and AF, as given by Eq. (4-15):

$$a = \frac{10\rho_g A}{(1-\varepsilon_{sd})\dot{m}_f AF} \qquad \textbf{(4-15)}$$

When Eq. (4-15) is substituted into Eq. (4-10), the entropy generation rate due to frictional pressure can be expressed in terms of the fuel mass flow rate and AF, as given by Eq. (4-16):

$$\dot{S}_{gen(p)} = \frac{\dot{m}_f (AF+1)(\rho_f - \rho_g) g \left[ \frac{(\varepsilon_{sd} - \varepsilon_{se})(1-\varepsilon_{sd})\dot{m}_f AF}{10\rho_g A} + H_t \varepsilon_{sd} + \ln\left( \frac{\varepsilon_{se} - \varepsilon_s^*}{\varepsilon_{sd} - \varepsilon_s^*} \right) \left( \frac{\varepsilon_{sd} - \varepsilon_s^*}{10\rho_g A} \right) (1-\varepsilon_{sd})\dot{m}_f AF \right]}{(\varepsilon_{se}\rho_f + (1-\varepsilon_{se})\rho_g) T_m} \qquad \textbf{(4-16)}$$

#### *4.2.1.3. Combustion entropy generation rate*

The entropy generation rate due to the combustion process is given by Eq. (4-17):

UNIVERSITEIT VAN PRETORIA
UNIVERSITY OF PRETORIA
YUNIBESITHI YA PRETORIA



$$\dot{S}_{gen(h)} = \frac{\dot{m}_f \Delta \bar{s}}{M_f} \quad \textbf{(4-17)}$$

The change in entropy $\dot{S}_{gen(h)}$ accounts for the increase in entropy as the fuel is oxidised by the oxygen in the air. The change in entropy is constituted by contributions from gaseous species and solid species, i.e. $\Delta \bar{s} = \Delta \bar{s}_g + \Delta \bar{s}_s$. The contribution to the entropy change from gaseous species is given by Eq. (4-18):

$$\Delta \bar{s}_g = \sum_{j=1}^{l} n_{pj} \left( \bar{s}^\circ - \bar{R} \ln(x) \right)_{Pj} - \sum_{j=1}^{m} n_{rj} \left( \bar{s}^\circ - \bar{R} \ln(x) \right)_{rj} \quad \textbf{(4-18)}$$

$M_j$ is the molecular weight of species $j$. The contribution to the entropy change from solid species is expressed by Eq. (4-19):

$$\Delta \bar{s}_s = \frac{\rho_{char}}{\rho_g} n_{char} c_{char} M_{char} \ln\left( T_{char} / 298 \right) - \frac{\rho_f}{\rho_g} n_f c_f M_f \ln\left( T_f / 298 \right) \quad \textbf{(4-19)}$$

$c_{char}$ is the specific heat constant for the char particles and $c_f$ is the specific heat constant for the solid fuel. When Eqs. (4-18) and (4-19) are substituted into Eq. (4-17), the entropy generation rate due to combustion can be expressed as given by Eq. (4-20):

$$\dot{S}_{gen(h)} = \frac{\dot{m}_f}{M_f} \left( \begin{array}{l} \sum_{j=1}^{l} n_{pj} \left( \bar{s}^\circ - \bar{R} \ln(x) \right)_{Pj} - \sum_{j=1}^{m} n_{rj} \left( \bar{s}^\circ - \bar{R} \ln(x) \right)_{rj} + \frac{\rho_{char}}{\rho_g} n_{char} c_{char} M_{char} \ln\left( T_{char} / 298 \right) \\ - \frac{\rho_f}{\rho_g} n_f c_f M_f \ln\left( T_f / 298 \right) \end{array} \right) \quad \textbf{(4-20)}$$

### 4.2.2. Entropy generation number and relative entropy generation rate

The entropy generation rate at any equivalent ratio is analysed further by means of two ratios. An equivalent ratio of 1 means complete combustion with theoretical amount of air, whereas an equivalent ratio above 1 signifies a rich mixture and that below 1 signifies a lean mixture.

UNIVERSITEIT VAN PRETORIA
UNIVERSITY OF PRETORIA
YUNIBESITHI YA PRETORIA



The first ratio is the entropy generation number, $N_s$ [4] which is the quotient of the entropy generation rate at any equivalence ratio and the minimum entropy generation rate, and is given by Eq. (4-21):

$$N_s = \frac{\dot{S}_{gen}}{\dot{S}_{gen,\min}} \quad \textbf{(4-21)}$$

Because $\dot{S}_{gen,\min}$ is the best possible solution at which the most exergy can be generated, $N_s$ measures the penalty paid in terms of lost exergy when deviating far from the point where the minimum entropy generation rate occurs. The second ratio is the relative generation rate, which is the quotient of the entropy generation rate at any equivalent ratio and the entropy generation rate when combustion occurred with theoretical air ratio, and is expressed by Eq. (4-22):

$$N_R = \frac{\dot{S}_{gen}}{\dot{S}_{gen,th}} \quad \textbf{(4-22)}$$

$\dot{S}_{gen,th}$ measures the entropy generation rate when complete combustion occurs with a theoretical amount of air. This point also happens to be where maximum possible temperature can be achieved. Therefore, $N_R$ can be a measure of gained or lost efficiency by sacrificing attainment of the maximum possible temperature in order to maximise exergy generation.

## 4.3. CFD MODEL

The adiabatic combustor produced 241 $kW_{th}$ when complete combustion of pitch pine wood occurred with a theoretical amount of air. The combustor had a diameter of 300 mm and a height of 7 000 mm, as illustrated in Figure 4-2.

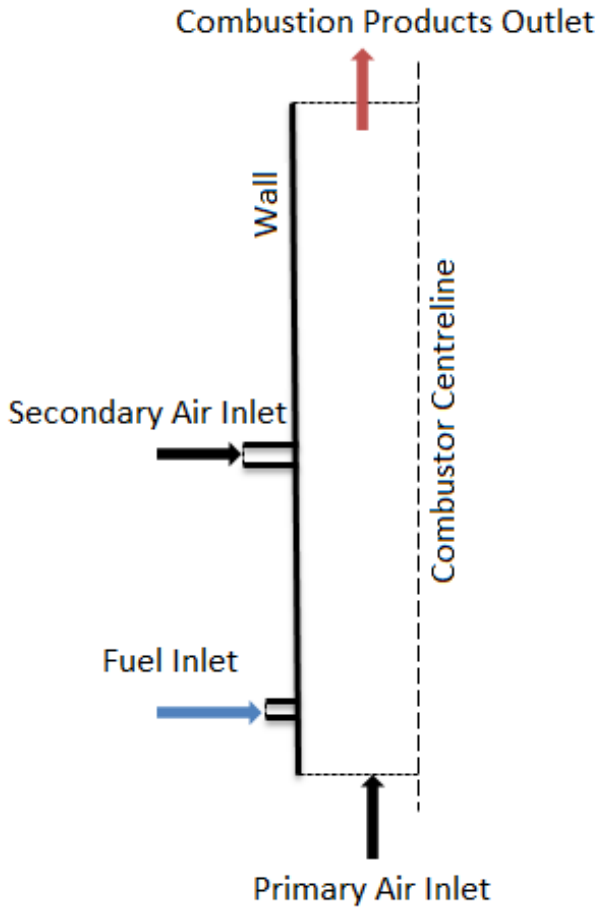


**Figure 4-2: Schematic of the adiabatic combustor showing boundary placements.**

The mass flow rate of the incoming solid fuel was fixed at a value of 0.015 kg/s so as to have a common maximum heat generation rate of 241 $kW_{th}$ because the lower heating value is fixed and unique for any particular fuel. ANSYS Fluent 14 [68] was used to simulate the combustion process inside the adiabatic combustor. The combustion process was modelled using the non-premixed combustion model because the solid fuel is only specified in ultimate analysis data, as given in Table 4-1, and the combustion model gives an option of specifying the fuel as an empirical stream. The inlet diffusion option was selected.

UNIVERSITEIT VAN PRETORIA
UNIVERSITY OF PRETORIA
YUNIBESITHI YA PRETORIA



**Table 4-1**: **Pitch pine ultimate analysis data (adapted from [67]).**

| Element | Value |
|---|---|
| C | 59.0 (%) |
| H | 7.2 (%) |
| O | 32.7 (%) |
| Ash | 1.13 (%) |
| HHV | 24220 (kJ/kg) |
| LHV | 16091.2 (kJ/kg) |
| Molecular weight | 98 (kg/kmol) |

The continuity and momentum equations [68], as expressed by Eq. (4-23) and Eq. (4-25) respectively, are solved for under steady-state condition.

$$\nabla \cdot \left(\rho \vec{v} \overline{f}\right) = \nabla \cdot \left(\frac{\mu_t}{\sigma_t} \nabla \overline{f}\right) + s_m \qquad \textbf{(4-23)}$$

$$\nabla \cdot \left(\rho \vec{v} \overline{f'^2}\right) = \nabla \cdot \left(\frac{\mu_t}{\sigma_t} \nabla \overline{f'^2}\right) + C_g \mu_t \left(\nabla \overline{f}\right)^2 - C_d \rho \frac{\varepsilon}{k} \overline{f'^2} \qquad \textbf{(4-24)}$$

$$\nabla \cdot \left(\rho \vec{v} \vec{v}\right) = -\nabla p + \nabla \cdot \left(\bar{\bar{\tau}}\right) + \rho \vec{g} + \vec{F} \qquad \textbf{(4-25)}$$

The stress tensor [68] is given by Eq. (4-26):

$$\bar{\bar{\tau}} = \mu \left[\left(\nabla \vec{v} + \nabla \vec{v}^T\right) - \frac{2}{3} \nabla \cdot \vec{v} \hat{i}\right] \qquad \textbf{(4-26)}$$

$\mu$ is the molecular viscosity of the continuous phase, $\vec{F}$ is the interactive body forces between the dispersed and the continuous phases, $S_m$ is the source term accounting for the mass transfer from the solid phase to the gas phase and $\hat{i}$ is a unit vector. $\overline{f}$ and $\overline{f'^2}$ are the mixture fraction and its variance, and are computed by applying an assumed shape

UNIVERSITEIT VAN PRETORIA
UNIVERSITY OF PRETORIA
YUNIBESITHI YA PRETORIA



probability density function ( $\beta$ -function) when modelling the turbulence-chemistry interaction.

The energy for the non-premixed combustion model [68] is expressed by Eq. (4-27):

$$\nabla \cdot \left( \rho \vec{v} H \right) = \nabla \cdot \left( \frac{k_t}{c_p} \nabla H \right) + S_h \qquad \textbf{(4-27)}$$

The total enthalpy $H$ is given by Eq. (4-28):

$$H = \sum_{j=1}^{m} Y_j \left( \int_{T_{ref,j}}^{T} c_{p,j} dT + h_j^0 \left( T_{ref,j} \right) \right) \qquad \textbf{(4-28)}$$

$Y_j$ is the mass fraction, $c_{p,j}$ is the specific heat and constant pressure and $h_j^0 \left( T_{ref,j} \right)$ is the enthalpy of formation of the $j^{th}$ species. $S_h$ is the source term due to viscous dissipation. The use of the chosen combustion model requires the use of a turbulent model because the combustion model is a mixture model. To this end, the $k-\varepsilon$ turbulent model with enhanced wall function option is chosen for all simulations.

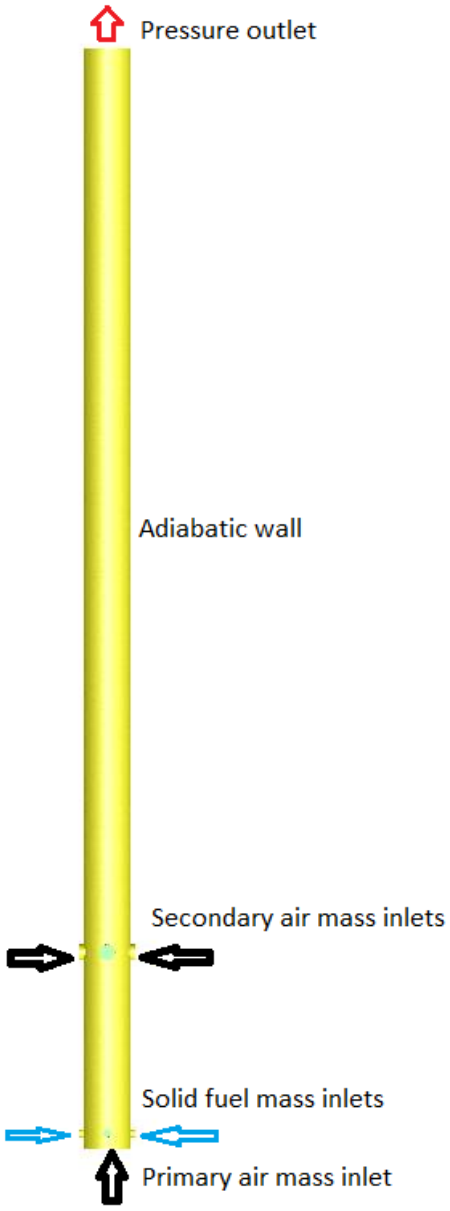


**Figure 4-3: Schematic of the geometry used in Ansys Fluent 14 [68] to model the adiabatic combustor.**

The adiabatic combustor had four mass flow inlets for the solid fuel as shown in Figure 4-3, each with equal mass flow rate of 0.00375 kg/s. The inlet temperature of the fuel at each inlet was set at 600K. The temperature value was selected to be the same as the devolatilisation

UNIVERSITEIT VAN PRETORIA
UNIVERSITY OF PRETORIA
YUNIBESITHI YA PRETORIA



temperature of pitch pine [67]. The oxidising air was split into the primary and secondary air, each making up half of the total air used in the oxidation of the fuel. The reason for splitting the oxidising air was to enable the modelling of incomplete combustion to take place. The primary air entered the combustor at the base with a single fixed mass inlet, with half of the total air mass flow rate. The four secondary air fixed mass inlets were situated a quarter of the height up the combustor, each having an eighth of the total air mass flow rate. The inlet temperature at all eight air inlets was set at 298K. The wall of the combustor was adiabatic. The data that was extracted from the simulations were the temperature at the pressure outlet boundary and the combustion products molar fractions. Figure 4-3 shows the placement and types of boundaries applied to the combustor.

Mesh independence of the solution was carried out for different mesh cell numbers. The figure of merit used to quantify mesh independence was $\Delta$, which was used to quantify the change in entropy generation rate because the number of cells in the computation domain was increased. The entropy generation rate is computed for the case of complete combustion with theoretical amount of air. It is computed as $\Delta = \left(\dot{S}_{gen,i} - \dot{S}_{gen,i-1}\right) / \dot{S}_{gen,i-1}$, and the results are tabulated in Table 4-2.

**Table 4-2: Mesh independence analysis results.**

| **Number of cells** | $\dot{S}_{gen}$ **(W/K)** | $\Delta$(%) |
|---|---|---|
| 438192 | 362.6218 | |
| 609857 | 362.6756 | 0.01% |
| 655783 | 362.7186 | 0.01% |
| 747055 | 364.1874 | 0.40% |
| 1188339 | 361.6429 | -0.70% |

The mesh used for the numerical simulations had 747 055 unstructured polyhedral cells. The Presto! scheme was used to solve for pressure and second-order upwind schemes were used to solve for the continuity, energy, turbulence and mass fraction. The results obtained when using Eq. (4-16) and Eq. (4-20) to process data from CFD simulations and data from the thermodynamics tables [2] were compared for the case of complete combustion with varying amounts of excess air, which were lean mixtures. It was found that the results from CFD data compared well with the results from the thermodynamics tables, as shown in Figure 4-4.

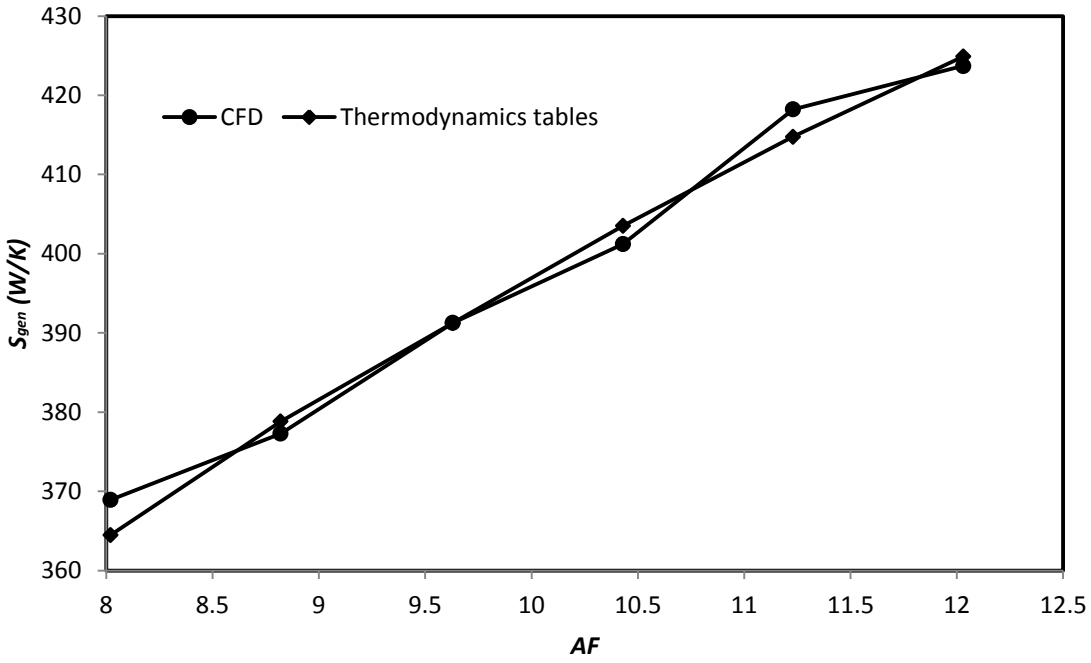


**Figure 4-4: The entropy generation rate profile as a function of AF in an adiabatic combustor for lean mixtures.**

## 4.4. RESULTS AND DISCUSSION

The entropy generation rate was almost entirely due to the combustion process, with negligible contribution from the component from frictional pressure drop, as can be seen from Figure 4-5.

UNIVERSITEIT VAN PRETORIA
UNIVERSITY OF PRETORIA
YUNIBESITHI YA PRETORIA



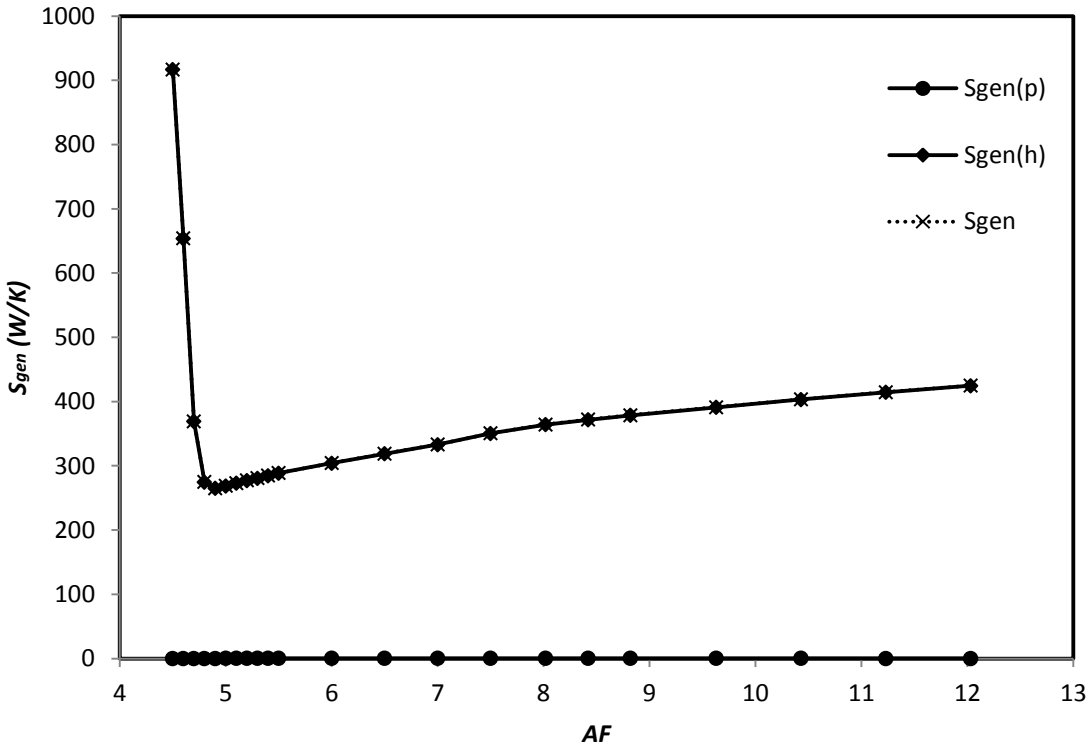


**Figure 4-5: The entropy generation rate profile as a function of AF in an adiabatic combustor.**

The change in the entropy generation rate as a function of AF was plotted, as shown in Figure 4-6. The figure shows that the entropy generation rate reaches a minimum at an AF of 4.9. This is well illustrated by the close-up plot, as shown by Figure 4-7. This ratio occurs when there is incomplete combustion inside the adiabatic combustor because complete combustion with theoretical amount of air occurs at 8.02. Figure 4-6 also shows the variation of the generated irreversibities with AF, which are computed from the entropy generation rate, as given by Eq. (4-2).

UNIVERSITEIT VAN PRETORIA
UNIVERSITY OF PRETORIA
YUNIBESITHI YA PRETORIA



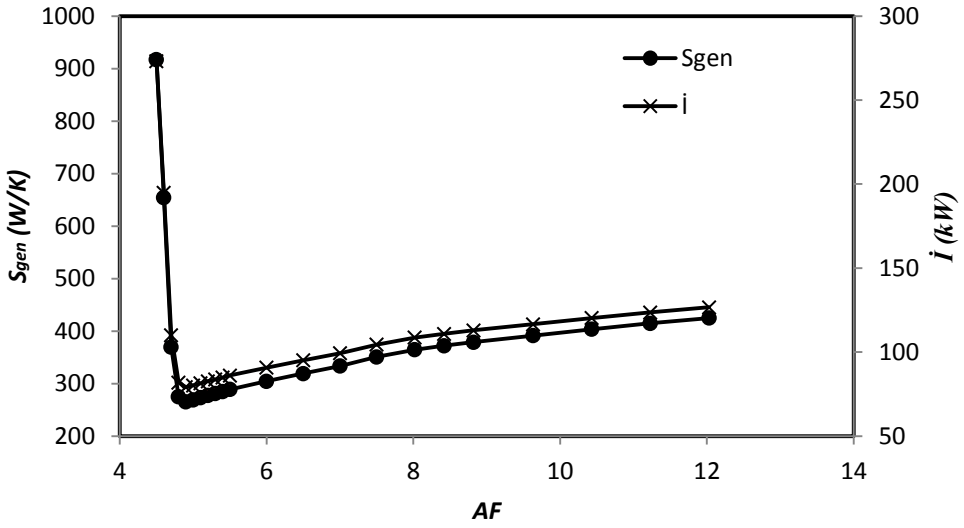


**Figure 4-6: Plots of the entropy generation rate and irreversibilities as functions of AF in an adiabatic combustor.**

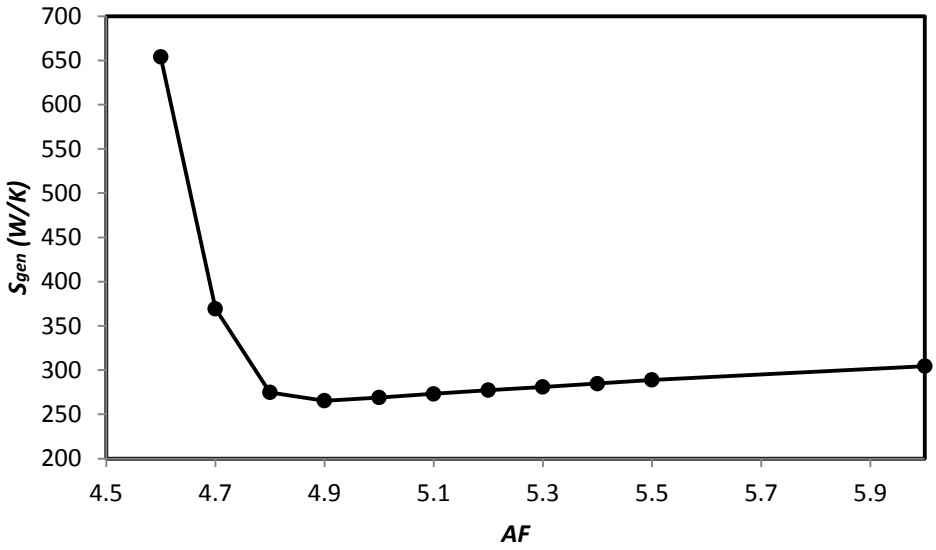


**Figure 4-7: Close-up of the entropy generation rate profile as a function of AF in an adiabatic combustor.**

UNIVERSITEIT VAN PRETORIA
UNIVERSITY OF PRETORIA
YUNIBESITHI YA PRETORIA



The computed values of the entropy generation rate due to the combustion process, frictional pressure drop, the overall entropy generation rate and the irreversibilities generated were also tabulated in Table 4-3 for all the plotted AF and corresponding equivalent ratios.

**Table 4-3: Computed values of the entropy generation rate and irreversibilities.**

| AF | Equivalent ratio | $\dot{S}_{gen(p)}$ (W/K) | $\dot{S}_{gen(h)}$ (W/K) | $\dot{S}_{gen}$ (W/K) | $\dot{I}$ (kW) |
|---|---|---|---|---|---|
| 4 | 2.005 | 0.237390033 | 3644.42 | 3644.66 | 1086.11 |
| 4.1 | 1.956098 | 0.240265992 | 2824.117687 | 2824.358 | 841.6587 |
| 4.2 | 1.909524 | 0.243068457 | 2036.776795 | 2037.02 | 607.0319 |
| 4.3 | 1.865116 | 0.245796486 | 1544.100364 | 1544.346 | 460.2152 |
| 4.4 | 1.822727 | 0.248450379 | 1242.88416 | 1243.133 | 370.4535 |
| 4.5 | 1.782222 | 0.251030896 | 916.5697472 | 916.8208 | 273.2126 |
| 4.6 | 1.743478 | 0.253537704 | 653.7978266 | 654.0514 | 194.9073 |
| 4.7 | 1.706383 | 0.25597112 | 369.1511782 | 369.4071 | 110.0833 |
| 4.8 | 1.670833 | 0.258330312 | 274.588215 | 274.8465 | 81.90427 |
| 4.9 | 1.636735 | 0.260615659 | 265.0651819 | 265.3258 | 79.06709 |
| 5 | 1.604 | 0.262827439 | 268.7854397 | 269.0483 | 80.17638 |
| 5.1 | 1.572549 | 0.264965702 | 272.828133 | 273.0931 | 81.38174 |
| 5.2 | 1.542308 | 0.26703045 | 277.0432976 | 277.3103 | 82.63848 |
| 5.3 | 1.513208 | 0.269021683 | 280.6182435 | 280.8873 | 83.70441 |
| 5.4 | 1.485185 | 0.270939401 | 284.5333752 | 284.8043 | 84.87169 |
| 5.5 | 1.458182 | 0.272783605 | 288.6333938 | 288.9062 | 86.09404 |
| 6 | 1.336667 | 0.280901916 | 304.1216374 | 304.4025 | 90.71196 |

| | | | | | |
|---|---|---|---|---|---|
| 6.5 | 1.233846 | 0.287182364 | 318.76 | 319.05 | 95.08 |
| 7 | 1.145714 | 0.291624947 | 332.9877197 | 333.2793 | 99.31724 |
| 7.5 | 1.069333 | 0.294229666 | 350.3486205 | 350.6429 | 104.4916 |
| 8.02 | 1 | 0.294988965 | 364.1874005 | 364.4824 | 108.6158 |
| 8.42 | 0.952494 | 0.294220374 | 371.7057442 | 372 | 110.856 |
| 8.82 | 0.909297 | 0.292275546 | 378.5330356 | 378.8253 | 112.8899 |
| 9.63 | 0.832814 | 0.284734689 | 390.9738209 | 391.2586 | 116.595 |
| 10.43 | 0.768936 | 0.27255259 | 403.2551109 | 403.5277 | 120.2512 |
| 11.23 | 0.714159 | 0.255665558 | 414.5166439 | 414.7723 | 123.6021 |
| 12.03 | 0.666667 | 0.234073594 | 424.663812 | 424.8979 | 126.6196 |

Figure 4-8 also shows the variation of entropy generation rate, but as a function of the equivalent ratio. An equivalent ratio of 1 means complete combustion with theoretical amount of air, whereas an equivalent ratio above 1 signifies a rich mixture. Figure 4-8 also shows that the entropy generation rate reaches a minimum at an equivalent ratio of 1.64 where incomplete combustion occurs. Both Figure 4-6 and Figure 4-8 show that when there is an increase in richness of the reactants mixture or deficiency in air, the entropy generation rate drops off gradually until minimum is reached. Then the entropy generation rate rises rapidly as the AF is decreased gradually.

UNIVERSITEIT VAN PRETORIA
UNIVERSITY OF PRETORIA
YUNIBESITHI YA PRETORIA



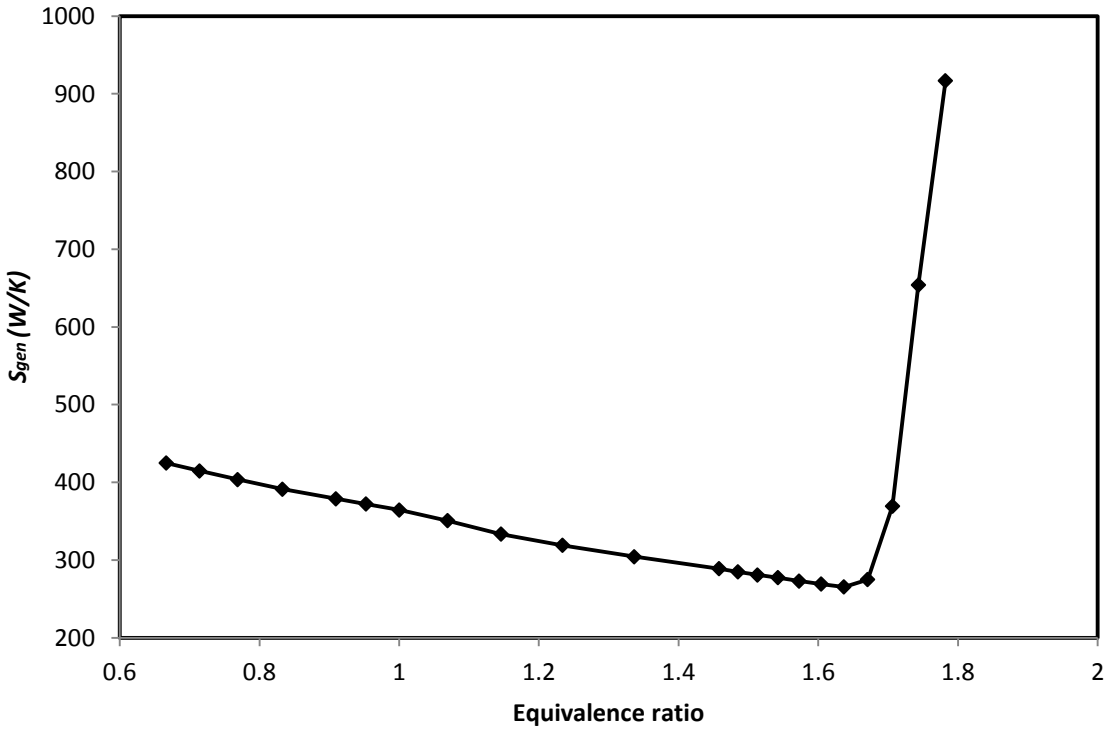


**Figure 4-8: Plot of entropy generation rate profile as a function of equivalent ratio in an adiabatic combustor.**

The entropy generation rate was normalised with respect to the value computed when combustion occurred with theoretical amount of air $N_R$, and this was plotted in Figure 4-9. Figure 4-9 shows that an AF of about 12 (which is a 50% excess air) resulted in a relative increase in entropy generation rate of 16.5%. However, an AF of 4.5 resulted in about 2.5 fold increase in entropy generation rate. Figure 4-9 also shows that at an AF of 4.7, entropy was generated at the same rate as when there was complete combustion with theoretical air ratio. Similarly, the relative entropy generation rate was plotted in Figure 4-10, but as a function of equivalent ratio.

Figure 4-9 and Figure 4-10 also show that the minimum entropy generation rate was about 73% of the value when combustion occurred with theoretical air ratio.

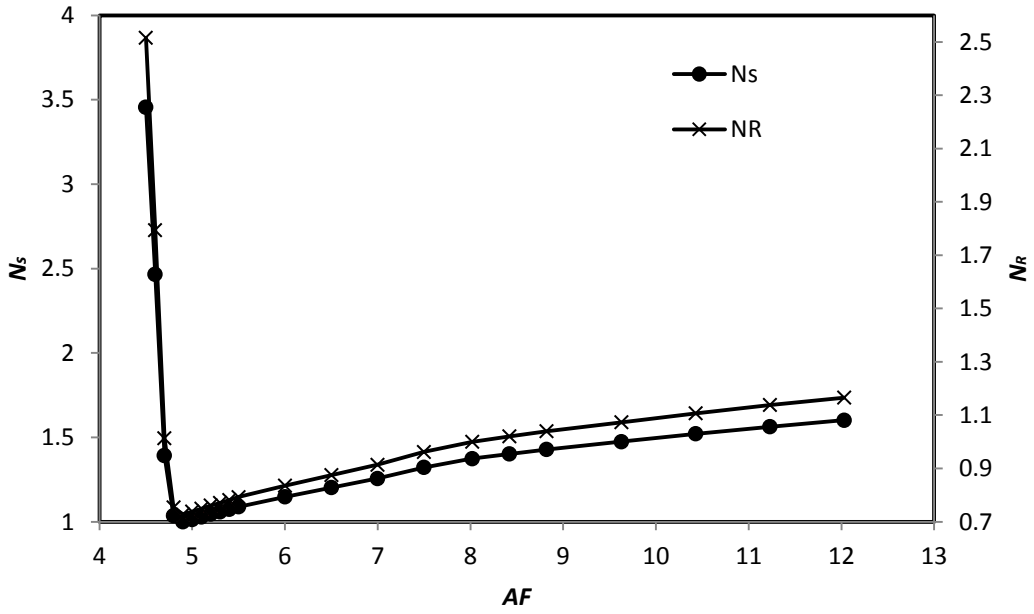


**Figure 4-9: Plot of entropy generation number and relative entropy generation rate as a function of AF in an adiabatic combustor.**

UNIVERSITEIT VAN PRETORIA
UNIVERSITY OF PRETORIA
YUNIBESITHI YA PRETORIA


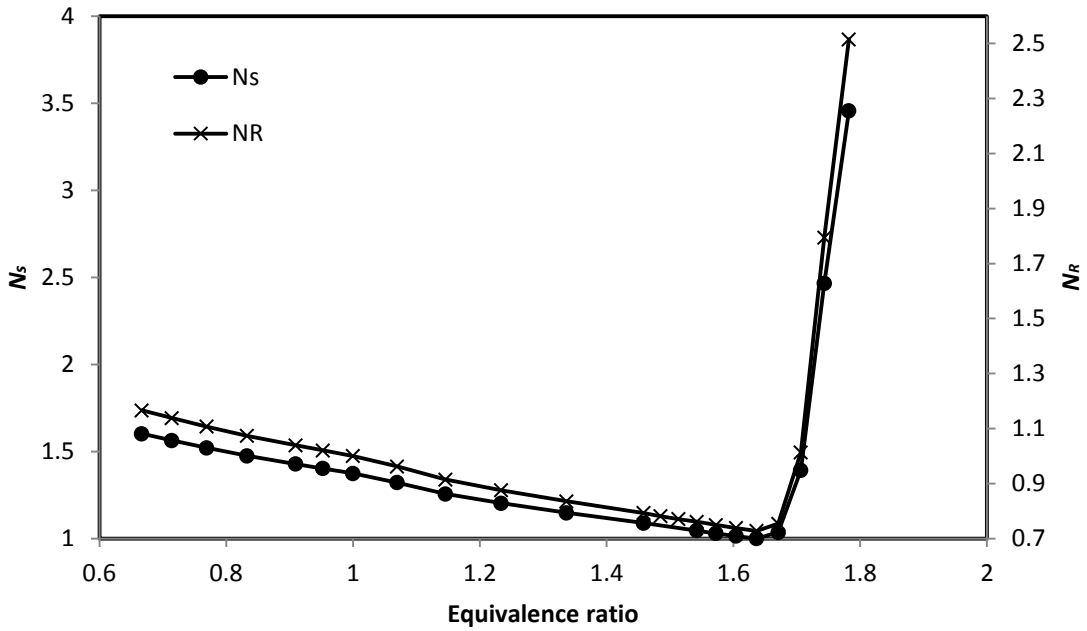


**Figure 4-10: Plot of entropy generation number and relative entropy generation rate as a function of equivalent ratio in an adiabatic combustor.**

However, the relative entropy generation rate was also computed with respect to the minimum value as an entropy generation number, $N_s$, and plotted in Figure 4-9. Figure 4-9 shows that the entropy generated when there was complete combustion with theoretical air ratio of 8.02 was about 37% more than the minimum rate. Combustion at an AF of 4.5 resulted in an entropy generation rate which was almost 3.5 times that of the minimum rate which occurred at an AF of 4.9. The entropy generation number was also plotted as a function of the equivalent ratio, as shown in Figure 4-10.

The temperature of the exiting combustion products mixture was plotted as a function of the AF, as shown by Figure 4-11. As expected, the highest temperature was achieved when combustion occurred with theoretical air ratio of 8.02, and it decreased as either a lean or rich mixture was combusted.

UNIVERSITEIT VAN PRETORIA
UNIVERSITY OF PRETORIA
YUNIBESITHI YA PRETORIA



The variation of molar fraction of combustion species was plotted as a function of the AF, as shown in Figure 4-12. The molar fraction for $N_2$ was not included in the plot because it was far bigger than the others, hence it would obscure the variations in the other molar fractions, and the fact that nitrogen was assumed to be inert to the combustion process. Figure 4-12 could hold a clue why the minimum entropy generation rate occurred at an AF of 4.9. It can be seen from the figure that at about an AF of 4.9, the molar fractions of $H_2$ and $H_2O$ are equal. This ratio also happened to be about the same point at which the molar fraction of $CO_2$ is at its lowest for a rich mixture. The other species are negligible in comparison. A consequent effect of this is that the combined contribution to total entropy generation rate from $H_2$, $H_2O$ and $CO_2$ is the lowest at an AF of 4.9 than at any other AF, because at an AF of 4.9, the molar fractions that are significant other than that of $N_2$ are those of $CO_2$, $H_2O$ and $H_2$, resulting in the lowest entropy generation rate occurring at an AF of 4.9. As mentioned in [73], the combustion model implemented in the CFD software of [32] over-predicts the presence of $O_2$. It was also mentioned in [73] that this had the effect of lowering the combustion products mixture temperature due to the presence of more species available to share in carrying the heat energy.

UNIVERSITEIT VAN PRETORIA
UNIVERSITY OF PRETORIA
YUNIBESITHI YA PRETORIA



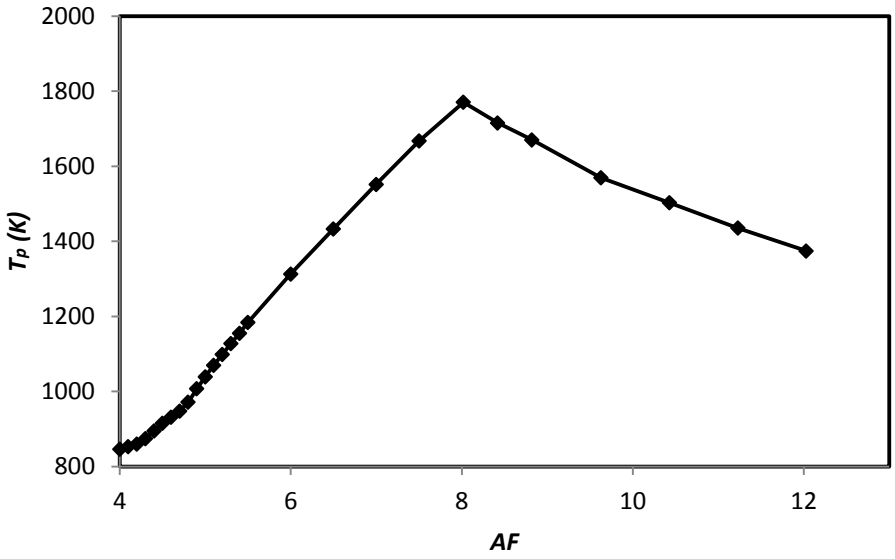


**Figure 4-11: Plot of combustion products mixture temperature as a function of AF in an adiabatic combustor.**

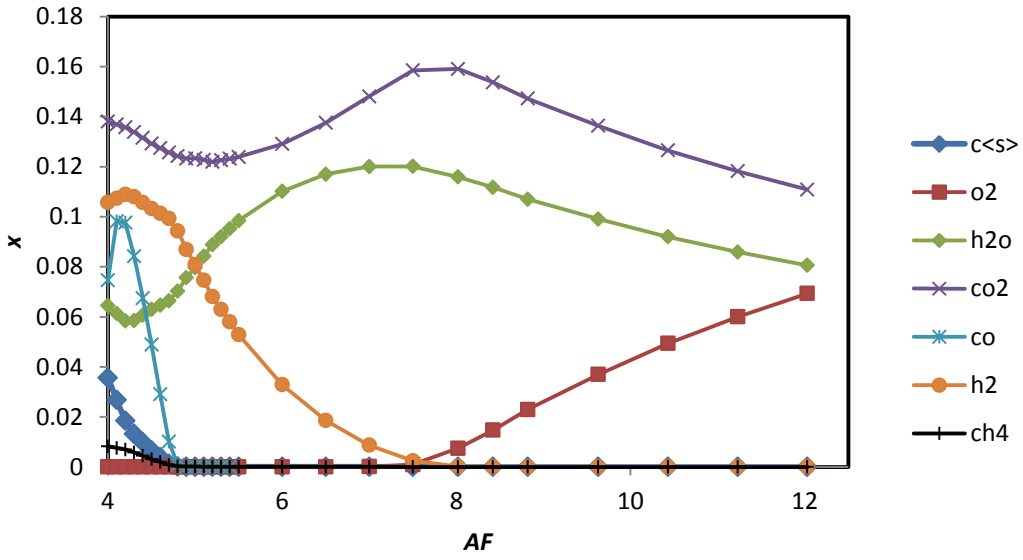


**Figure 4-12: Plot of variation with AF in molar fraction of combustion products species in an adiabatic combustor.**

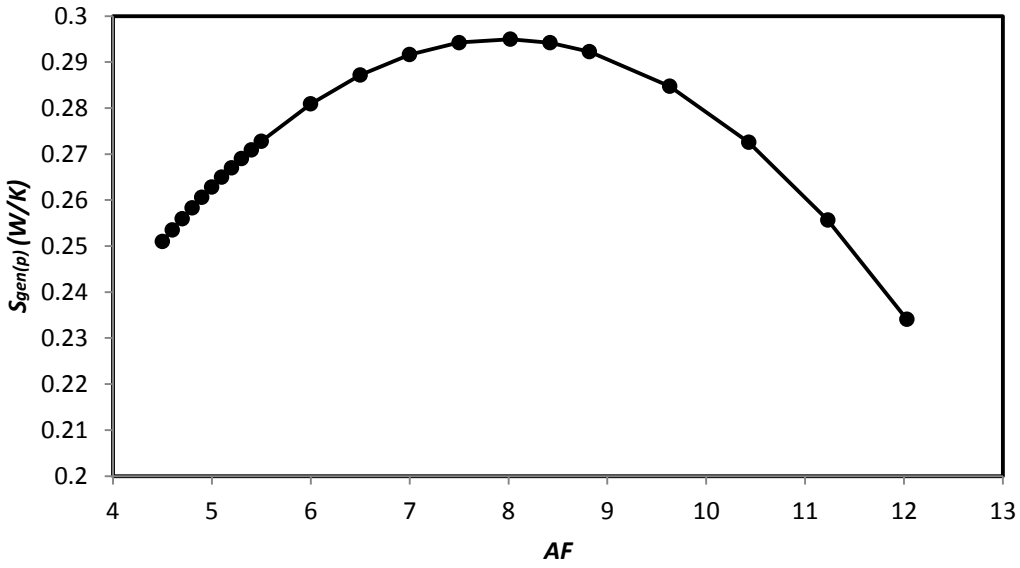


**Figure 4-13: Plot of entropy generation rate due to frictional pressure drop as a function of AF in an adiabatic combustor.**

As mentioned earlier, the entropy generation rate due to frictional pressure drop is negligible compared with that due to the combustion process. However, for the geometric configuration used in this study, the entropy generation rate due to combustion cannot tell if the flow process is physically possible or not. For this, the entropy generation rate was used due to frictional pressure drop to see where it became negative to know whether it would occur or not in the physical world. For the current geometric and flow configuration, Figure 4-13 shows that the flow process is physically possible because $\dot{S}_{gen(p)}$ is positive throughout the AF range under consideration. Because it is negligible in magnitude in comparison with the entropy generation rate due to combustion, the entropy generation rate due to frictional pressure drop was plotted on its own as a function of the AF, as shown in Figure 4-13. Whereas a minimum is observed for the overall entropy generation rate, Figure 4-13 predicts

UNIVERSITEIT VAN PRETORIA
UNIVERSITY OF PRETORIA
YUNIBESITHI YA PRETORIA



a maximum for the frictional pressure drop entropy generation rate. The maximum value occurred at an AF of about 8, which was almost an AF of 8.02, where complete combustion occurred with theoretical air ratio. Section plots of contours of temperature (in Kelvins) through the adiabatic combustor for the case with AF of 4.9 and 8.02 were plotted respectively in Figure 4-14 and Figure 4-15. From the two figures, it can be seen that the average adiabatic temperatures plotted in Figure 4-11 were arrived at by averaging over a temperature range at the outlet of the combustor.

UNIVERSITEIT VAN PRETORIA
UNIVERSITY OF PRETORIA
YUNIBESITHI YA PRETORIA



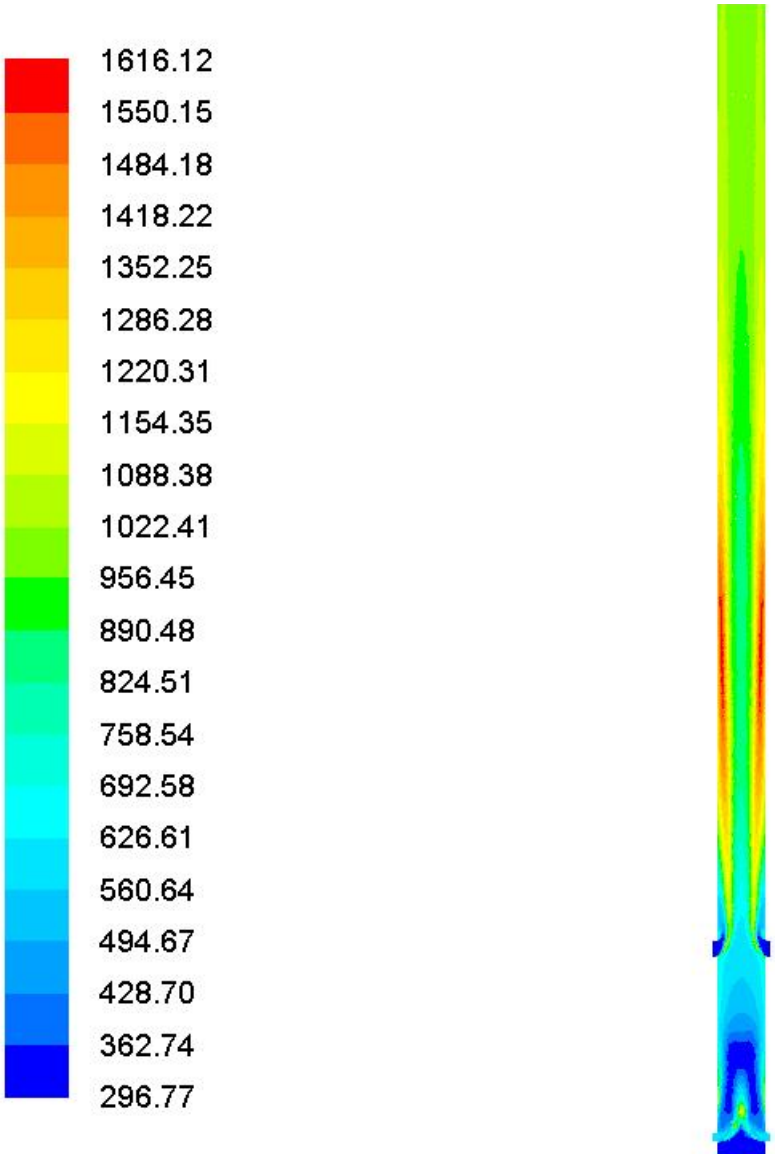


**Figure 4-14: Section plot of filled temperature contours (Kelvins) for the case with AF of 4.9.**

UNIVERSITEIT VAN PRETORIA
UNIVERSITY OF PRETORIA
YUNIBESITHI YA PRETORIA



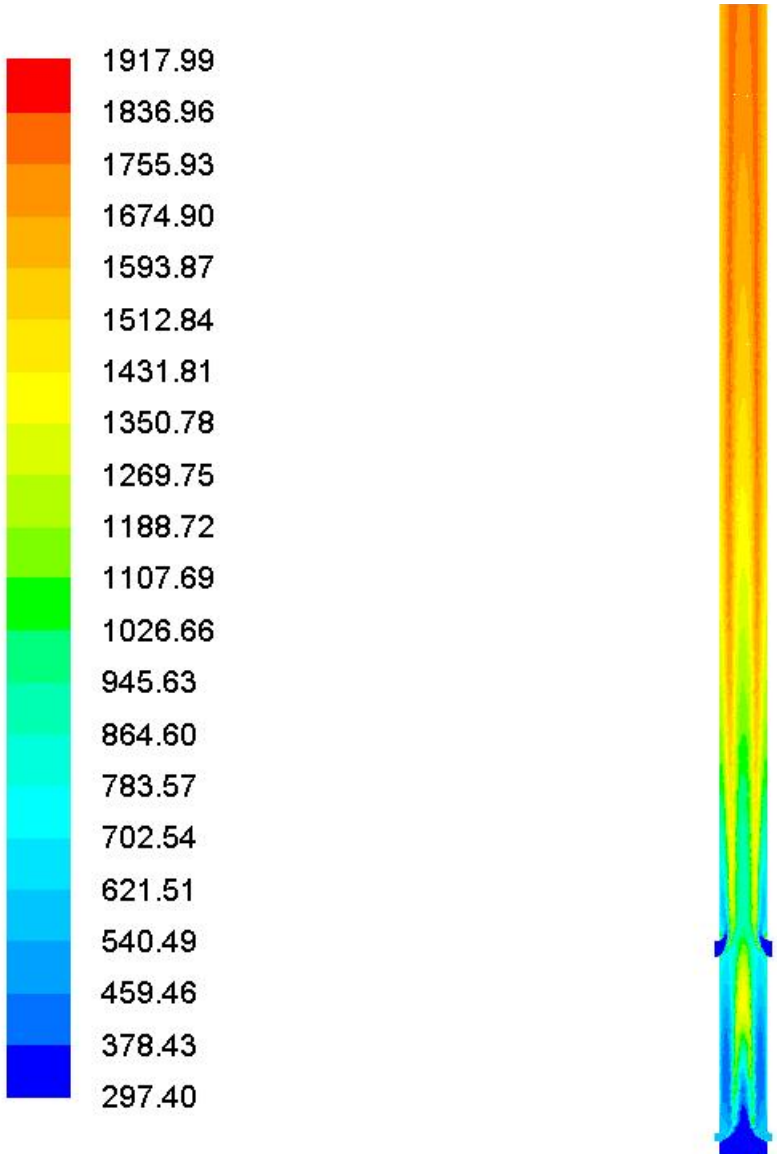


**Figure 4-15: Section plot of filled temperature contours (Kelvins) for the case with AF of 8.02.**

## 4.5. CONCLUSION

The entropy generation rates due to the combustion and frictional pressure drop processes were analysed in order to calculate the irreversibilities generated in the adiabatic combustor. It was found that the entropy generation rate due to frictional pressure drop was negligible

when compared with that due to combustion. The analysis of the irreversibilities generated during the combustion process of an adiabatic combustor with a fixed geometry was conducted and it was found that a minimum was reached when the air-fuel mass ratio was 4.9. At about this air-fuel mass ratio, the molecular hydrogen and water vapour were at equal amounts of molar fraction and the carbon dioxide molar fraction was at its minimum for a rich mixture. This resulted in the combined contribution from $H_2$, $H_2O$ and $CO_2$ to the entropy generation rate being the lowest at an AF of 4.9 than at any other AF; hence a minimum entropy generation rate because they had the most significant molar fractions other than $N_2$.

UNIVERSITEIT VAN PRETORIA
UNIVERSITY OF PRETORIA
YUNIBESITHI YA PRETORIA



# Chapter 5. THERMODYNAMIC OPTIMISATION OF A WOOD-FIRED COMBUSTOR: THE INFLUENCE OF WALL HEAT FLUX, WALL THICKNESS AND AIR INLET TEMPERATURE

## 5.1. INTRODUCTION

The focus of the world is the reduction of greenhouse gases such as carbon dioxide. Because most of the carbon dioxide emitted into the atmosphere is from fossil fuel combustion, alternative energy sources were developed and others are currently under study to see whether they will be good alternatives. One of these alternative sources of energy is the combustion of wood in place of coal. However, wood has lower calorific heat rates than coal, hence the investigation of better conditions under which to run combustion chambers burning wood is paramount if wood is to make a good alternative source of energy. The effect of changing the wall conditions from adiabatic to heat loss was numerically analysed by Hua et al. [36] when they investigated combustion chambers burning a hydrogen-air mixture as they varied from millimetre to micro-scale size, in which they found that the heat loss had the effect of quenching, even extinguishing, the combustion process inside the chamber as the chamber narrowed. The micro-combustor investigated by [36] was optimised by [83] to arrive at the best equivalent ratio to operate the combustor. Norton and Vlachos [37] found two modes of flame blowout, one due to thick wall thermal conductivities and another due to low flow velocities when they numerically studied the effects of wall thickness and flow velocities on the combustion characteristics and flame stability in a premixed methane-air mixture micro-burner. Louis et al. [8] discovered that it was important to include the mixing,

combustion and heat loss in a non-adiabatic model of an air-cooled syngas combustion chamber if the NO formation in flames with heat loss was to be predicted accurately. The stainless steel micro-tube burning a methane-oxygen mixture was found by [9] to have heat loss due to radiation of about 70% of the total heat loss. For a small tube with an axial temperature gradient at the wall burning an air-methane mixture, Feng et al. [38] found through their numerical studies that the higher the wall temperature, the more stable the flame that can be realised for a given tube size. Ziviani et al. [94] numerically modelled an organic Rankine cycle (ORC) system using available literature, aimed at exploiting low temperature energy sources. They found that their model provided a robust and powerful tool to describe in detail the components making up the ORC system. Toffolo et al. [95] optimised ORC systems that used low to medium temperature heat sources running on isobutene and R134a in the temperature interval between 130 and 180 °C. They found the maximum power output was for a system running on R134a for all temperatures considered. Zhang et al. [96] used a heat recovery steam generator (HRSG) to enhance the energy efficiency of a polygeneration plant. By optimising the HRSG, using the mixed-integer non-linear programming approach, they found that the optimum depended on the HRSG type and model specification. Li, Wang and Ding [97] developed a methodology to design large-scale gas liquefaction using genetic algorithm and exergy efficiency analysis. They found that the optimum design resulted in a maximum exergy efficiency of 52% if the liquefaction process was for hydrogen and 58% for methane and nitrogen. Lian et al. [98] analysed the thermoeconomic potential of biomass-fired steam-turbine plant used for trigeneration by looking at its exergy. They found about 60% of the exergy destruction occurred in the furnace and the component with the second-most exergy destruction of between 11% and 16% was the steam drum. Qian et al. [99]

UNIVERSITEIT VAN PRETORIA
UNIVERSITY OF PRETORIA
YUNIBESITHI YA PRETORIA


conducted a thermoeconomic analysis of a polygeneration plant that produced chemical products such as propylene and ethylene and electricity by using the internal rate of return (IRR) and exergy efficiency. The polygeneration system was found to have an IRR and an exergy efficiency which were higher by 18.9% and 49.9% respectively when compared with a natural gas methanol to olefin system. Blanco-Marigorta et al. [100] conducted an exergy analysis on a biodiesel production process from Jatropha curca oil in which they found that 95% of the exergy destruction occurred in the transesterification reactor, and the exergy efficiency of the overall process was 63%. Kohl et al. [101] analysed the exergetic and economic performance of three biomass upgrading processes where three fuels, namely wood pellets, torrefied wood pellets and a mixture of pyrolysis char and oil, were put through a pyrolysis process. They found that most of the exergy destruction occurred in the combustion equipment, but the exegetic efficiencies for the three fuels were improved by 22%, 26% and 31% for the mixture of pyrolysis char and oil, torrefied wood pellets and wood pellets respectively. However, the economic performance was best for the mixture of pyrolysis char and oil. Li et al. [102] analysed the exergy performance of three coals to synthetic natural gas and power cogeneration systems with or without carbon dioxide capture. They found the system with carbon dioxide capture had more exergy loss than the system without, and the cogeneration systems had lower exergy input requirements when compared with the single product systems. McTigue et al. [103] did a thermodynamic analysis of a pumped thermal electric storage system, which consisted of hot and cold packed bed thermal stores. They conducted parametric studies and optimised the system such that as long as the efficiencies of the compression and expansion processes of the reciprocating devices were maintained after optimisation, high energy storage densities close to 200 $MJm^{-3}$ comparable with pumped

UNIVERSITEIT VAN PRETORIA
UNIVERSITY OF PRETORIA
YUNIBESITHI YA PRETORIA


hydroschemes could be attained. Arjmandi and Amani [104] numerically investigated and compared two methods of computing the entropy generated in a combustion chamber; the first of which was based on the overall entropy balance of the system and the second based on the local entropy generation rate. They found that the two methods predicted the total entropy generated, which was 6.4% different from each other. They also found that combustion and heat transfer accounted for most of the total entropy generation. Exergy efficiency of turboprop engine components was dynamically modelled by Baklacoiglu et al. [105] by using a hybrid model of genetic algorithm-artificial neural networks on dynamic variables of power, torque, fuel flow, gas generator speed and engine mass air flow. They found that the model they developed improved the accuracy greatly when compared with a trial-and-error case as measured by their reference data. Blanco-Marigorta et al. [106] conducted an exergy analysis of the components of a reverse osmosis desalination plant in the pursuit of improving the environmental impact of the plant. They found that the first-stage reverse osmosis membrane module and the high pressure pump were responsible for most of the exergy destruction of the plant, and that these two components were also responsible for most of the negative environmental impact of the plant. Safari et al. [107] used a large eddy simulation that incorporated the entropy transport equation to analyse entropy generation in a turbulent non-premixed flame. They found chemical reaction and heat conduction were the main sources of irreversiblities in the flame. Nguyen et al. [108] conducted a thermodynamic evaluation of oil and gas platforms to find system efficiencies over the life cycle of the platforms. They found about 50% of the inefficiencies were due to chemical exergy inefficiencies, 20% due to thermal exergy inefficiencies and 15% due to mechanical exergy efficiencies. Ramakrishnan and Edwards [109] and Ramakrishnan and Edwards [110]

UNIVERSITEIT VAN PRETORIA
UNIVERSITY OF PRETORIA
YUNIBESITHI YA PRETORIA


developed and employed a method they called attractor trajectory optimisation, which used chemical equilibrium attractor states in the thermodynamic state space, on steady flow combustion engines. They asserted that their method allowed for optimisation of the engine cycle and the cycle parameters all at once as physics permitted. And because the resultant optimised engine cycle burnt the fuel by splitting into the adiabatic segment and the isothermal segment, it was more efficient than a traditional Brayton cycle, which used adiabatic combustion or a fully reheat cycle, which used isothermal combustion. Hagi et al. [111] conducted an exergy analysis on oxy-fire pulverised coal power plants in the pursuit of minimising the exergy losses while taking into account the technological and operational constraints. The plants looked at were the conventional cold flue gas recycle scheme and three alternative flue gas recirculation schemes. They found that the alternative scheme with recirculation of the flue gas before the regenerative heat with advanced air separation unit and a double column compression and purification unit had the highest net plant efficiency. Feng et al. [112] optimised the exergy efficiency and the heat exchanger area per unit net power output of a regenerative organic Rankine cycle as compared with a basic organic Rankine cycle. They found that the regenerative organic Rankine cycle had an exergy efficiency of 8.1% higher and the heat exchanger area per unit net power output 15.9% lower than those of a basic organic Rankine cycle. Tapasvi et al. [113] numerically studied the torrefication of wood by gasification through minimising the Gibbs free energy of the product gases that resulted in chemical equilibrium in the gasification process. They found that the torrefied wood had improved energy and exergy efficiencies when compared with untreated wood. Li et al. [114] developed a theoretical framework for the exergy analysis of a biomass boiler by conducting sensitivity studies of several design parameters such as excess air, steam

parameters and biomass moisture. They found that most of the exergy destruction occurred in the combustion process, followed by water walls and radiation superheater, and then the low temperature superheater.

The technique of analysing and minimising the entropy generation rate of a process was demonstrated with good effect in studies by [84-87]. In furtherance of the work done in Baloyi et al. [84] and Baloyi et al. [88], in this study, the effects, firstly, of changing the incoming air temperature in an adiabatic circulating fluidised bed combustor from 298 K to 400 K on the air-fuel mass ratio value at which minimum irreversibilities were generated were investigated. Secondly, the effect of changing the wall condition on a circulating fluidised bed combustor from adiabatic to negative heat flux (that is heat leaving the system) on the air-fuel mass ratio value at which minimum irreversibilities were generated was also investigated. Because the sum of the molar fractions of the combustion products species must add up to one, when the molar fraction of one of the species increases, the molar fractions of the other species will either increase or decrease to result in a sum of one. With this fact in mind, the link between the change in optimum air-fuel mass ratio and the balance between the molar fractions of the combustion products species were also investigated. The third part of the study was analysing the effect of a change in combustor diameter and wall thickness on irreversibilities in a combustor with a negative wall heat flux.

## 5.2. Thermodynamic model

### 5.2.1. Exergy analysis

The irreversibility generation rate that results from the combustion heat transfer and frictional pressure drop processes taking place in a combustor is defined by Eq. (5-1) [1-3]. As in [84], the different states of complete/incomplete combustion were attained by changing the mass

UNIVERSITEIT VAN PRETORIA
UNIVERSITY OF PRETORIA
YUNIBESITHI YA PRETORIA


flow rate of the incoming oxidising air, thereby varying the air-fuel mass ratio (AF). The chemical formula of the solid fuel as computed in [88] was given by $C_{4.9}H_{7.2}O_2$, the lower heating value of the fuel from [88] was given as 16 091.2 kJ/kg and the molecular weight of the fuel was calculated as 98 kg/kmol. The specific heat at constant pressure was also given as 1.680 kJ/kg.K.

$$\dot{I} = T_{ref}\dot{S}_{gen} \quad \textbf{(5-1)}$$

where $\dot{S}_{gen}$ is the entropy generation rate.

The study was conducted in three parts. The first part of the study focused on comparing two adiabatic combustors burning pitch pine wood, one with incoming air temperature of 298 K (Case 2 as listed in Table 5-1) as investigated in [84], and the second one for incoming air temperature of 400 K (Case 1 as listed in Table 5-1), as investigated in [88]. The second part of the study focused on comparing the combustor with an adiabatic wall condition and incoming air temperature of 400 K (Case 1) with a combustor with a negative heat flux wall condition (Case 3 as listed in Table 5-1), also with an incoming air temperature of 400 K.

**Table 5-1: Description of the three cases.**

| | |
|---|---|
| Case 1 | Combustor with adiabatic wall condition and incoming air temperature at 400 K |
| Case 2 | Combustor with adiabatic wall condition and incoming air temperature at 298 K |
| Case 3 | Combustor with -7500 W/m$^2$ wall condition and incoming air temperature at 400 K |

### 5.2.2. Adiabatic combustor

For an adiabatic combustor (as shown in Figure 5-1), the entropy generation rate is constituted by the frictional pressure drop and combustion heat transfer terms [4].

UNIVERSITEIT VAN PRETORIA
UNIVERSITY OF PRETORIA
YUNIBESITHI YA PRETORIA


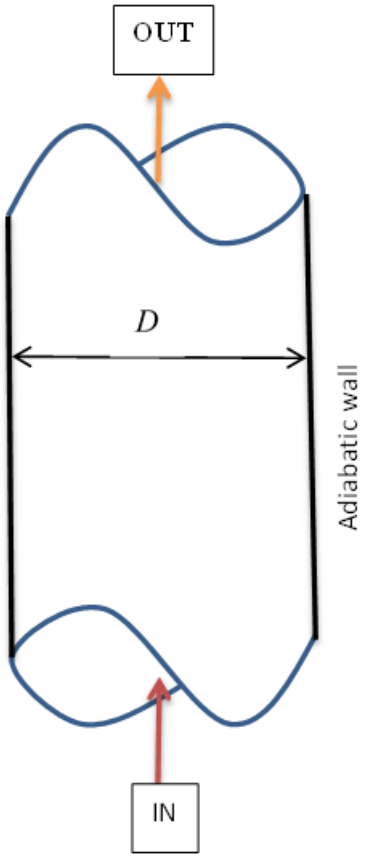


**Figure 5-1: Schematic of a section of an adiabatic combustor.**

The frictional pressure drop term, due to the air-fuel mixture as it flows through the riser [28], was derived in [84] and is given by Eq. (5-2):

$$\dot{S}_{gen(p)} = \frac{\dot{m}_f (AF+1)(\rho_f - \rho_g) g \left[ \frac{(\varepsilon_{sd} - \varepsilon_{se})(1-\varepsilon_{sd})\dot{m}_f AF}{10\rho_g A} + H_t \varepsilon_{sd} + \ln\left( \frac{\varepsilon_{se} - \varepsilon_s^*}{\varepsilon_{sd} - \varepsilon_s^*} \right) \left( \frac{\varepsilon_{sd} - \varepsilon_s^*}{10\rho_g A} \right) (1-\varepsilon_{sd})\dot{m}_f AF \right]}{(\varepsilon_{se}\rho_f + (1-\varepsilon_{se})\rho_g) T_m} \quad \textbf{(5-2)}$$

$\Delta P$ is the pressure drop across the combustor, $\dot{m}_f$ is the fuel mass flow rate, $\rho_m$ is the mixture density, $T_m$ is the mixture temperature, $\varepsilon_{mf}$ is the minimum fluidisation solid volume fraction, $\rho_f$ is the char density, $\rho_g$ is the gaseous density, $\varepsilon_{sd}$ is the solid volume fraction in the bed region of the riser, $\varepsilon_{se}$ is the solid volume fraction at the exit of the riser, $H_t$ is the total height

UNIVERSITEIT VAN PRETORIA
UNIVERSITY OF PRETORIA
YUNIBESITHI YA PRETORIA


of the riser, $A$ is the combustor cross-sectional area and $\varepsilon_s^*$ is the minimum value that $\varepsilon_{se}$ can be assumed.

The combustion heat transfer term, due to combustion and/or heat transfer processes, was also derived in [84] and is given by Eq. (5-3):

$$\dot{S}_{gen(h)} = \frac{\dot{m}_f}{M_f}\left(\begin{array}{l}\sum_{j=1}^{l} n_{pj}\left(\bar{s}^\circ - \bar{R}\ln(x)\right)_{Pj} - \sum_{j=1}^{m} n_{rj}\left(\bar{s}^\circ - \bar{R}\ln(x)\right)_{rj} + \frac{\rho_{char}}{\rho_g} n_{char} c_{char} M_{char} \ln\left(T_{char}/298\right) \\ -\frac{\rho_f}{\rho_g} n_f c_f M_f \ln\left(T_f/298\right)\end{array}\right) \quad \textbf{(5-3)}$$

where $c_{char}$ is the specific heat constant for the char particles and $c_f$ is the specific heat constant for the solid fuel. The specific entropy is given by Eq. (5-4):

$$\bar{s}_{pi} = \bar{s}^\circ_{pi}(T) - \bar{R}\ln(Px_{pi}/P_{ref}) \quad \textbf{(5-4)}$$

The static pressure in the combustor is the same as the reference static pressure, i.e. $P = P_{ref}$, and the molar fraction of each product species, $x_{pi}$, is given by Eq. (5-5):

$$x_{pi} = n_{pi}\Big/\sum_{i=1}^{l} n_{pi} \quad \textbf{(5-5)}$$

$n_{pi}$ is the stoichiometric coefficient of combustion product species *i*. The same expressions apply for reactants. $\bar{h}$ is the specific enthalpy, $\bar{s}^\circ_{pi}$ is the absolute entropy, $\bar{R}$ is the universal gas constant, $p$ is the static pressure, $P_{ref}$ is the reference static pressure of the environment and $T_{ref}$ is the reference temperature of the environment. The specific entropy of the solid fuel was computed by defining [33], as given by Eq. (5-6):

$$\bar{s} = \bar{c}\ln\left(T_f/298\right) \quad \textbf{(5-6)}$$

$\bar{c}$ is the molar specific heat of the solid fuel.

UNIVERSITEIT VAN PRETORIA
UNIVERSITY OF PRETORIA
YUNIBESITHI YA PRETORIA


### 5.2.3. Combustor with heat flux wall condition and an infinitely thin wall

A negative wall heat flux of 7 500 W/m$^2$ was applied over the wall of the combustor cases with AF varying from 4.5 to 10 for an air inlet temperature of 400 K, as shown in Figure 5-2. The selected range of AF corresponds to mixture varying from a rich mixture to a lean mixture.

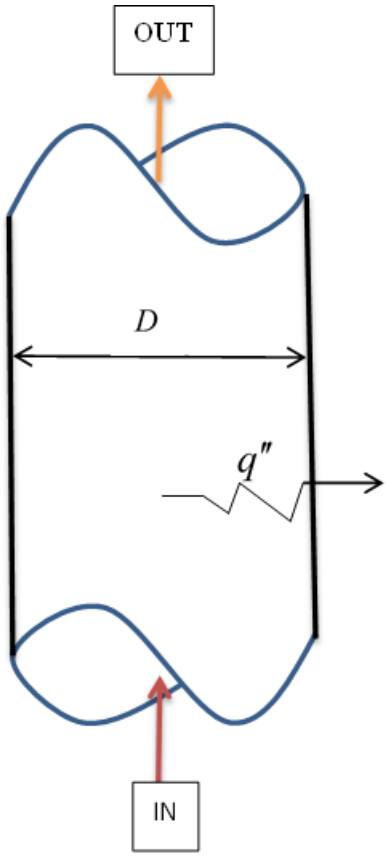


**Figure 5-2: Sketch of a combustor section with negative heat flux wall condition and zero wall thickness.**

The analysis of the entropy generation rate is the same as that of [84] except that there is an additional term due to heat transfer [4] through the wall of the combustor, and this term is expressed by Eq. (5-7):

$$\dot{S}_{gen(h-t)} = -\frac{2\pi LDq''}{T_m + \Delta T} \qquad \textbf{(5-7)}$$

where $L$ is the length of the combustor, $D$ is the diameter of the combustor, $q''$ is the wall heat flux and $\Delta T$ is the change in temperature across the length of the combustor. The only term that is unknown in Eq. (5-7) is $\Delta T$, which can be described by Eq. (5-8):

$$\Delta T = \frac{q''}{c_p G St} \tag{5-8}$$

where $G = \dot{m}_f (AF + 1)/A$ is the mixture mass flux and $St = Nu/(\mathrm{Re}_D \mathrm{Pr})$ is the Stanton number. The Prandtl number $\mathrm{Pr}$ is assumed to be 0.69 [89] for the gas species mixture involved in the combustion process and $\mathrm{Re}_D$ is the Reynolds number based on the combustor diameter. The Nusselt number [4] is given by Eq. (5-9), assuming fully turbulent internal flow.

$$Nu = 0.023 \mathrm{Re}_D^{0.8} \mathrm{Pr}^{0.4} \tag{5-9}$$

Substituting Eq. (5-10) into Eq. (5-9) and taking all the above into consideration, Eq. (5-10) becomes:

$$\Delta T = \frac{\pi D^2 q''}{0.1148 c_p \dot{m}_f (AF + 1) \mathrm{Re}_D^{-0.2}} \tag{5-10}$$

Substituting Eq. (5-10) into Eq. (5-7) results in:

$$\dot{S}_{gen(h-t)} = -\frac{0.2296 \pi L D c_p \dot{m}_f (AF + 1) q'' \mathrm{Re}_D^{-0.2}}{0.1148 c_p \dot{m}_f (AF + 1) T_m \mathrm{Re}_D^{-0.2} + \pi D^2 q''} \tag{5-11}$$

When Eq. (5-11) is added to Eq. (5-3), what results is an equation that describes the entropy generation rate due to combustion and heat transfer through a wall for the combustor with a heat flux wall condition, as expressed by Eq. (5-12):

UNIVERSITEIT VAN PRETORIA
UNIVERSITY OF PRETORIA
YUNIBESITHI YA PRETORIA



$$\dot{S}_{gen} = \frac{\dot{m}_f}{M_f}\left(\begin{array}{l}\sum_{j=1}^{l} n_{pj}\left(\bar{s}^\circ - \bar{R}\ln(x)\right)_{Pj} - \sum_{j=1}^{m} n_{rj}\left(\bar{s}^\circ - \bar{R}\ln(x)\right)_{rj} + \frac{\rho_{char}}{\rho_g} n_{char} c_{char} M_{char} \ln\left(T_{char}/298\right) \\ -\frac{\rho_f}{\rho_g} n_f c_f M_f \ln\left(T_f/298\right)\end{array}\right)$$
$$-\frac{0.2296\pi L D c_p \dot{m}_f (AF+1) q'' \mathrm{Re}_D^{-0.2}}{0.1148 c_p \dot{m}_f (AF+1) T_m \mathrm{Re}_D^{-0.2} + \pi D^2 q''} \quad \textbf{(5-12)}$$

where the Reynolds number is expressed by Eq. (5-13):

$$\mathrm{Re}_D = \frac{4\dot{m}_f (AF+1)}{\pi \mu_m D} \quad \textbf{(5-13)}$$

where $\mu_m$ is the mixture dynamic viscosity.

When taking all the terms that constitute the entropy generation rate into account by adding Eq. (5-12) to Eq. (5-2), the total entropy generation rate is expressed by Eq. (5-14):

$$\dot{S}_{gen} = B_1\left[\frac{X_1}{\pi D^2} + B_3 + \frac{4X_2}{\pi D^2}\right] + B_4$$
$$-\frac{X_3 D \mathrm{Re}_D^{-0.2}}{B_6 \mathrm{Re}_D^{-0.2} + X_4 D^2} \quad \textbf{(5-14)}$$

where

$$B_1 = \frac{\dot{m}_f (AF+1)(\rho_f - \rho_g) g}{\left[\varepsilon_{se}\rho_f + (1-\varepsilon_{se})\rho_g\right] T_m} \quad \textbf{(5-15)}$$

$$B_3 = H_t \varepsilon_{sd} \quad \textbf{(5-16)}$$

$$B_4 = \dot{S}_{gen(h)} =$$
$$\frac{\dot{m}_f}{M_f}\left(\begin{array}{l}\sum_{j=1}^{l} n_{pj}\left(\bar{s}^\circ - \bar{R}\ln(x)\right)_{Pj} \\ -\sum_{j=1}^{m} n_{rj}\left(\bar{s}^\circ - \bar{R}\ln(x)\right)_{rj} \\ +\frac{\rho_{char}}{\rho_g} n_{char} c_{char} M_{char} \ln\left(T_{char}/298\right) \\ -\frac{\rho_f}{\rho_g} n_f c_f M_f \ln\left(T_f/298\right)\end{array}\right) \quad \textbf{(5- 17)}$$

$$B_6 = 0.1148 c_p \dot{m}_f (AF+1) T_m \quad \textbf{(5-18)}$$

UNIVERSITEIT VAN PRETORIA
UNIVERSITY OF PRETORIA
YUNIBESITHI YA PRETORIA



$$X_1 = \frac{(\varepsilon_{sd} - \varepsilon_{se})(1-\varepsilon_{sd})\dot{m}_f AF}{10\rho_g} \quad \textbf{(5-19)}$$

$$X_2 = \frac{\dot{m}_f AF}{10\rho_g} \ln\left(\frac{\varepsilon_{se} - \varepsilon_s^*}{\varepsilon_{sd} - \varepsilon_s^*}\right)(\varepsilon_{sd} - \varepsilon_s^*)(1-\varepsilon_{sd}) \quad \textbf{(5-20)}$$

$$X_3 = 0.2296\pi L c_p \dot{m}_f (AF+1) q'' \quad \textbf{(5-21)}$$

$$X_4 = \pi q'' \quad \textbf{(5-22)}$$

The entropy generation rate in Eq. (5-14) can be expressed as a function of Reynolds number, as given by Eq. (5-23):

$$\dot{S}_{gen} = \left[\frac{\pi B_1 X_1 \mu^2}{4\dot{m}_f^2 (AF+1)^2} + \frac{\pi B_1 X_2 \mu^2}{4\dot{m}_f^2 (AF+1)^2}\right] \mathrm{Re}_D^2 + B_1 B_3 + B_4 - \frac{4\pi\mu X_3 \dot{m}_f (AF+1)\mathrm{Re}_D^{0.8}}{\pi^2 \mu^2 B_6 \mathrm{Re}_D^{1.8} + 16 X_4 \dot{m}_f^2 (AF+1)^2} \quad \textbf{(5-23)}$$

The entropy generation number, $N_s$ [84], which is the quotient of the entropy generation rate at any Reynolds number and the minimum entropy generation rate, was used to analyse the penalty paid by running the combustor at a Reynolds number other than the optimum and is given by Eq. (5-24):

$$N_s = \frac{\dot{S}_{gen}}{\dot{S}_{gen,\min}} \quad \textbf{(5-24)}$$

The relative generation rate, $N_R$ [84], which is the quotient of the entropy generation rate at any equivalence ratio, and the entropy generation rate when combustion occurred with theoretical air ratio, is expressed by Eq. (5-25):

$$N_R = \frac{\dot{S}_{gen}}{\dot{S}_{gen,th}} \quad \textbf{(5-25)}$$

### 5.2.4. Combustor with heat flux wall condition and varying wall thickness

The third part of the study was to analyse the effect of a change in combustor diameter and wall thickness on irreversibilities in a combustor with a negative wall heat flux. When the

UNIVERSITEIT VAN PRETORIA
UNIVERSITY OF PRETORIA
YUNIBESITHI YA PRETORIA


thickness, $t$, of the combustor is taken into account (as shown in Figure 5-3), the heat flux through the inner wall can be related to the heat flux through the outer wall, as given by Eq. (5-26):

$$q'' = q_o''\left(\frac{2t}{D}+1\right) \tag{5-26}$$

Substituting Eq. (5-26) and Eq. (5-13) into Eq. (5-23) and eliminating $D$ result in an expression given by Eq. (5-27):

$$\dot{S}_{gen} = \left[\frac{\pi B_1 X_1 \mu^2}{4\dot{m}_f^2 (AF+1)^2} + \frac{\pi B_1 X_2 \mu^2}{4\dot{m}_f^2 (AF+1)^2}\right] \mathrm{Re}_D^2 + B_1 B_3 + B_4 - \frac{4\pi\mu X_5 \dot{m}_f (AF+1)\mathrm{Re}_D^{0.8}}{\pi^2 \mu^2 B_6 \mathrm{Re}_D^{1.8} + 4\pi\dot{m}_f (AF+1) q_o''\left[2\pi\mu_m t\,\mathrm{Re}_D + 4\dot{m}_f (AF+1)\right]} \tag{5-27}$$

where:

$$X_5 = 0.2296\pi L c_p \dot{m}_f (AF+1) q_o'' \tag{5-28}$$

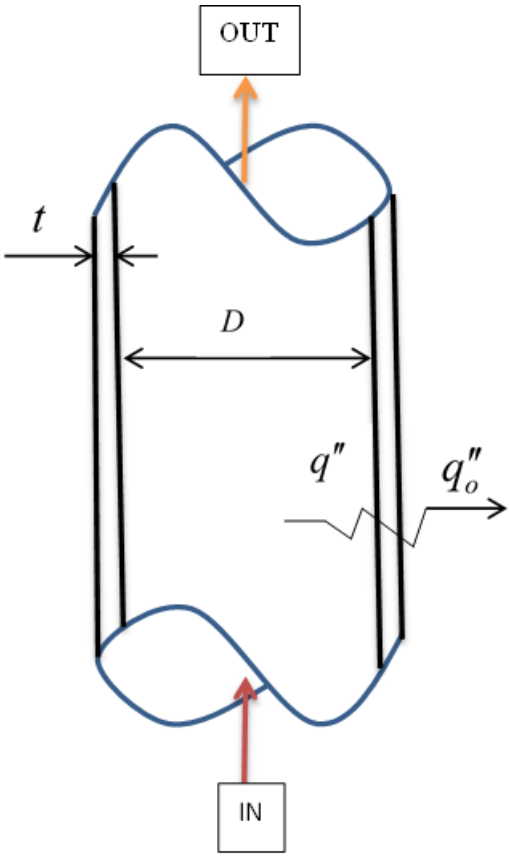

UNIVERSITEIT VAN PRETORIA
UNIVERSITY OF PRETORIA
YUNIBESITHI YA PRETORIA



**Figure 5-3: Sketch of a combustor section with negative heat flux wall condition and arbitrary wall thickness.**

### 5.3. Numerical model

ANSYS FLUENT 16.2 [93] was used to simulate the combustion process inside the combustor. The combustion process was modelled using the non-premixed combustion model that was implemented by using the mixture fraction theory. This combustion model was chosen because the solid fuel was only specified in the form of ultimate analysis data [67], as given in Table 5-2, and the combustion model gave an option of specifying the fuel as an empirical stream. The inlet diffusion option was selected.

**Table 5-2: Pitch pine ultimate analysis data (adapted from [67]).**

| Element | Value |
|---|---|
| C | 59.0 (%) |
| H | 7.2 (%) |
| O | 32.7 (%) |
| Ash | 1.13 (%) |
| HHV | 24220 (kJ/kg) |
| LHV | 16091.2 (kJ/kg) |
| Molecular weight | 98 (kg/kmol) |

The continuity equations for continuous phase (Eq. (5-29)), dispersed phase (Eq. (5-30) and Eq. (5-31)) and momentum equation [93], as expressed by Eq. (5-32), were solved for under steady-state condition.

$$\nabla \cdot \left(\rho \vec{v}\right) = -s_m \quad \textbf{(5-29)}$$

$$\nabla \cdot \left(\rho \vec{v} \overline{f}\right) = \nabla \cdot \left(\frac{\mu_t}{\sigma_t} \nabla \overline{f}\right) + s_m \quad \textbf{(5-30)}$$

UNIVERSITEIT VAN PRETORIA
UNIVERSITY OF PRETORIA
YUNIBESITHI YA PRETORIA


$$\nabla\cdot\left(\rho\vec{v}\overline{f'^2}\right)=\nabla\cdot\left(\frac{\mu_t}{0.85}\nabla\overline{f'^2}\right)+2.86\mu_t\left(\nabla\overline{f}\right)^2-2.0\rho\frac{\varepsilon}{k}\overline{f'^2} \quad \textbf{(5-31)}$$

$$\nabla\cdot\left(\rho\vec{v}\vec{v}\right)=-\nabla p+\nabla\cdot\left(\bar{\bar{\tau}}\right)+\rho\vec{g}+\vec{F} \quad \textbf{(5-32)}$$

The stress tensor [93] is given by Eq. (5-33):

$$\bar{\bar{\tau}}=\mu\left[\left(\nabla\vec{v}+\nabla\vec{v}^T\right)-\frac{2}{3}\nabla\cdot\vec{v}\hat{i}\right] \quad \textbf{(5-33)}$$

$\mu$ is the molecular viscosity of the continuous phase, $\vec{F}$ is the interactive body forces between the dispersed and the continuous phases, $S_m$ is the source term accounting for the mass transfer from the solid phase to the gas phase and $\hat{i}$ is a unit vector. $\overline{f}$ and $\overline{f'^2}$ are the mean mixture fraction and the mixture fraction variance, and are computed by applying an assumed shape probability density function ($\beta$-function) when modelling the turbulence-chemistry interaction. Because $\bar{f}=f-f'$ (where $f$ is the mixture fraction), the mean mixture fraction can be related to the air-fuel mass ratio (AF) by $f=ER/(ER+AF)$. $ER$ is the equivalent ratio.

The assumed shape probability density function ($\beta$-function) is given by Eq. (5-34):

$$p(f)=\frac{f^{\alpha-1}(1-f)^{\beta-1}}{\int f^{\alpha-1}(1-f)^{\beta-1}df} \quad \textbf{(5-34)}$$

where $\alpha=\bar{f}\left[\bar{f}\left(1-\bar{f}\right)/\overline{f}'^2-1\right]$ and $\beta=\left(1-\bar{f}\right)\left[\bar{f}\left(1-\bar{f}\right)/\overline{f}'^2-1\right]$.

Figure 5-4 shows the computed mean temperature as a function of mean mixture fraction inside the combustor, with a mean mixture fraction of 1 corresponding to 100% fuel with no air.

UNIVERSITEIT VAN PRETORIA
UNIVERSITY OF PRETORIA
YUNIBESITHI YA PRETORIA



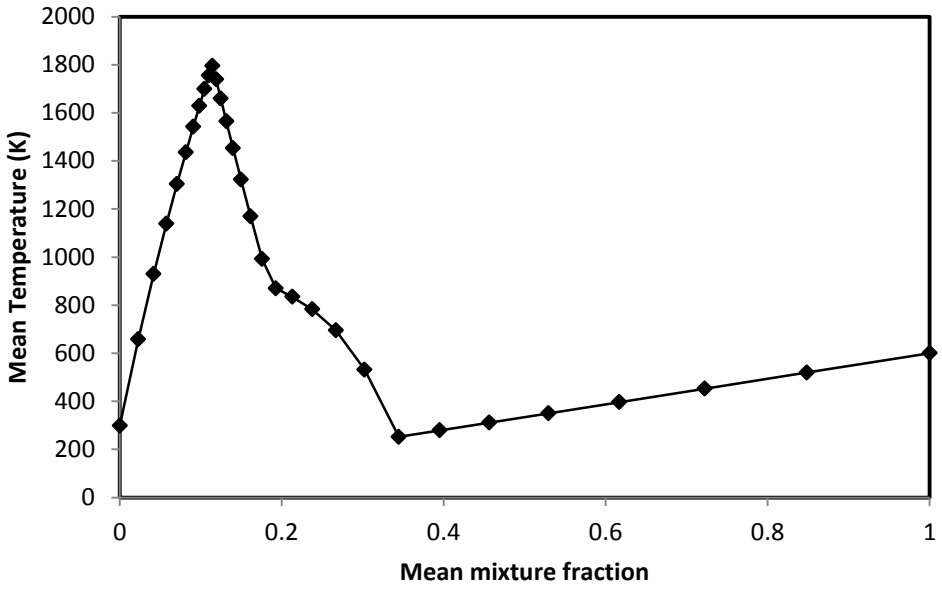


**Figure 5-4: The computed mean temperature distribution of the pitch pine wood combustion in air as a function of mean mixture fraction.**

The energy for the non-premixed combustion model [93] was as expressed by Eq. (5-35):

$$\nabla \cdot \left(\rho \vec{v} H\right) = \nabla \cdot \left(\frac{k_t}{c_p} \nabla H\right) + S_h \qquad \textbf{(5-35)}$$

The total enthalpy $H$ is given by Eq. (5-36):

$$H = \sum_{j=1}^{m} Y_j \left( \int_{T_{ref,j}}^{T} c_{p,j} dT + h_j^0 \left(T_{ref,j}\right) \right) \qquad \textbf{(5-36)}$$

$Y_j$ is the mass fraction, $c_{p,j}$ is the specific heat and constant pressure and $h_j^0\left(T_{ref,j}\right)$ is the enthalpy of formation of the $j^{th}$ species. $S_h$ accounts for source terms due to radiation, heat transfer to wall boundaries and heat exchange with the dispersed phase. The use of the chosen combustion model required the use of a turbulent model, because the combustion model is a mixture model. To this end, the $k-\varepsilon$ turbulent model with enhanced wall function option was chosen for all simulations. The P1 model included in the ANSYS FLUENT 16.2 code [93] was used to model radiation. The Presto! scheme was used to solve for pressure and

UNIVERSITEIT VAN PRETORIA
UNIVERSITY OF PRETORIA
YUNIBESITHI YA PRETORIA


second-order upwind schemes were used to solve for the continuity, energy, turbulence and mass fraction.

### 5.3.1. Part 1: Adiabatic combustors

The combustor had a cylinder shape with four inlets for the fuel as shown in Figure 5-5, each inlet with a mass flow rate of 0.00375 kg/s, which added to a total of 0.015 kg/s. The inlet temperature of the fuel at each inlet was set to 600 K. The temperature value was selected to be the same as the devolatilisation temperature of pitch pine [67].

The air inlets were divided into a primary air inlet used to devolatilise the fuel and four secondary air inlets, which were needed to complete the combustion of the fuel. The inlet temperature of air at each inlet was set to 400 K for Case 1 and 298 K for Case 2. The primary air entered the combustor at the base with a single fixed mass inlet, with half of the total air mass flow rate. The four secondary air fixed mass inlets were situated a quarter of the height up the combustor, each having an eighth of the total air mass flow rate. The combustor produced 241 $kW_{th}$ when complete combustion of pitch pine wood occurred with a theoretical amount of air. The air-fuel mass ratio was varied from 4.5 to 10. The combustor had a diameter of 300 mm and a height of 7 000 mm, as illustrated in Figure 5-5. The wall condition was made to be adiabatic. The data that was extracted from the simulations were the temperature at the pressure outlet boundary and the combustion products molar fractions also at the pressure outlet boundary.

UNIVERSITEIT VAN PRETORIA
UNIVERSITY OF PRETORIA
YUNIBESITHI YA PRETORIA


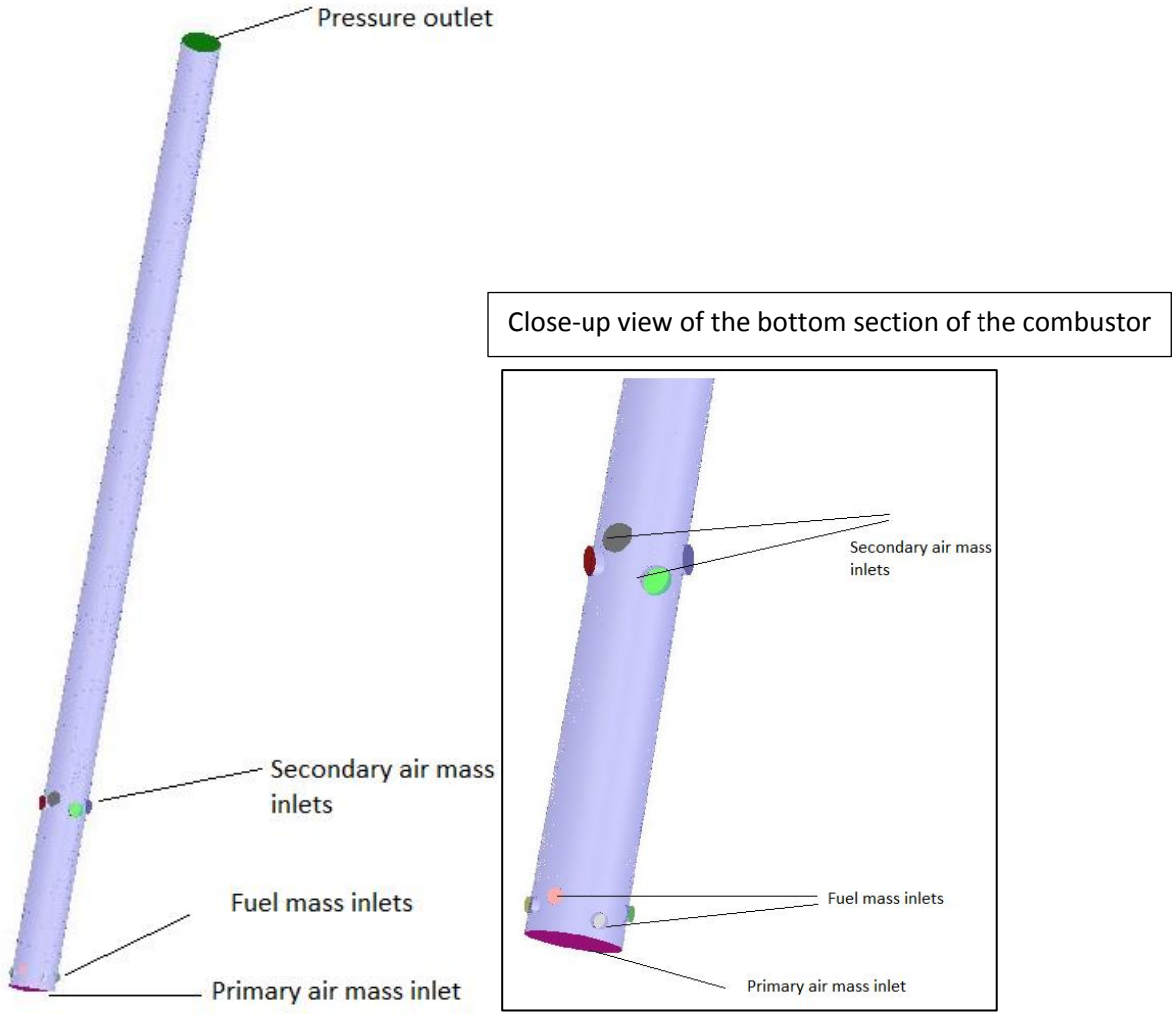


**Figure 5-5: Schematic of the combustor showing boundary placements.**

### 5.3.2. Part 2: Combustors with incoming air at 400K, one with adiabatic and the other with wall heat flux conditions

The combustors used in the second part of the study had exactly the same dimensions and operating conditions as the combustor shown in Figure 5-5 for the first part of the study. Firstly, the difference is that the incoming air temperature was fixed at 400K for both combustors. Secondly, for the combustor with a wall heat flux condition, the heat flux was set at -7500 $W/m^2$.

### 5.3.3. Part 3: Combustors with wall heat flux condition and wall thickness

The combustors used in the third part of the study had exactly the same height of 7 m and operating conditions as the combustor shown in Figure 5-5 for Part 1and Part 2 of the study. However, the combustors had diameters varying from 0.1 m to 1 m. The outer-wall heat flux was fixed to a value of 7272.9 W/m$^2$ for all combustors and for each combustor diameter, the wall thickness was varied from a value of zero to 0.05 m.

### 5.3.4. Mesh independence

A mesh independence exercise was done to remove any numerical effects on the results due to the mesh used to run the simulations. The dependence of the entropy generation rate of the combustor was plotted against the number of polyhedral cells shown in Figure 5-6. The figure shows that the mesh size had little effect on computing the entropy generation rate, therefore a mesh size of 747 055 was chosen for Parts 1 and 2 of the study and mesh sizes above or about 747 000 were chosen for Part 3.

UNIVERSITEIT VAN PRETORIA
UNIVERSITY OF PRETORIA
YUNIBESITHI YA PRETORIA


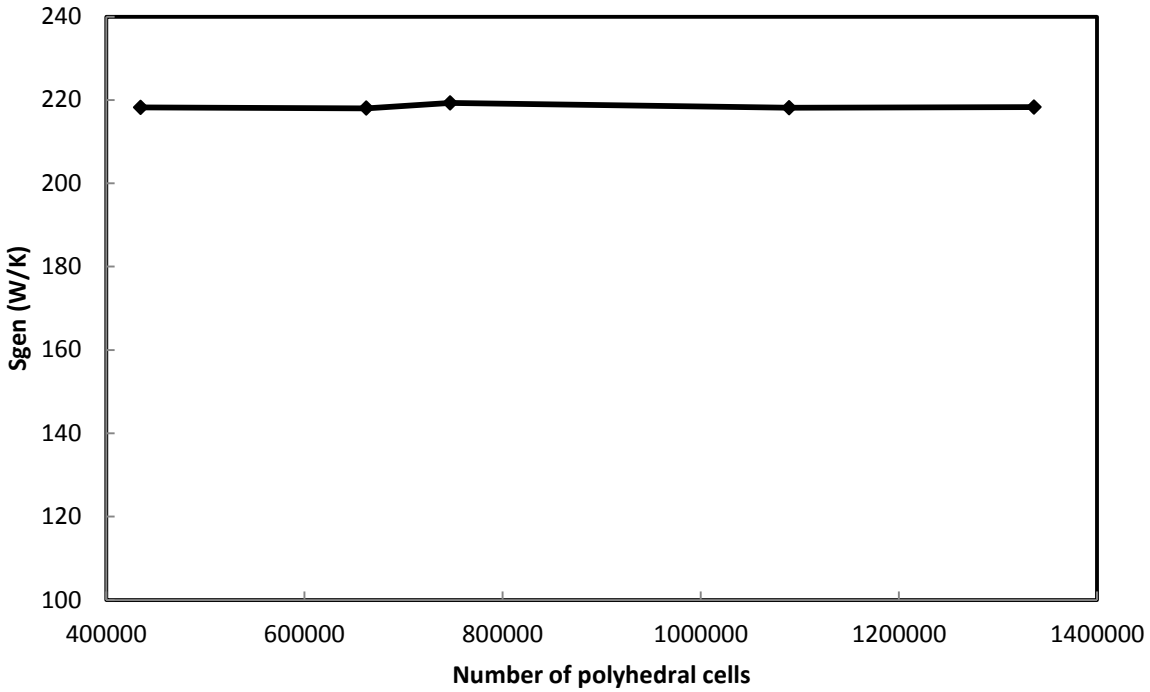


**Figure 5-6: Mesh independence exercise for a combustor with a diameter of 0.3 m, simulated at AF of 6.**

### 5.3.5. Validation of CFD simulations

The results obtained when using Eq. (5-2) and Eq. (5-3) to process data from numerical simulations and data from the thermodynamics tables [1] were compared for the case of complete combustion with varying amounts of excess air, which were lean mixtures. It was found that the results from numerical simulations compared well with the results from the thermodynamics tables, as shown in Figure 5-7.

UNIVERSITEIT VAN PRETORIA
UNIVERSITY OF PRETORIA
YUNIBESITHI YA PRETORIA


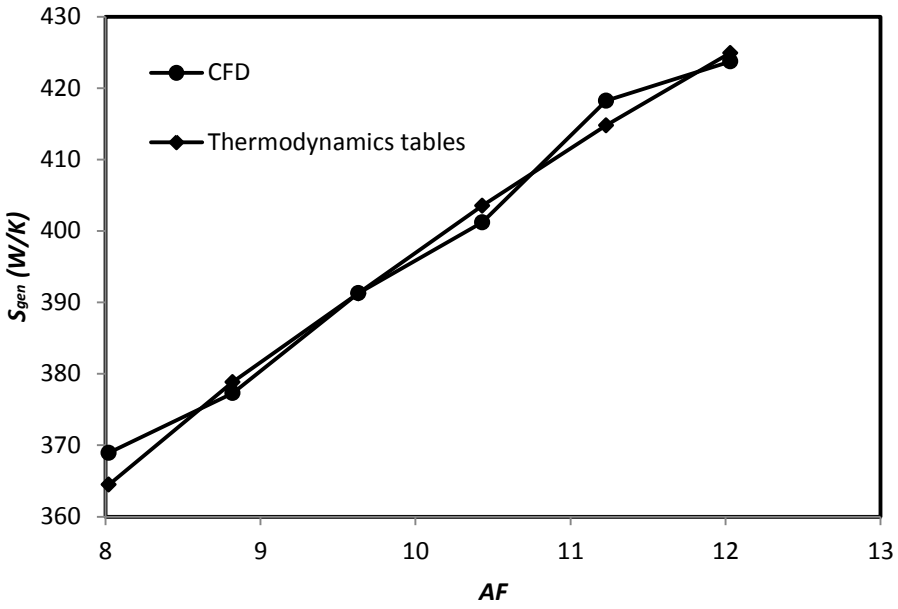


**Figure 5-7: The entropy generation rate profile as a function of AF in an adiabatic combustor for lean mixtures.**

## 5.4.Results and discussion

The results from the study are presented and discussed focusing first on comparing the two adiabatic cases (Case 1 and Case 2) in Part 1, followed by comparing the cases each with incoming air temperature of 400 K, but one case with adiabatic wall condition (Case 1) and the case with a negative heal flux wall condition (Case 3) in Part 2.

### 5.4.1. Part 1: Case 1 vs. Case 2

The entropy generation rate and irreversibilities of Case 1 and Case 2 were compared simultaneously in order to observe the effect of a change in incoming air temperature from 298 K to 400 K, and the results are presented in Figure 5-8. It can be seen from Figure 5-8 that the increase in incoming air temperature had the effect of lowering the minimum values of the entropy generation rate and irreversibilities. This can clearly be seen in Figure 5-9

UNIVERSITEIT VAN PRETORIA
UNIVERSITY OF PRETORIA
YUNIBESITHI YA PRETORIA


where a plot, with a bound range in the AF axis, of the entropy generation rate was plotted around the AF value where the minima occurred. From Figure 5-9, it can be seen that the AF at which the minimum occurred for an incoming temperature of 298 K changed from 4.9 to 4.8 for an incoming air temperature of 400 K.

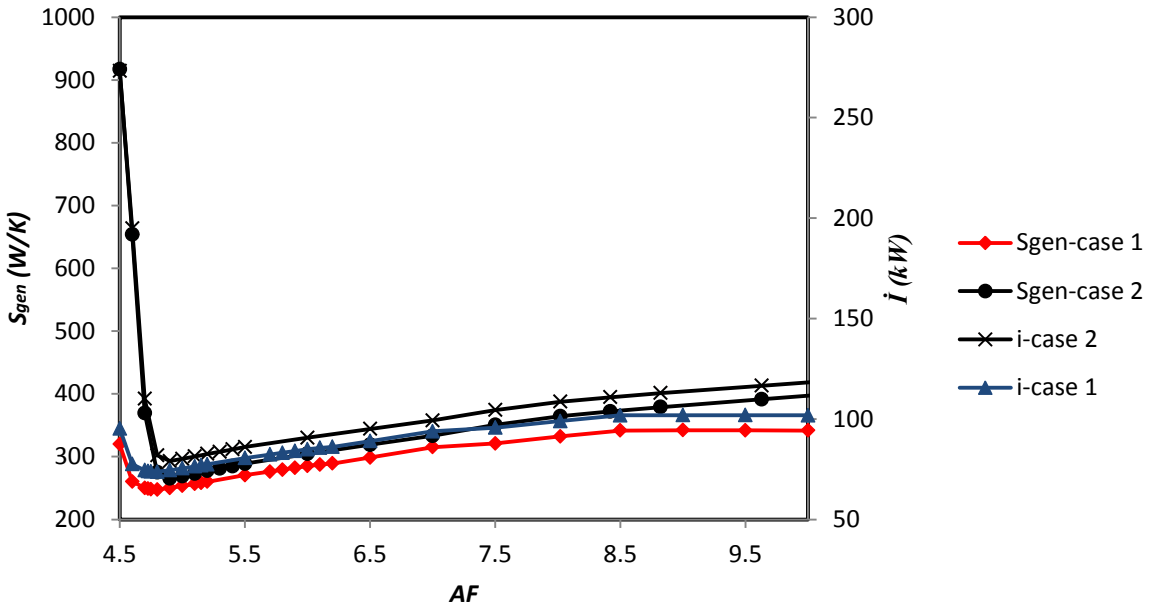


**Figure 5-8: Plots of the variation of entropy generation rate and irreversibilities with AF for Case 1 and Case 2.**

UNIVERSITEIT VAN PRETORIA
UNIVERSITY OF PRETORIA
YUNIBESITHI YA PRETORIA



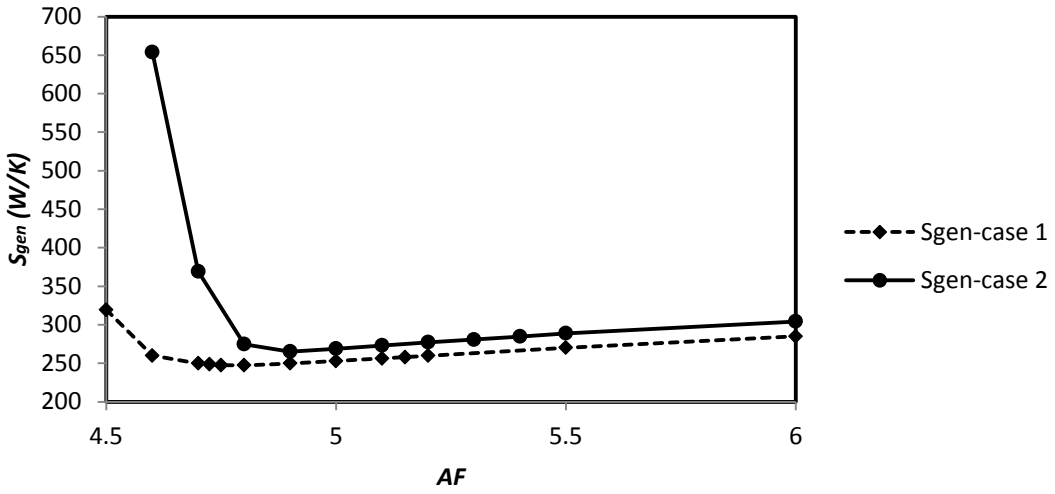


**Figure 5-9: Close-up of plots of the variation of entropy generation rate with AF for Case 1 and Case 2.**

The reason for this improvement in performance could be that the amount of unburnt solid fuel as represented by char, C<s>, had considerably gone down with a rise in incoming air temperature as can be seen when comparing Figure 5-10 and Figure 5-11. The combusted char (C<s>) was converted to CO, as can be observed from Figure 5-10, with a considerable increase in the molar fraction of CO.

UNIVERSITEIT VAN PRETORIA
UNIVERSITY OF PRETORIA
YUNIBESITHI YA PRETORIA



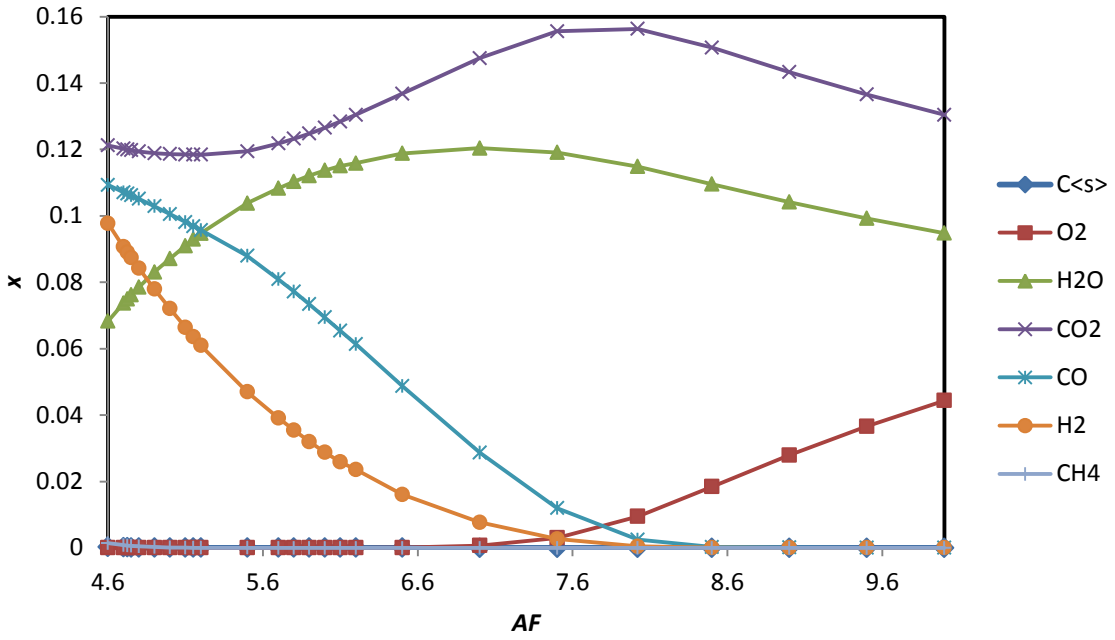


**Figure 5-10: Plot of variation with AF in molar fraction of combustion product species for Case 1.**

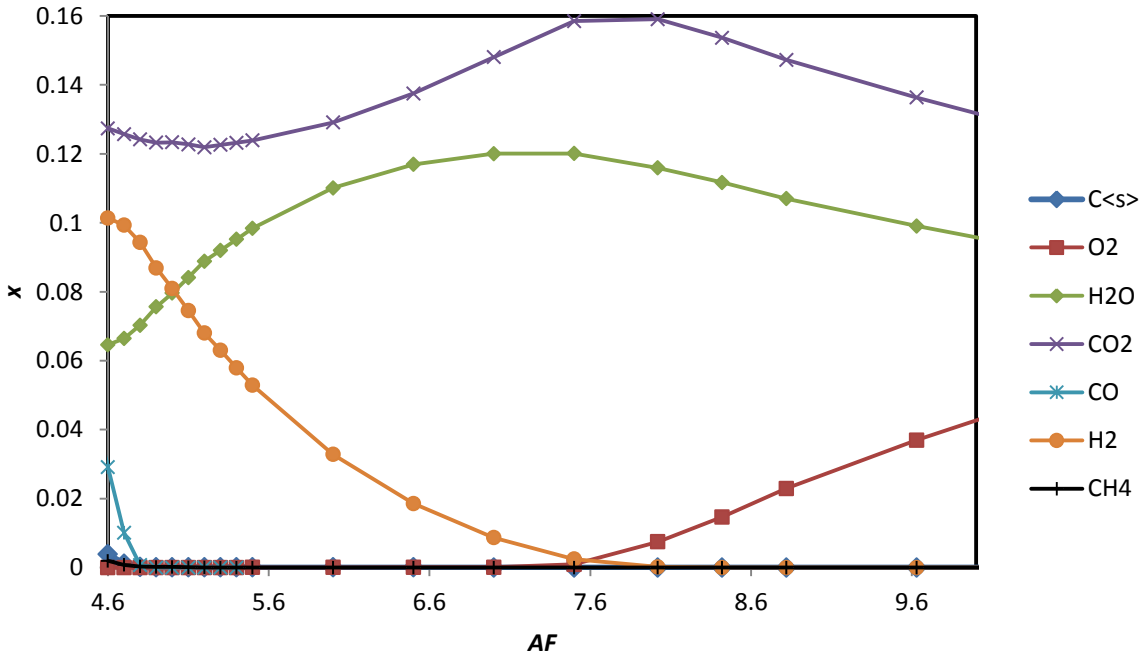


**Figure 5-11: Plot of variation with AF in molar fraction of combustion product species for Case 2.**

UNIVERSITEIT VAN PRETORIA
UNIVERSITY OF PRETORIA
YUNIBESITHI YA PRETORIA


As was discussed in [84], the minima entropy generation rates occurred around AF where molar fractions of $H_2O$ and $H_2$ were equal, as can be seen in plots in Figure 5-12 and Figure 5-13. This was also the point at which the molar fraction of $CO_2$ was the lowest. It was furthermore discussed in [84] that when the combined contribution to the total entropy generation rate from $H_2O$, $H_2$ and $CO_2$ was the lowest, the minimum total entropy generation rate would occur. Figure 5-13 shows that the change in AF value when the incoming air temperature changes from 298 K to 400 K is small.

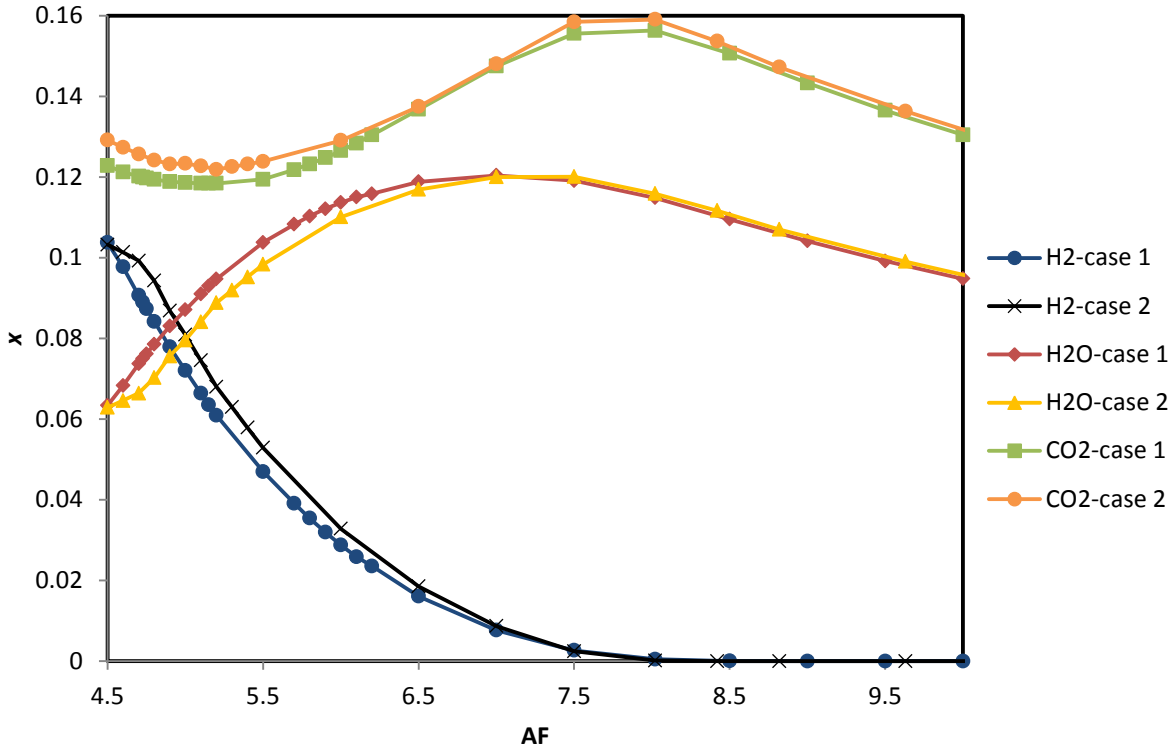


**Figure 5-12: Plot comparing the variation of molar fractions of selected combustion product species with AF for Case 1 and Case 2.**

UNIVERSITEIT VAN PRETORIA
UNIVERSITY OF PRETORIA
YUNIBESITHI YA PRETORIA


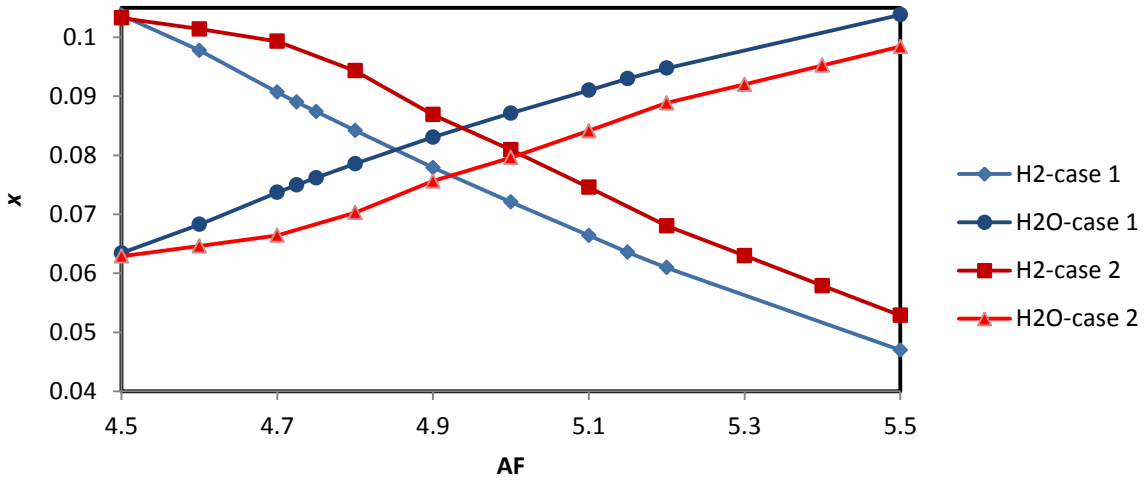


**Figure 5-13: Plot comparing the variation of molar fractions of H2 and H2O with AF for Case 1 and Case 2.**

When $N_s$ and $N_R$ between the two cases were compared, as shown in Figure 5-14, more insights were gained. When the incoming air temperature was changed from 298 K to 400 K, the penalty paid for deviating from the AF with minimum entropy generation rate was reduced drastically. For example, this was illustrated for the case of AF = 4.6 where for the case with incoming air temperature of 298 K, Ns = 1.46, whereas for the case with incoming air temperature of 400 K, Ns = 1.05. At the same AF = 4.6, the corresponding NR for the case with incoming air temperature of 298 K was 1.79, whereas for the case with incoming air temperature of 400 K, NR = 0.78.

UNIVERSITEIT VAN PRETORIA
UNIVERSITY OF PRETORIA
YUNIBESITHI YA PRETORIA



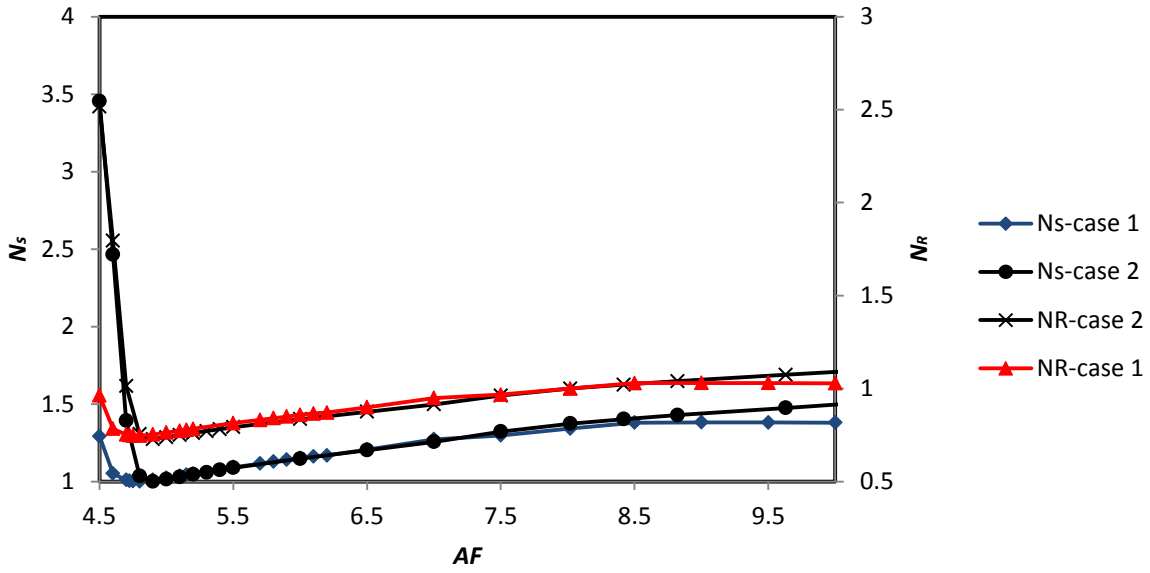


**Figure 5-14: Plot of entropy generation number and relative entropy generation rate as a function of AF for Case 1 and Case 2.**

As reported in [85], the changing of incoming air temperature from 298 K to 400 K had the effect of raising the adiabatic combustor's outlet mixture temperature, as shown in Figure 5-15. As expected, the maximum temperature occurred for the AF of 8.02, corresponding to combustion with a theoretical amount of air.

UNIVERSITEIT VAN PRETORIA
UNIVERSITY OF PRETORIA
YUNIBESITHI YA PRETORIA


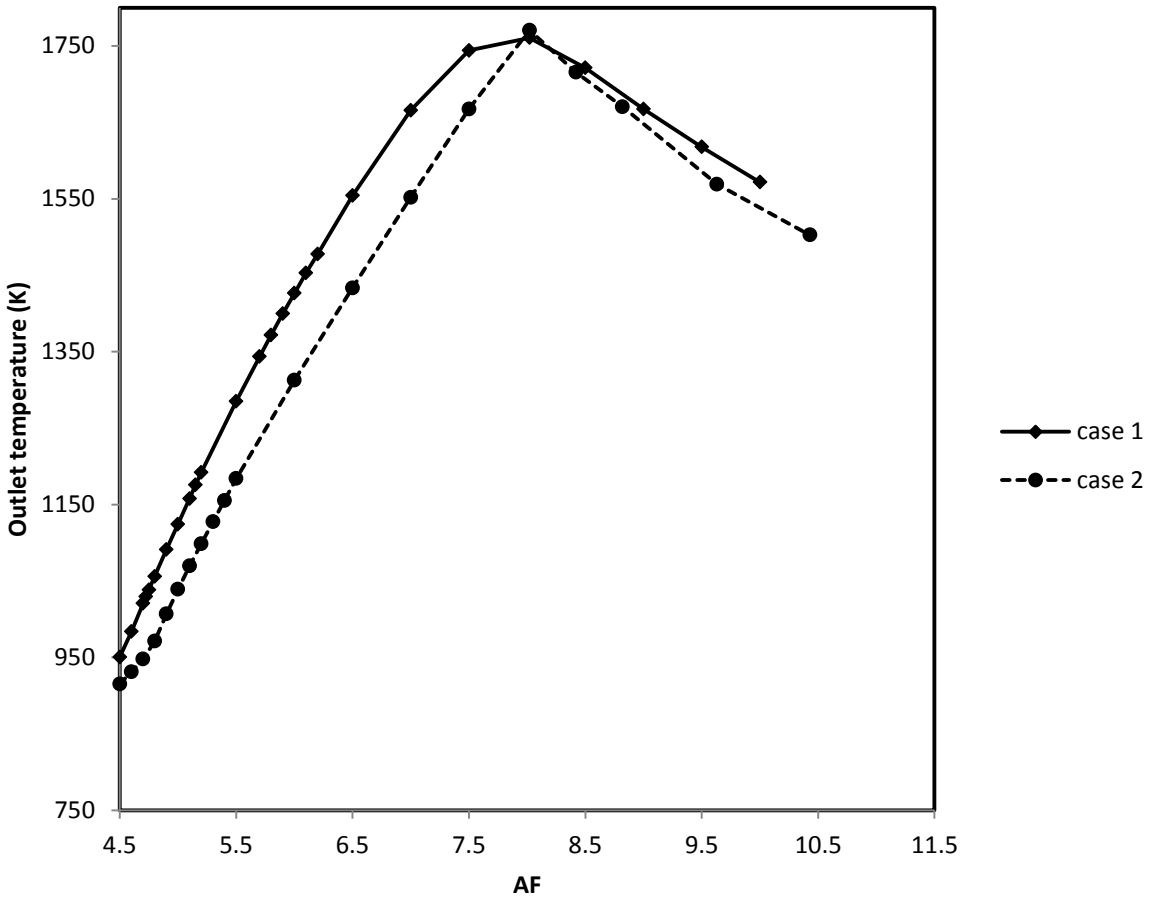


**Figure 5-15: Plot of combustion products mixture temperature as a function of AF for Case 1 and Case 2.**

### 5.4.2. Part 2: Case 1 vs. Case 3

The entropy generation rate and irreversibilities of Case 1 and Case 3 were compared in order to observe the effect of a wall heat flux, and the results are presented in Figure 5-16. It can be seen from Figure 5-16 that the application of a negative heat flux resulted in a drastic increase in the entropy generation rate. By changing the wall condition from adiabatic (Case 1) to negative heat flux (Case 3), the AF at which the minimum entropy generation rate and irreversibilities occurred changed from 4.8 to 6. This can clearly be seen in Figure 5-17 where a plot, with a bound range in the AF axis, of the entropy generation rate was plotted

UNIVERSITEIT VAN PRETORIA
UNIVERSITY OF PRETORIA
YUNIBESITHI YA PRETORIA


around the AF value where the minima occurred. From Figure 5-17, it can be seen that the AF at which the minimum occurred for an adiabatic wall changed from 4.8 to 6 for a wall with a negative heat flux of 7 500 W/m$^2$.

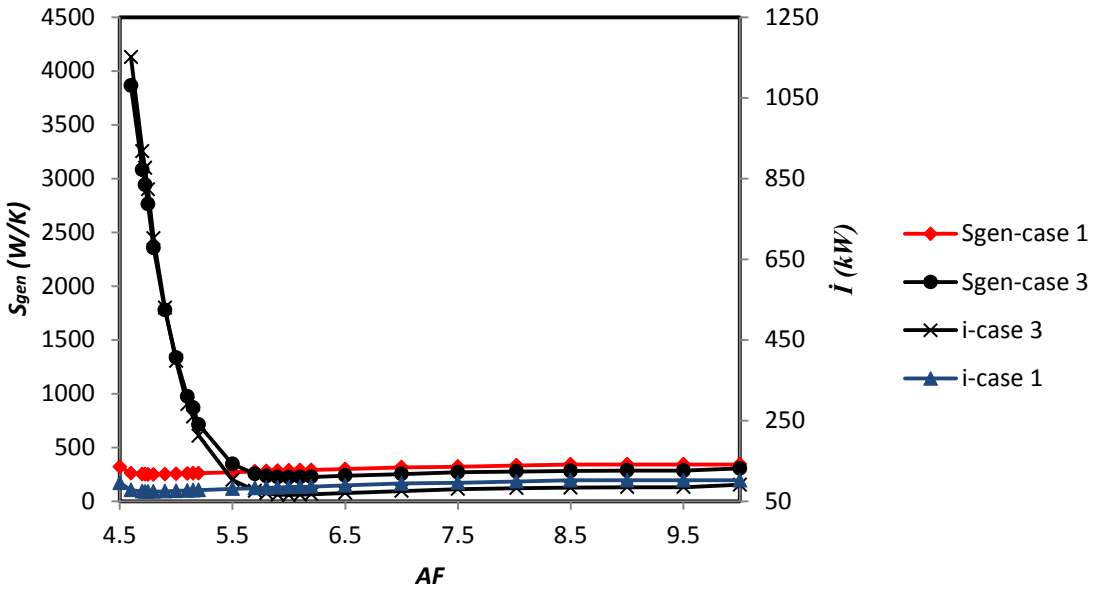


**Figure 5-16: Plots of the variation of entropy generation rate and irreversibilities with AF for Case 1 and Case 3.**

UNIVERSITEIT VAN PRETORIA
UNIVERSITY OF PRETORIA
YUNIBESITHI YA PRETORIA


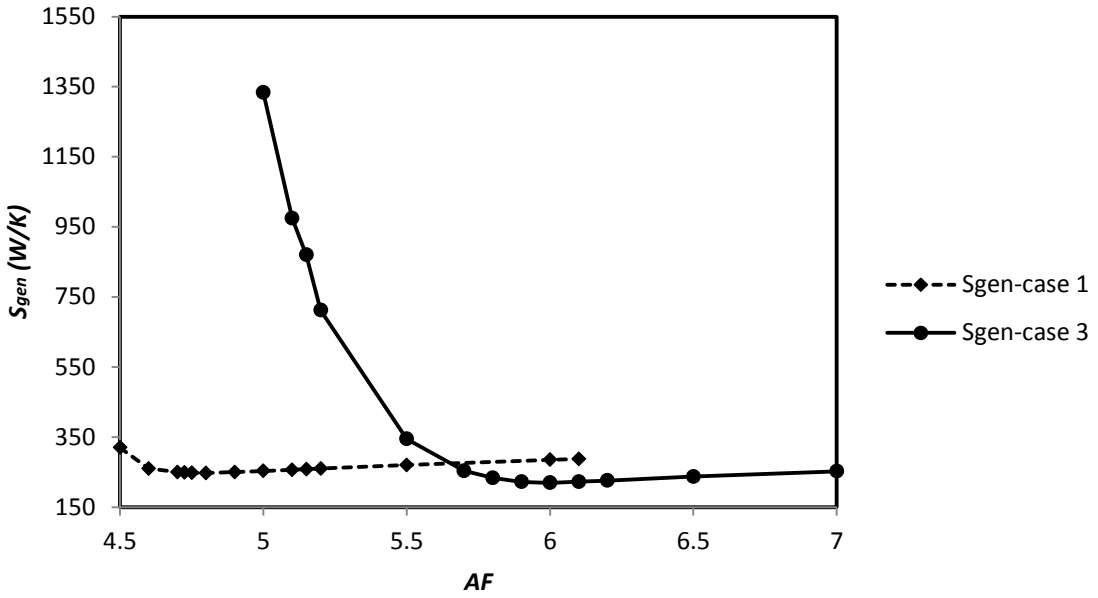


**Figure 5-17: Close-up of plots of the variation of entropy generation rate with AF for Case 1 and Case 3.**

The reason for the deterioration in performance for Case 3 could be that the amount of unburnt solid fuel as represented by char, C<s>, had considerably gone up with a change in wall condition from adiabatic to negative heat flux as can be seen when comparing Figure 5-10 and Figure 5-18. The molar fraction of CO did not rise as high for Case 3 as for Case 1 when comparing Figure 5-10 and Figure 5-18.

UNIVERSITEIT VAN PRETORIA
UNIVERSITY OF PRETORIA
YUNIBESITHI YA PRETORIA



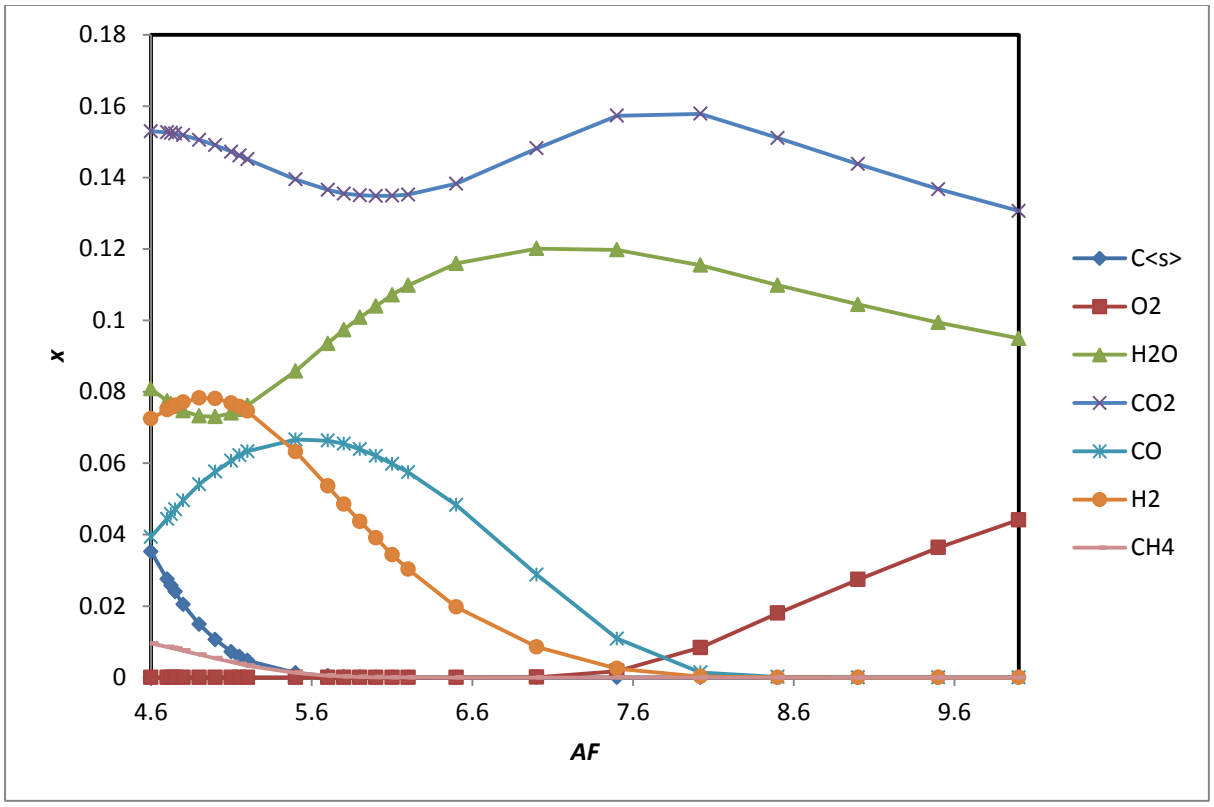


**Figure 5-18: Plot of variation with AF in molar fraction of combustion product species for Case 3.**

As was discussed in [84] and also from observing Figure 5-10, Figure 5-11 and Figure 5-12, the minima entropy generation rates occurred around AF where molar fractions of $H_2O$ and $H_2$ were equal. This was also the point at which the molar fraction of $CO_2$ was the lowest. However, Figure 5-18 and Figure 5-19 show that the minimum entropy generation rate occurred only at an AF when the molar fraction $CO_2$ was the lowest, and not when the molar fractions of $H_2$ and $H_2O$ were equal. Figure 5-18 and Figure 5-19 also show that the molar fractions of $H_2$ and $H_2O$ were equal at two points, which was not observed before with Case 1 and Case 2 when the wall condition was adiabatic. Figure 5-20 shows a plot, with a bound range in the AF axis, of the molar fraction plots of $H_2$ and $H_2O$ for Case 1 and Case 3,

highlighting the difference in response of the combustion products mixture components to a change in wall condition from adiabatic to negative heat flux.

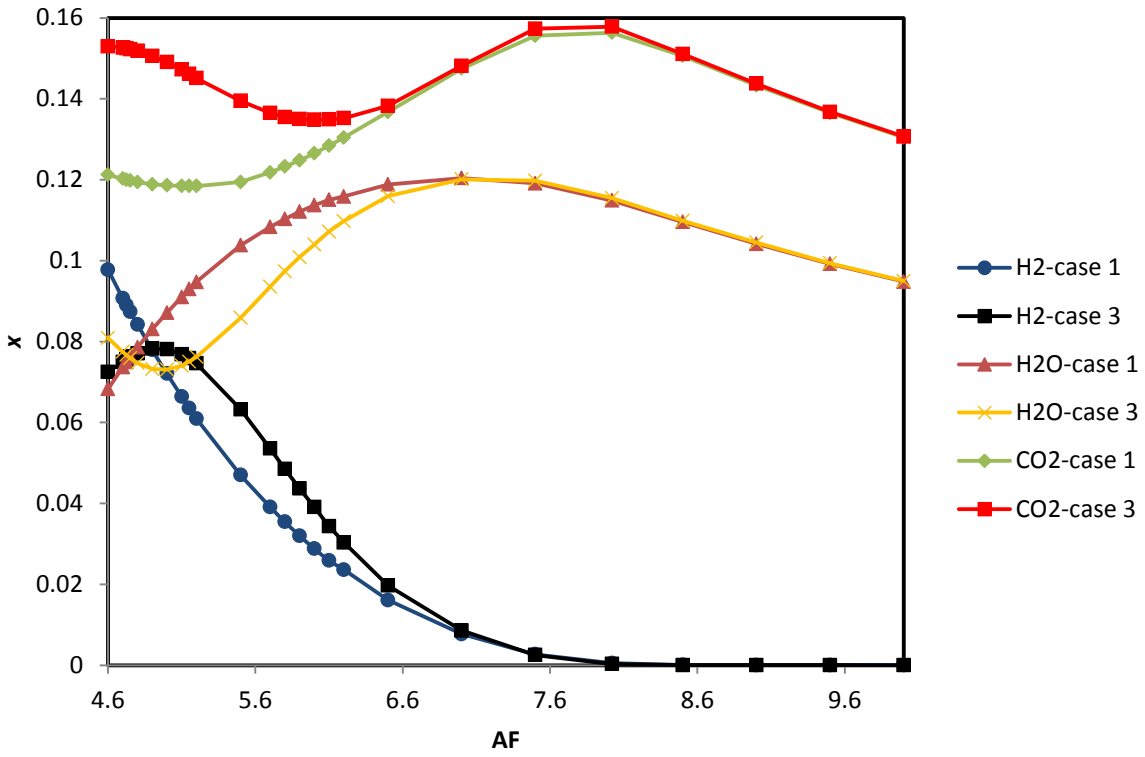


**Figure 5-19: Plot comparing the variation of molar fractions of selected combustion product species with AF for Case 1 and Case 3.**

UNIVERSITEIT VAN PRETORIA
UNIVERSITY OF PRETORIA
YUNIBESITHI YA PRETORIA


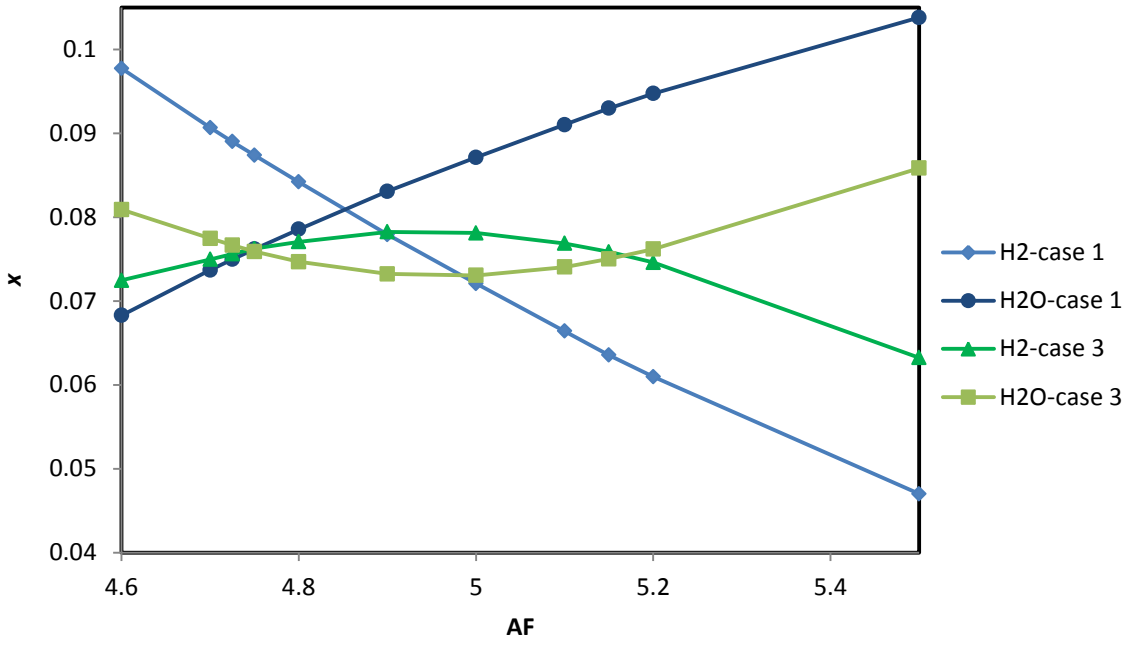


**Figure 5-20: Plot comparing the variation of molar fractions of H2 and H2O with AF for Case 1 and Case 3.**

When the wall condition was changed from adiabatic to negative heat flux, the penalty paid for deviating from the AF with minimum entropy generation rate was increased drastically, as shown in Figure 5-21. This was illustrated, for example, for the case of AF = 4.6 where for Case 3 with a negative heat flux wall condition, Ns = 17.62, whereas for Case 1 with an adiabatic wall condition, Ns = 1.05. At the same AF = 4.6, the corresponding NR for Case 3 with a negative heat flux wall condition was 13.96, whereas for Case 1 with an adiabatic wall condition, NR = 0.78.

UNIVERSITEIT VAN PRETORIA
UNIVERSITY OF PRETORIA
YUNIBESITHI YA PRETORIA


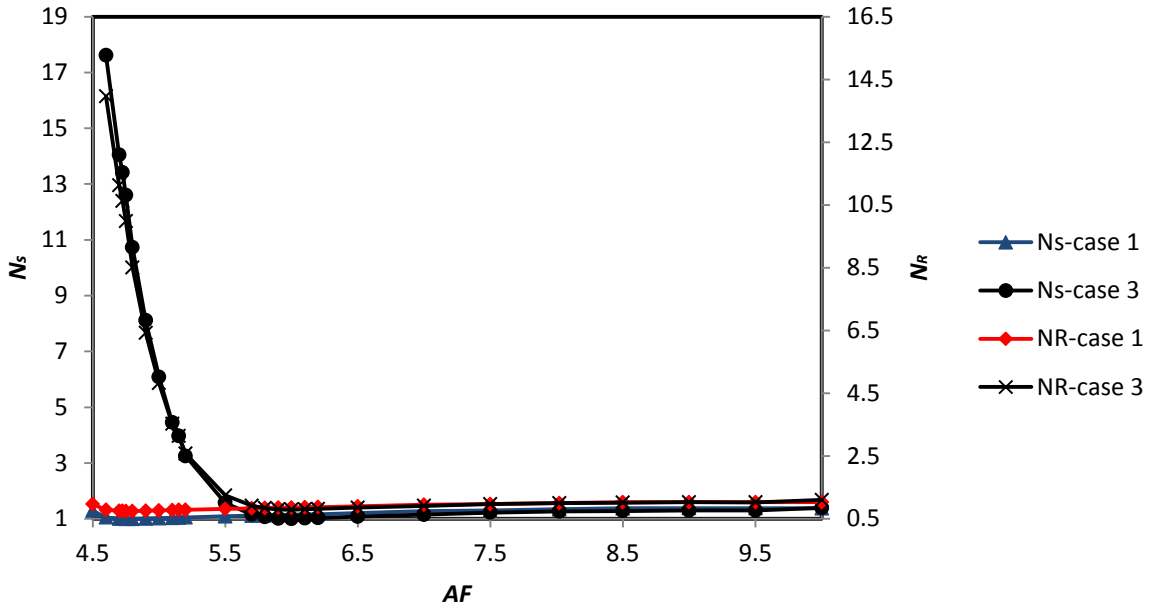


**Figure 5-21: Plot of entropy generation number and relative entropy generation rate as a function of AF for Case 1 and Case 3.**

Changing the wall condition from adiabatic to negative heat flux had the effect of lowering the combustor's outlet mixture temperature, as shown in Figure 5-22. As mentioned earlier, this was due to the presence of unburnt fuel at the exit in the form of char (C<s>).

UNIVERSITEIT VAN PRETORIA
UNIVERSITY OF PRETORIA
YUNIBESITHI YA PRETORIA


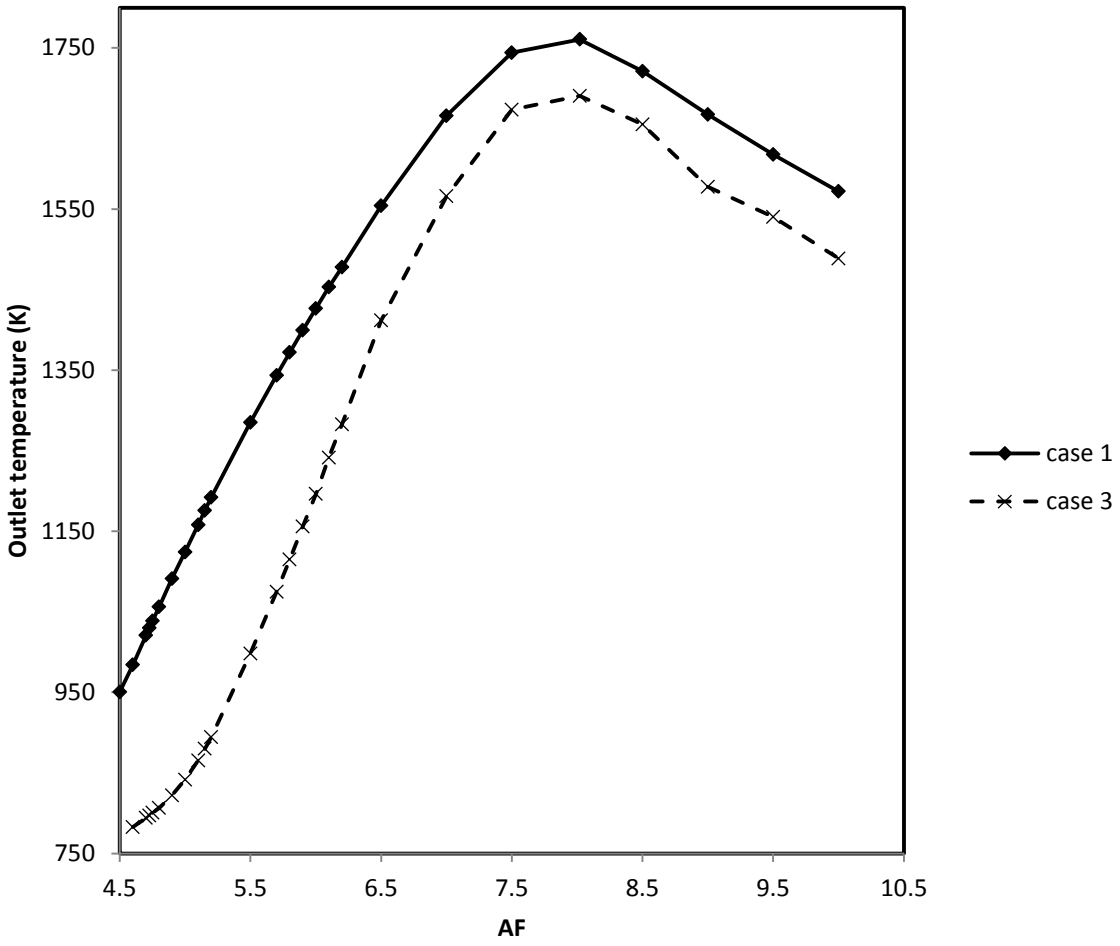


**Figure 5-22: Plot of combustion products mixture temperature as a function of AF for Case 1 and Case 3.**

Filled contour plots of temperature on a section through the geometry of the combustor and the cylinder wall were created for Case 3 at condition when it achieved the minimum entropy generation rate, and were plotted in Figure 5-23 and Figure 5-24 respectively. More filled contour plots of temperature in the combustor are shown in figures in Appendix C.

UNIVERSITEIT VAN PRETORIA
UNIVERSITY OF PRETORIA
YUNIBESITHI YA PRETORIA



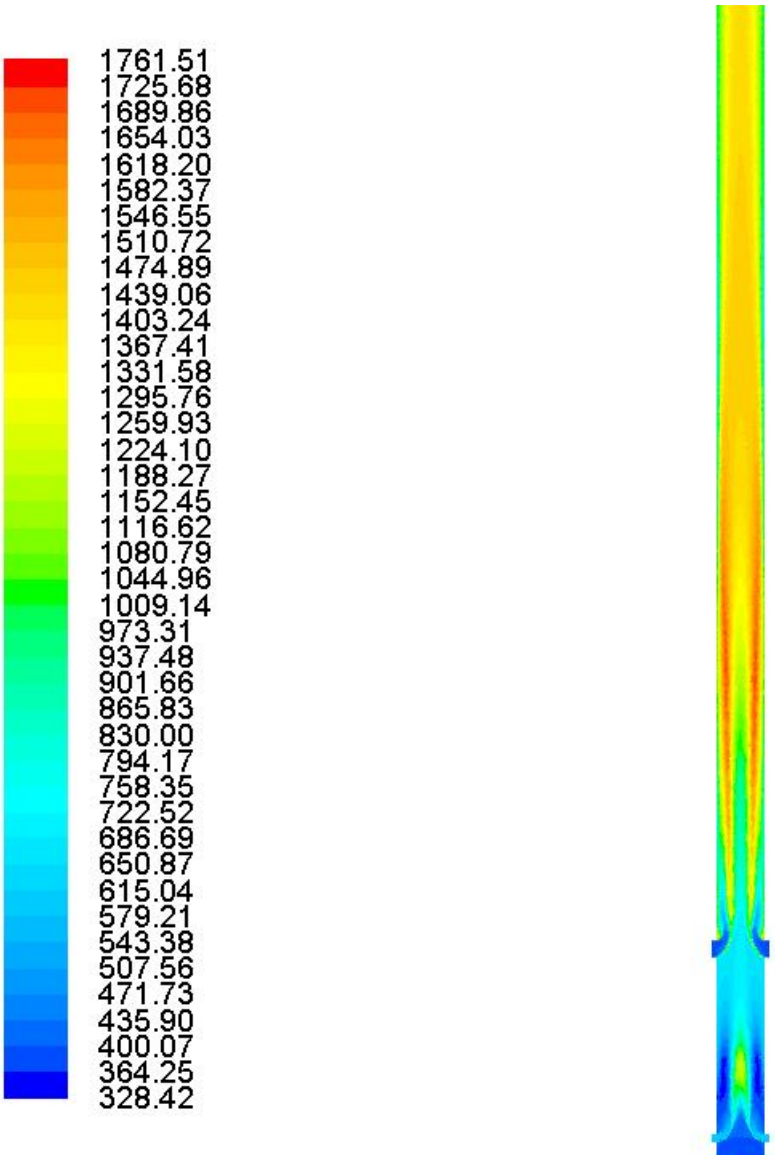


**Figure 5-23: Section plot of filled temperature contours (Kelvins) for Case 3 with AF of 6.0.**

UNIVERSITEIT VAN PRETORIA
UNIVERSITY OF PRETORIA
YUNIBESITHI YA PRETORIA



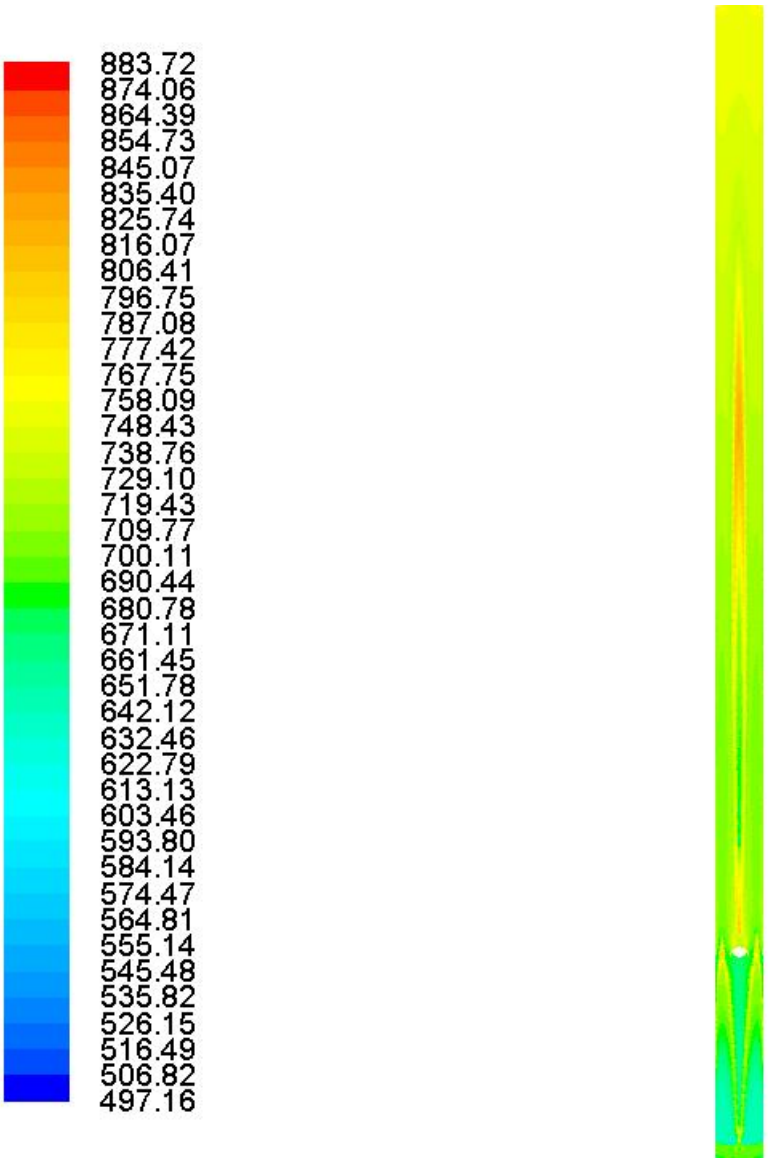


**Figure 5-24: Wall plot of filled temperature contours (Kelvins) for Case 3 with AF of 6.0.**

### 5.4.3. Part 3: Combustors with wall heat flux condition and wall thickness

The molar fractions of combustion products were incorporated into Eq. (5-27) in order to compute the entropy generation rate of the combustor. The computed entropy generation rate for a wide range of Reynolds numbers based on the combustor diameter was plotted in Figure 5-25. The figure shows that the minimum entropy generation rate of about 218 W/K occurred at a Reynolds number of about 25 000, when the combustor with an infinitesimally thin wall (

UNIVERSITEIT VAN PRETORIA
UNIVERSITY OF PRETORIA
YUNIBESITHI YA PRETORIA


$t = 0mm$) was simulated.

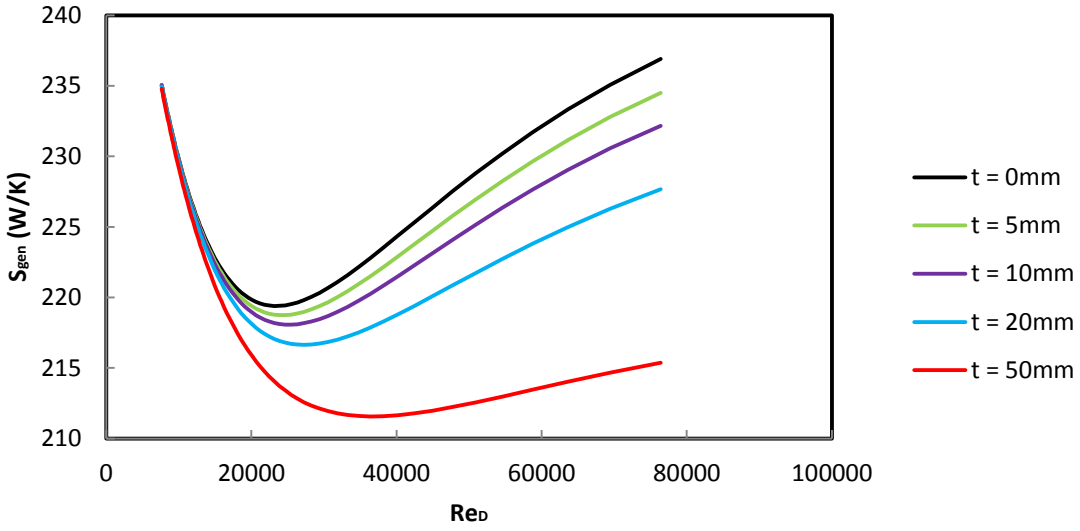


**Figure 5-25 Entropy generation rate profile as a function of Reynolds number for combustors with various wall thicknesses all ran at an AF of 6 (equivalent ratio of 1.34.)**

This Reynolds number corresponded to a combustor diameter of 0.32 m, as shown by Figure 5-26. Because the AF had been fixed at a value of 6, the entropy generation rate term due to combustion remained constant even when the there was a change in combustor diameter. Also given that the contribution of the pressure loss term was negligible, as discovered in [84], all changes in the entropy generation rate were due to the heat transfer term through the wall of the combustor. This meant that the optimum diameter discovered in this study was unique for a combustor run at an AF of 6.

UNIVERSITEIT VAN PRETORIA
UNIVERSITY OF PRETORIA
YUNIBESITHI YA PRETORIA


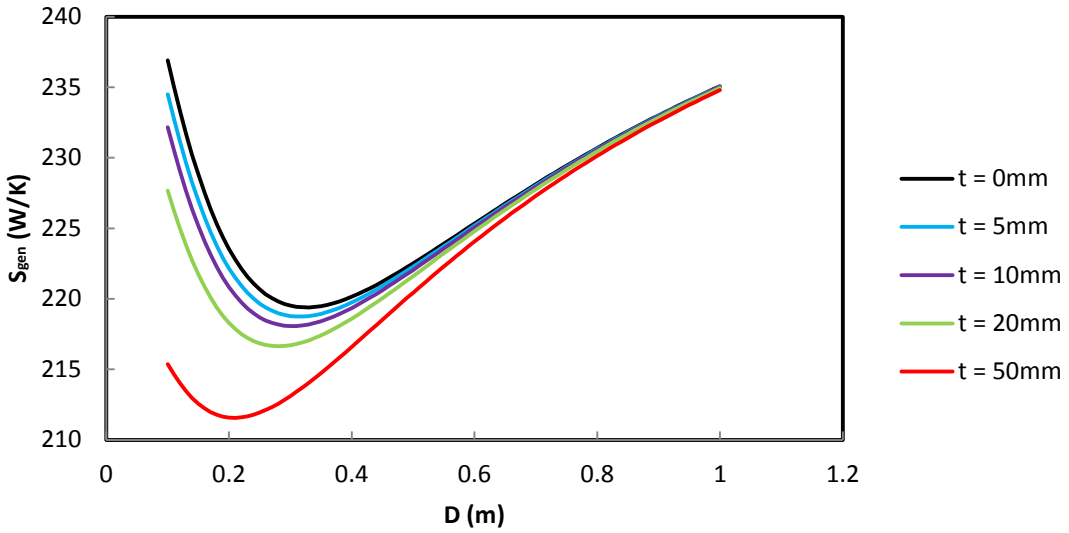


**Figure 5- 26: Entropy generation rate profile as a function of combustor diameter for combustors with various wall thicknesses all ran at an AF of 6 (equivalent ratio of 1.34.)**

The introduction of wall thickness unlocked further optimisation of the diameter of the combustor. With an increase in wall thickness, there was a decrease in the optimum diameter of the combustor, as shown in Figure 5-26. This decrease in optimum diameter that resulted in minimum entropy generation rate could be that the Nusselt number (as given by Eq. (5-9)), which increased with decreasing diameter, indicated improved convective heat transfer from the combustion products to the combustor wall. It is worth noting that the sum of the optimum diameter and twice the thickness of the wall always added up to the optimum diameter when the wall thickness was infinitesimally small, that is $t = 0mm$.

The effect of improved convective heat transfer can also be seen clearly in Figure 5-25 where an increase in wall thickness resulted in slower increase of entropy generation rate when there was an increase in Reynolds number (Reynolds number was inversely proportional to combustor diameter, as given by Eq. (5-13)). Both Figure 5-25 and Figure 5-26 show that when there was an increase in diameter (decrease in Reynolds number), the advantage of

improved convective heat transfer diminished to the point where for any wall thickness value, the entropy generation rate was the same as for an infinitesimally thin wall. The corresponding irreversibilities to the entropy generation rate shown in Figure 5-25 are shown in Figure 5-27.

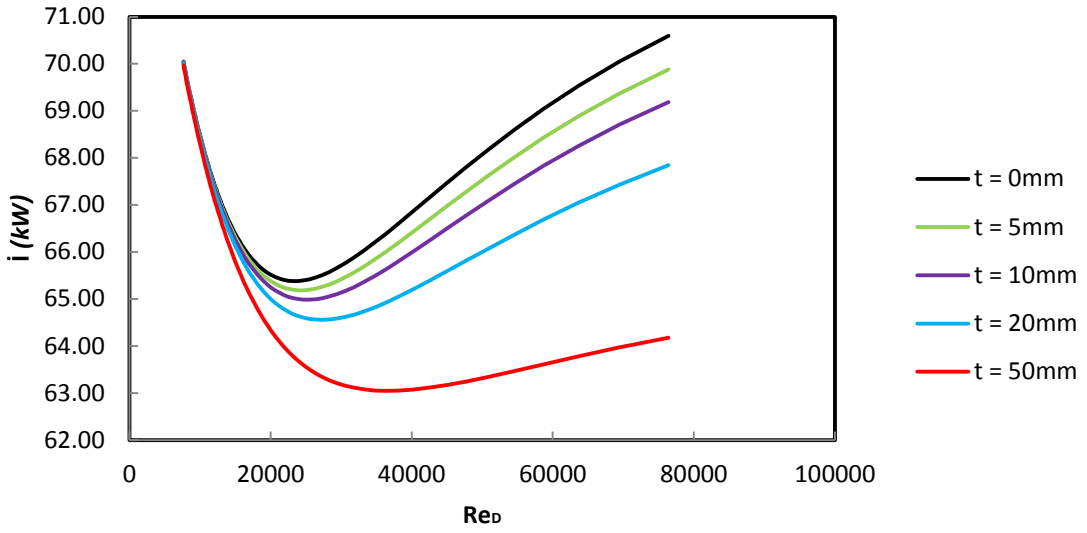


**Figure 5-27: Irreversibilities profile as a function of Reynolds number for combustors with various wall thicknesses all ran at an AF of 6 (equivalent ratio of 1.34.)**

The penalty that was paid when the combustor had a diameter that was not optimum was also computed as represented by $N_s$, as can be seen in Figure 5-28. The figure shows that at diameters of 0.1 m and 0.97, the penalty paid was an extra 7% in entropy generation rate for an optimum diameter of 0.32 m, but this penalty decreased with increasing wall thickness of the combustor.

UNIVERSITEIT VAN PRETORIA
UNIVERSITY OF PRETORIA
YUNIBESITHI YA PRETORIA


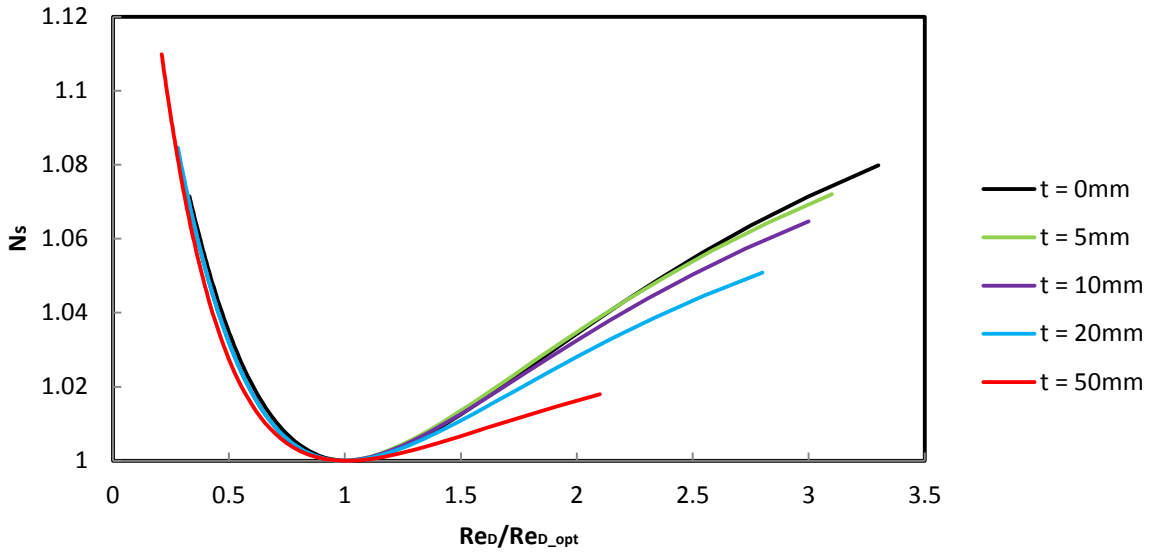


**Figure 5-28: The entropy generation number profile as a function of Reynolds number for combustors with various wall thicknesses all ran at an AF of 6 (equivalent ratio of 1.34.)**

## 5.5. CONCLUSION

The changing of incoming air temperature into a circulating fluidised bed adiabatic combustor from 298 K to 400 K resulted in a small change in AF, at which minimum entropy generation rate occurred, from 4.9 to 4.8. The penalty paid when deviating from that point reduced drastically from 46% for Case 2 with incoming air temperature of 298 K to 5% for Case 1 with incoming air temperature of 400 K when the combustor was run at an AF of 4.6. On the other hand, the changing of the wall condition from adiabatic to a negative heat flux resulted in a change in AF, at which minimum entropy generation rate occurred, from 4.8 to 6. For a combustor with a heat flux of -7 500 W/m2 wall condition and an infinitesimally thin wall simulated at an AF of 6, an optimum diameter of 0.32 m resulted in the minimum entropy generation rate. However, when the combustor wall thickness was taken into consideration, the optimum diameter got smaller with increasing wall thickness. It was also

UNIVERSITEIT VAN PRETORIA
UNIVERSITY OF PRETORIA
YUNIBESITHI YA PRETORIA


found that the sum of twice the wall thickness and the optimum diameter always added up to the optimum diameter when the wall thickness was infinitesimally small. Taking into account the wall thickness resulted in lower entropy generation rates and this was attributed to improved convective heat transfer when the optimum diameter got smaller. The penalty paid for deviating from the optimum diameter was also reduced with increased wall thickness for smaller diameters, as measured by the entropy generation number.

UNIVERSITEIT VAN PRETORIA
UNIVERSITY OF PRETORIA
YUNIBESITHI YA PRETORIA


# Chapter 6. OPTIMUM GEOMETRY OF SOLID POROUS SPHERES WITH HEAT GENERATION

## 6.1. INTRODUCTION

The storage of spent nuclear fuel is complicated by the need to manage the decay heat generated by the fuel. The spent nuclear fuel has to be cooled so that heat generated does not melt the containment system, which can lead to the unintentional release of radioactive material to the surroundings. A similar scenario takes place, although innocuous, where a pile of stones (heated as an energy storage mechanism) is cooled by a fluid flowing through gaps between the stones. The heat transfer mechanisms involved in the cooling in both instances have historically been analysed by assuming that the fluid and solid phases are at local thermal equilibrium (LTE) in order to simplify the analysis. However, in general, models created with this assumption in mind do not give accurate results because the local temperature difference between the solid and fluid phases can be too big for the LTE assumption to be valid. In order to remedy this shortcoming, local thermal non-equilibrium (LTNE) has been taken as the general condition which is assumed to prevail between the solid and fluid phases.

Using the LTNE condition between the two phases, many researchers [39-44] created models in an attempt to solve the heat transfer problem for porous media and they showed that these models asymptoted into LTE models at special conditions. Concurrently, [45-52] compared the LTNE and LTE models for cases from metallic and non-metallic packed beds to microchannel heat sinks and annulus partially filled with porous media. They came up with criteria under which the LTE assumption was valid. Reddy and Narasimhan [53] numerically

UNIVERSITEIT VAN PRETORIA
UNIVERSITY OF PRETORIA
YUNIBESITHI YA PRETORIA


investigated a similar case where there was interplay between internal heat generation and externally driven natural convection inside a vertical porous annulus under steady-state conditions.

Whitaker [54] discusses constraints that should be satisfied when LTE is assumed. He suggests that these constraints must be satisfied when the following conditions are imposed: the solid and fluid phases' thermal diffusivities ratio must be equal, the thermal conductivities ratio must be equal, and the non-slip condition must hold. [55] and [56] developed LTE models for metallic foams porous channels where they respectively discovered that the LTE assumption was valid even if the solid thermal conductivity was markedly higher than that of the fluid, and developed an algorithm that did away with the need to conduct numerical calculations. Alazmi and Vafai [39] investigated the proper boundary condition to be used for a porous channel bounded by walls having a constant heat flux. They found that the Darcy number, porosity, solid-fluid thermal conductivity ratio and Reynolds number all had a significant effect on the results of the different boundary conditions tested, and this was when thermal dispersion and porosity variation were not considered. For a porous matrix with a stagnant fluid and a heat flux, Lage [58] shows that if the fluid and solid phases are in thermal equilibrium at the boundaries, they will then be in thermal equilibrium throughout the entire domain. Kou and Huang [57] investigated the effect of thermal boundary conditions applied to a vertical annular duct embedded in a porous medium. Teng and Zhao [59] developed a model that attempted to extend the applicability of Darcy's law beyond the laminar flow regime as defined by the microscopic Reynolds number of about 10. Optimisation of the performance and configuration of porous structures and systems were the subject of research [60- 65] in which analytical models were developed to that end.

UNIVERSITEIT VAN PRETORIA
UNIVERSITY OF PRETORIA
YUNIBESITHI YA PRETORIA



Effective cooling of a porous medium made up of solid spheres with internal heat generation rate depends on the minimisation of the thermal resistance between the porous matrix and the fluid. Conditions under which minimisation of the thermal resistance can take place include the surfaces of the solid spheres and the fluid cooling them being in LTE with one another. The porous matrix under consideration was made up of solid spheres and the determination of the optimum porous properties would essentially mean the determination of the optimum sphere diameter at which the thermal resistance was minimised, for a given porosity. Therefore, the aim of the study was to determine the optimum diameter of the same size solid spheres with internal heat generation forming a porous matrix that resulted in minimum thermal resistance of the porous medium as the spheres were being cooled by air flowing through the porous matrix. This was done for a forced convection laminar flow under steady-state conditions.

## 6.2. ANALYTICAL LTE MODEL

The case under investigation was a cylindrical porous domain with adiabatic walls, saturated with a fluid, as shown in Figure 6-1.

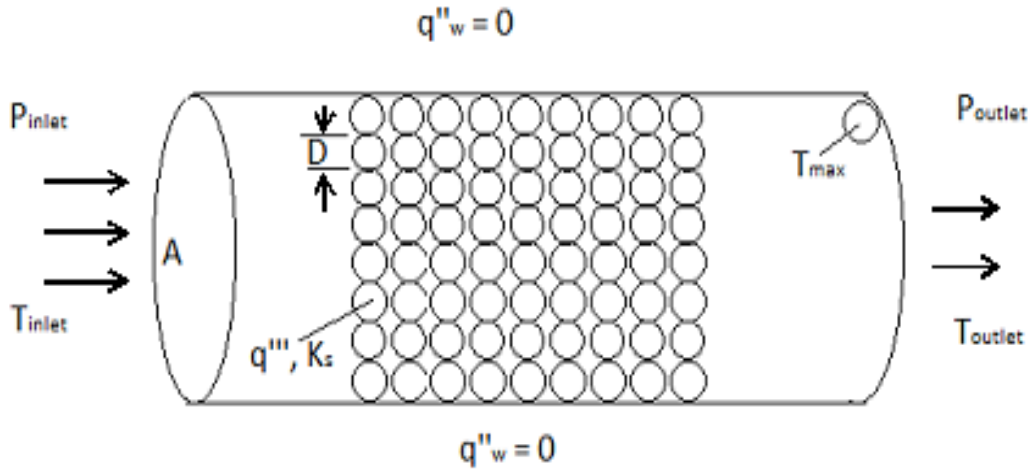


**Figure 6-1: Sketch of the porous medium domain.**

UNIVERSITEIT VAN PRETORIA
UNIVERSITY OF PRETORIA
YUNIBESITHI YA PRETORIA



Thermal resistance between the point at a temperature $T_{\max}$ and the point at a temperature $T_{\min}$, as shown in Figure 6-1 in a porous medium, as given by Eq. (6-1), shows that it is directly proportional to the temperature difference between the two points, if the rate of heat transfer is assumed to be constant. In this instance, the heat transferred was due to the internal heat generation density, $q''$, inside the solid spheres. Here the inlet temperature is defined as the domain minimum temperature, i.e. $T_{inlet} = T_{\min}$.

$$R_T = \frac{\left(T_{\max} - T_{\min}\right)}{q} \qquad \textbf{(6-1)}$$

From this expression, it can be seen that in order to minimise the thermal resistance, all that is required is to minimise the temperature difference. Because the porous medium was made up of air and solid spheres with internal heat generation, the rate of heat transfer is given by $q = (1-\phi)q'''AL$, where $\phi, q''', A$ and $L$ are the porosity, Heat density, cross-sectional area and the length of the porous medium respectively. However, this rate of heat transfer must equal the rate of heat removal by the air flowing through the porous medium, as given by Eq. (6-2), because steady-state conditions were assumed.

$$q = \dot{m}c_p\left(T_{outlet} - T_{\min}\right) \qquad \textbf{(6-2)}$$

$\dot{m}$ is the fluid mass flow rate, $c_p$ is the heat capacity of the fluid at constant pressure and $T_{\max}$ is the maximum temperature at the centre of a sphere. The mass flow rate of the air flowing with an average superficial velocity $u$ through the porous medium is $\dot{m} = \rho A u$, where $\rho$ is the density of the fluid. Given that laminar flow was assumed for the air flowing through the porous medium, Darcy's law [91] was used to express the superficial velocity for a unidirectional driven flow, as given by Eq. (6-3):

$$u = \frac{K\Delta P}{\mu L} \qquad \textbf{(6-3)}$$

UNIVERSITEIT VAN PRETORIA
UNIVERSITY OF PRETORIA
YUNIBESITHI YA PRETORIA



Where $K, \Delta P$ and $\mu$ are the porous medium permeability, pressure drop and fluid dynamic viscosity. Because the solid matrix of the porous medium was made up of solid spheres, the permeability is given by the Carman-Kozeny equation [91], as expressed by Eq. (6-4):

$$K = \frac{D^2 \phi^3}{180(1-\phi)^2} \tag{6-4}$$

$D$ is the sphere diameter. The temperature difference between the outlet and inlet of the porous medium can be expressed in terms of the diameter of the solid spheres by simply substituting Eqs. (6-3, 6-4), into Eq. (6-2), and rearranging the terms to give Eq. (6-5):

$$T_{outlet} - T_{\min} = 180\left(\frac{1-\phi}{\phi}\right)^3 \frac{\mu q''' L^2}{\rho c_p \Delta P D^2} \tag{6-5}$$

The temperature profile of the hottest solid sphere is $T_{\max} - T_{outlet} = q''' D^2 / 24 k_s$. Combining the temperature profile of the hottest solid sphere with Eq. 7-5 results in an expression for the temperature difference between two points in the porous medium having the maximum and minimum temperatures, as given by Eq. (6-6):

$$T_{\max} - T_{\min} = \frac{q''' D^2}{24 k_s} + 180\left(\frac{1-\phi}{\phi}\right)^3 \frac{\mu q''' L^2}{\rho c_p \Delta P D^2} \tag{6-6}$$

However, the aim of the analysis is the minimisation of $T_{\max} - T_{\min}$ with respect to $D$. This results in the optimum sphere diameter as given by Eq. (6-7):

$$D_{opt} = 8.107\left(\frac{1-\phi}{\phi}\right)^{3/4} \sqrt[4]{\frac{\mu k_s L^2}{\rho c_p \Delta P}}$$

$$D_{opt} = 8.107\left(\frac{1-\phi}{\phi}\right)^3 L \gamma^{1/4} Be^{-1/4} \tag{6-7}$$

where $\gamma = k_s / k_f$ is the solid/fluid thermal conductivity ratio and $Be = \Delta P L^2 / \alpha \mu$ is the Bejan number [92, 93] representing the dimensionless pressure drop across the porous medium. $\alpha = k_f / \rho c_p$ is the thermal diffusivity of the fluid.

UNIVERSITEIT VAN PRETORIA
UNIVERSITY OF PRETORIA
YUNIBESITHI YA PRETORIA



The minimum temperature difference that corresponds to the optimum diameter is given by Eq. (6-8):

$$\left(T_{\max}-T_{\min}\right)_{\min}=5.477\left(\frac{1-\phi}{\phi}\right)^{3/2}\frac{q'''L^2}{k_f}Be^{-1/2}\gamma^{-1/2} \qquad \textbf{(6-8)}$$

When Eq. (6-8) is substituted into Eq. (6-1), the result is the minimum thermal resistance, as given by Eq. (6-9):

$$\left(R_T\right)_{\min}=5.477\frac{(1-\phi)^{1/2}}{\phi^{3/2}}\frac{LBe^{-1/2}\gamma^{-1/2}}{Ak_f} \qquad \textbf{(6-9)}$$

Eqs. (6-8 and 6-9) express the minima temperature difference and thermal resistance in terms of porosity respectively; however, it is also useful to express both minima in terms of the optimum diameter by substituting Eq. (6-7) into Eqs. (6-8 and 6-9). The expression for the minimum temperature difference as a function of optimum diameter is given by Eq. (6-10) and that for the minimum thermal resistance is given by Eq. (6-11). Note the disappearance of $q'''$ and *Be* in Eq. (6-11) when expressed in terms of $D_{opt}$.

$$\left(T_{\max}-T_{\min}\right)_{\min}=\frac{q'''D_{opt}^2}{12k_s} \qquad \textbf{(6-10)}$$

$$\left(R_T\right)_{\min}=\frac{D_{opt}^2}{12ALk_s(1-\phi)} \qquad \textbf{(6-11)}$$

The optimum diameter, the minimum temperature difference and minimum thermal resistance are all normalised with respect to their respective values at a porosity of $\phi=0.1$. The normalised optimum diameter, $\psi_{opt}$, the minimum temperature difference, $\theta_{\min}$ and minimum thermal resistance, $\eta_{\min}$ are given by Eqs. (6-12, 6-13 and 6-14) respectively:

UNIVERSITEIT VAN PRETORIA
UNIVERSITY OF PRETORIA
YUNIBESITHI YA PRETORIA



$$\psi_{opt} = \frac{D_{opt}}{\left(D_{opt}\right)_{\phi=0.1}} = \frac{\left(\frac{1-\phi}{\phi}\right)^{3/4}}{\left(\frac{1-\phi}{\phi}\right)^{3/4}_{\varphi=0.1}} \quad \textbf{(6-12)}$$

$$\theta_{\min} = \frac{\left(\frac{1-\phi}{\phi}\right)^{3/2}}{\left(\frac{1-\phi}{\phi}\right)^{3/2}_{\phi=0.1}} = \psi_{opt}^{2} \quad \textbf{(6-13)}$$

$$\eta_{\min} = \frac{\left[\frac{(1-\phi)^{1/2}}{\phi^{3/2}}\right]}{\left[\frac{(1-\phi)^{1/2}}{\phi^{3/2}}\right]_{\phi=0.1}} = \frac{0.9}{(1-\phi)}\psi_{opt}^{2} \quad \textbf{(6-14)}$$

## 6.3. NUMERICAL ANALYSIS

The numerical porous medium model in ANSYS Fluent 14.0 [94] was used to conduct comparative simulations for the study. Unlike the analytical model, Eq. (6-6), where the porous medium and the heat conduction inside the solid spheres were modelled, the numerical model modelled only the porous medium. The flow was driven by a unidirectional pressure gradient across the porous medium.

Steady state was assumed and a three-dimensional domain was also assumed. A further assumption made was that the flow was laminar. With all these assumptions in mind, the flow physics in the porous medium is given by Eqs. (6-15 to 6-17).

The continuity equation for the porous medium is given by:

$$\nabla.(\rho u) = 0 \quad \textbf{(6-15)}$$

The momentum equation is given by Darcy's law:

$$-\frac{dP}{dx} = \frac{\mu u}{K} \quad \textbf{(6-16)}$$

The energy equation is given by:

UNIVERSITEIT VAN PRETORIA
UNIVERSITY OF PRETORIA
YUNIBESITHI YA PRETORIA


$$\rho C_p \vec{v}.\nabla T = k_m \nabla^2 T + q'''_m \quad \textbf{(6-17)}$$

where

$$k_m = \phi k_f + (1-\phi)k_s \quad \textbf{(6-18)}$$

and

$$q'''_m = (1-\phi)q''' \quad \textbf{(6-19)}$$

The optimum diameter as given by Eq. (6-7) is used together with the Carman-Kozeny equation Eq. (6-4) to compute the viscous resistance to be inserted into the numerical model. The diameter and length of the porous domain are both 2000 mm.

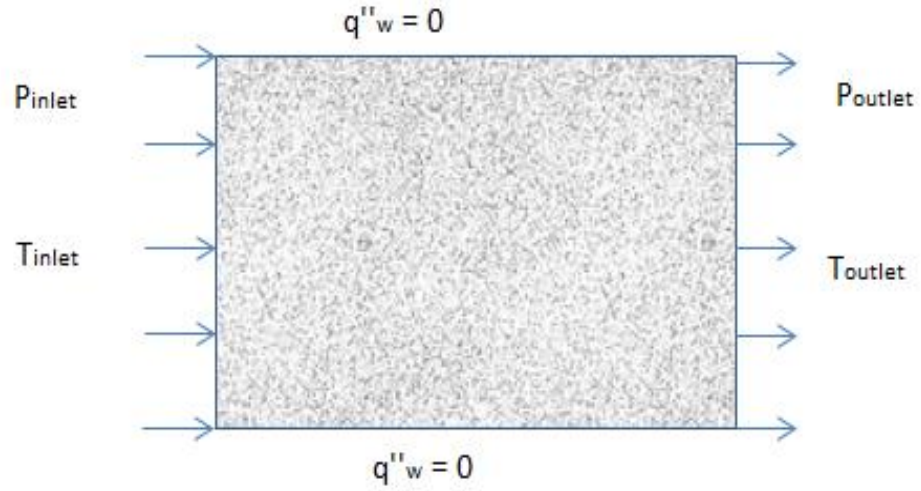


**Figure 6-2: Sketch of the numerical porous medium domain with boundary conditions.**

The porous medium domain as represented by Figure 6-2 was sandwiched between an upstream and a downstream domain (which are not shown in Figure 6-2 for clarity) used for implementing the inlet and outlet conditions because ANSYS Fluent 14.0 [94] did not allow direct application of inlet and outlet boundaries on porous domains. The upstream domain was a fluid domain that was made up of an adiabatic circumferential wall boundary with a non-slip condition and a pressure inlet boundary. The third boundary was simply an interface between the domain and the porous domain connected to it. The static pressure on the inlet

UNIVERSITEIT VAN PRETORIA
UNIVERSITY OF PRETORIA
YUNIBESITHI YA PRETORIA



boundary was set equal to the operating pressure and the temperature was set at 25 °C. This domain had 8 535 hexahedral cells.

The porous domain was made up of an adiabatic non-slip circumferential wall boundary and two interface boundaries connecting it to the upstream and downstream domains. The domain had 17 070 hexahedral cells. The downstream domain was a fluid domain. The domain had an interface boundary connecting it to the porous domain, a non-slip adiabatic circumferential wall boundary and a pressure outlet boundary. The change in pressure difference was modelled by varying the gauge pressure of the pressure outlet boundary. The domain had 17 070 hexahedral cells. The grid independence of the numerical solution was conducted using the temperature difference, $\Delta T = T_{outlet} - T_{inlet}$ as the figure of merit. This was conducted for $q''' = 10^5 W/m^3$ , $\Delta P = P_{inlet} - P_{outlet} = 6kPa$ and $\phi = 0.1$. The relative change metric used to check the change in temperature difference from a coarser grid to a finer grid was simply $\left(\Delta T_{finer} - \Delta T_{coarser}\right)/\Delta T_{finer}$. As can be seen from Table 6-1, the change from 2 460 cells through to 17 070 cells was constant. For this reason, the 17 070 cells were chosen for the numerical simulations since there was no computational time penalty.

**Table 6-1: Grid independence study using air as the fluid and wood as the solid, for ΔP = 6 kPa and φ = 0.1.**

| Number of cells | ΔT (°C) | Relative change |
|---|---|---|
| 1230 | 56.51124 | |
| 2460 | 57.72587 | 0.021 |
| 4920 | 58.33546 | 0.0104 |
| 17070 | 57.73561 | 0.0104 |

UNIVERSITEIT VAN PRETORIA
UNIVERSITY OF PRETORIA
YUNIBESITHI YA PRETORIA



The implicit pressure-based solver was selected, with the superficial velocity for the porous formulation. The PRESTO! [94] discretisation scheme was used for the pressure, and the second-order upwind schemes were selected for the density, energy and mass discretisation.

Two cases were run where the fluid phase was modelled by first using air and then liquid water. An assumption was made that the fluid (except for the density of air) and thermal properties of the solid spheres and fluid were constant. The heat generation rate density that came from the solid phase used in the numerical simulations was $q''' = 10^5 W/m^3$. For the LTE assumption to be valid for the porosity range of $0.1 \le \phi \le 0.9$, the thermal conductivities of the fluid and solid phases making up the porous medium had to be of the same order of magnitude. For this reason, wood properties (which is important in biomass energy systems) with $k_s = 0.173 W/m.K$ and silica/sand properties (which is important in coal bubbling bed boilers systems) with $k_s = 0.2 W/m.K$ were used to model the solid phase properties in the ANSYS Fluent 14 porous medium model. The thermal conductivities of air and liquid water were 0.0242 W/m.K and 0.6 W/m.K respectively.

## 6.4. RESULTS AND DISCUSSION

From Eq. (6-7), it followed that the optimum diameter did not depend on the internal heat generation rate from the solid spheres, suggesting that this optimum diameter solution was robust when applied to a porous medium. This same quality of robustness was also observed with respect to the minimum thermal resistance, as expressed by Eq. (6-11), because it too was independent of the internal heat generation rate from the solid spheres. The normalised optimum diameter was evaluated for a porosity range of $0.1 \le \phi \le 0.9$, and this was plotted in Figure 6-3.

UNIVERSITEIT VAN PRETORIA
UNIVERSITY OF PRETORIA
YUNIBESITHI YA PRETORIA



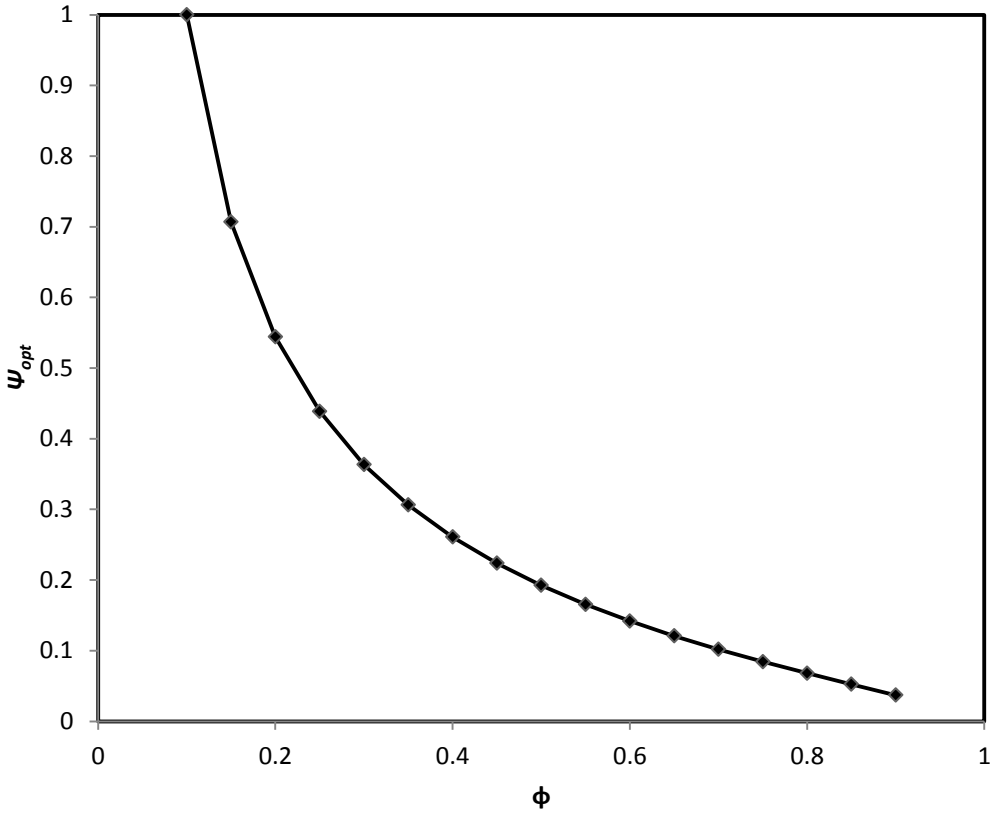


**Figure 6-3: The variation of the normalised optimum diameter with porosity.**

Figure 6-3 shows that the optimum diameter decreases non-linearly with increasing porosity. The comparison between the results from Eq. (6-13) and those from the normalised ANSYS Fluent 14 (for both air and liquid water) for the normalised minimum temperature difference with respect to the result at a porosity of $\phi = 0.1$ is shown in Figure 6-4 as functions of normalised optimum diameter. Results for the normalised minimum thermal resistance were

UNIVERSITEIT VAN PRETORIA
UNIVERSITY OF PRETORIA
YUNIBESITHI YA PRETORIA


also plotted on the same figure.

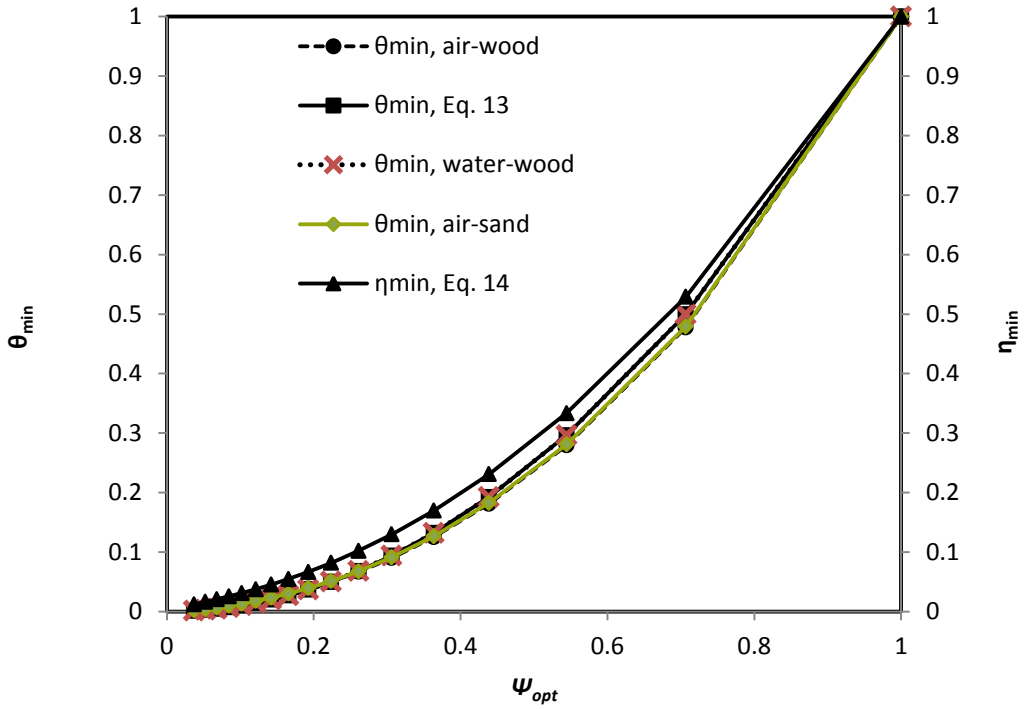


**Figure 6-4: The variation of the normalised minima temperature difference and thermal resistance with normalised optimum sphere diameter.**

Figure 6-4 shows that the analytical solution compares very well with numerical results for both air and liquid water. This shows that the LTE assumption made in the derivation of the analytical model was valid because the fluid to solid thermal conductivities ratio for both air and liquid water was close to unity or less. From Figure 6-4, it can also be seen that the analytical solution compared much better with the liquid water numerical results than with those of air. This could be the result of the densities of the liquid water and wood being of the same order of magnitude. This follows from one of the criteria proposed by Whitaker [16], namely that the thermal diffusivities ratio of the fluid and solid phases should be of the same order of magnitude.

The normalised minimum temperature differences together with the normalised minimum thermal resistance were also plotted against the porosity to illustrate the direct relationship between the minima temperature difference and thermal resistance with porosity. As was the case for Figure 4, this comparison between the analytical model and the numerical model was done for both air and liquid water, and was plotted in Figure 6-5.

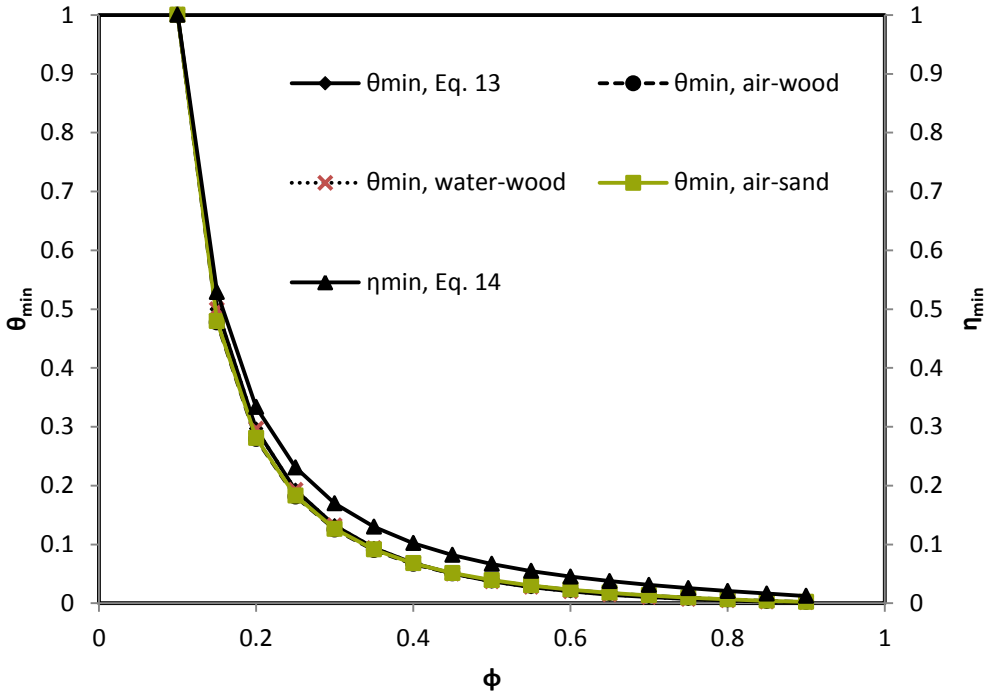


**Figure 6-5: The variation of the normalised minima temperature difference and thermal resistance with porosity.**

Again the analytical solution compared very well with both numerical solutions, but compared much better with the liquid water numerical solution because of the thermal diffusivities of the fluid and solid phases being of the same order of magnitude.

Another observation is that the absolute value of the minimum temperature difference predicted by ANSYS Fluent 14 was about half the value predicted by the analytical model, as expressed by Eq. (6-10). This is illustrated in Figures 6-6 and 6-7 where

UNIVERSITEIT VAN PRETORIA
UNIVERSITY OF PRETORIA
YUNIBESITHI YA PRETORIA



$\Delta T_{\min} = \left(T_{\max} - T_{\min}\right)_{\min}$. Figure 6-6 shows the comparison results for air-wood porous medium, and Figure 6-7 shows the comparison for liquid water-wood porous medium.

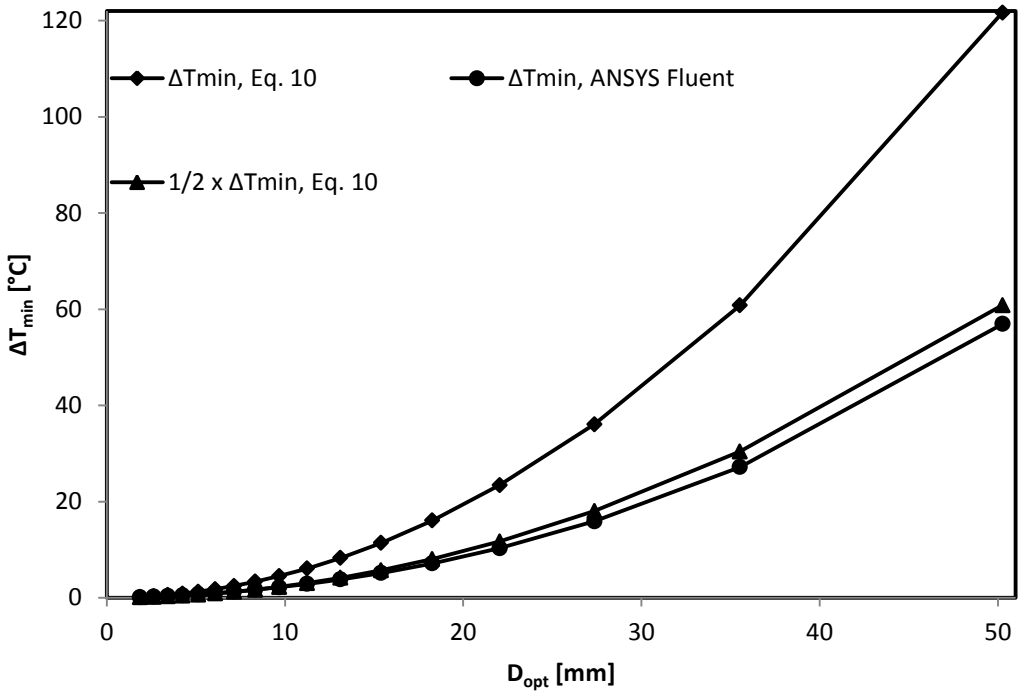


**Figure 6-6: The variation of the minimum temperature difference with optimum sphere diameter for air-wood porous medium.**

UNIVERSITEIT VAN PRETORIA
UNIVERSITY OF PRETORIA
YUNIBESITHI YA PRETORIA


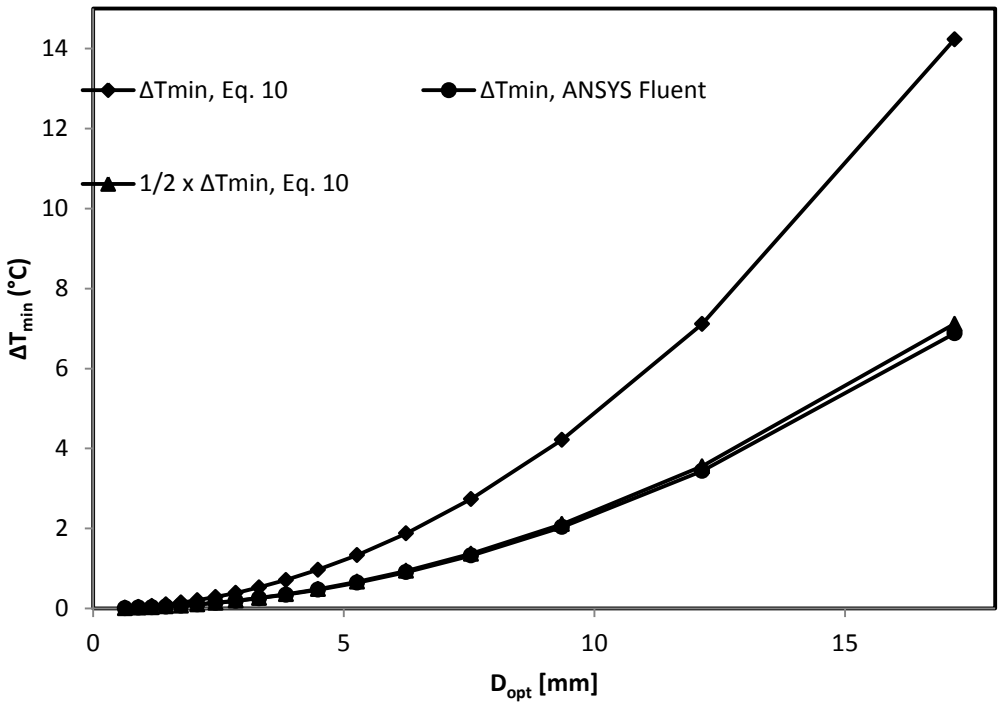


**Figure 6-7: The variation of the minimum temperature difference with optimum sphere diameter for liquid water-wood porous medium.**

For both Figure 6-6 and Figure 6-7, half the value from the analytical solution was also plotted to illustrate the point that the porous model in ANSYS Fluent 14 predicted half the value of the minimum temperature difference of that predicted by the analytical model. This meant that for optimum sphere diameter, the temperature difference between the centre of the hottest solid sphere and its surface was equal to the temperature difference between the sphere surface and the coolest point in the porous medium. This prediction of half the value by ANSYS Fluent 14 was because the numerical code only modelled heat transfer between the surfaces of the spheres and the fluid.

## 6.5. CONCLUSION

The optimum sphere diameter expression was determined analytically and was found to be independent of the heat generation rate of the solid spheres. This quality was found to be the

UNIVERSITEIT VAN PRETORIA
UNIVERSITY OF PRETORIA
YUNIBESITHI YA PRETORIA



same for the corresponding minimum thermal resistance. It can be concluded that the optimum solid sphere diameter and the minimum thermal resistance were both robust when applied to a porous medium where the LTE assumption was valid. The minimum temperature difference analytical solution compared very well with the numerical solutions when air and liquid water properties were used for the fluid phase and wood and silica properties were used for the solid phase. The absolute value of the minimum temperature difference predicted by the ANSYS Fluent 14 was about half the value predicted by the derived analytical model. Because the minimum thermal resistance was directly proportional to the minimum temperature difference, the same conclusion could be drawn, namely that the absolute value of the minimum thermal resistance predicted by ANSYS Fluent 14 would be about half the value predicted by the analytical model.

UNIVERSITEIT VAN PRETORIA
UNIVERSITY OF PRETORIA
YUNIBESITHI YA PRETORIA


# Chapter 7. CONCLUSIONS AND RECOMMENDATIONS

## 7.1. INTRODUCTION

The study focused on the search of the most optimum operating conditions that can make the case of the viability of wood combustion as an alternative to coal combustion as an energy source. The conclusions to each phenomena studied are presented individually in the next section. Recommendations in terms of furthering the study are also given.

## 7.2. CONCLUSIONS

- The second law efficiency of a pine wood-fired adiabatic combustor was found to drop as the air excess percentage of air was increased from that needed for theoretical combustion. However, the efficiency was found to increase as the incoming air temperature was increased from the reference value of 298 K. This phenomenon was observed to continue until the efficiency exceeded that of theoretical combustion for incoming air temperature of 1 100 K and greater. This observed phenomenon was even more pronounced for CFD results.
- The entropy generation rates due to the combustion and frictional pressure drop processes were analysed in order to calculate the irreversibilities generated in the adiabatic combustor. It was found that the entropy generation rate due to frictional pressure drop was negligible when compared with that due to combustion. An analysis was conducted of the irreversibilities generated during the combustion process of an adiabatic combustor with a fixed geometry and it was found that a minimum was reached when the air-fuel mass ratio was 4.9. At about this air-fuel mass ratio, the molecular hydrogen and water vapour were at equal amounts of molar

fraction and the carbon dioxide molar fraction was at its minimum for a rich mixture. This resulted in the combined contribution from $H_2$, $H_2O$ and $CO_2$ to the entropy generation rate being the lowest at an AF of 4.9 than at any other AF; hence a minimum entropy generation rate since they have the most significant molar fractions other than $N_2$.

- The changing of incoming air temperature into a circulating fluidised bed adiabatic combustor from 298 K to 400 K resulted in a small change in AF, at which minimum entropy generation rate occurred, from 4.9 to 4.8. The penalty paid when deviating from that point reduced drastically from 46% for Case 2 with incoming air temperature of 298 K to 5% for Case 1 with incoming air temperature of 400 K when the combustor was run at an AF of 4.6. On the other hand, the changing of the wall condition from adiabatic to a negative heat flux resulted in a change in AF, at which minimum entropy generation rate occurred, from 4.8 to 6. For a combustor with a heat flux of -7 500 W/m2 wall condition and an infinitesimally thin wall simulated at an AF of 6, an optimum diameter of 0.32 m resulted in the minimum entropy generation rate. However, when the combustor wall thickness was taken into consideration, the optimum diameter got smaller with increasing wall thickness. It was also found that the sum of twice the wall thickness and the optimum diameter always added up to the optimum diameter when the wall thickness was infinitesimally small. Taking into account the wall thickness resulted in lower entropy generation rates and this was attributed to improved convective heat transfer when the optimum diameter got smaller. The penalty paid for deviating from the optimum diameter was also reduced with increased wall thickness for smaller diameters, as measured through the entropy generation number.

UNIVERSITEIT VAN PRETORIA
UNIVERSITY OF PRETORIA
YUNIBESITHI YA PRETORIA


- The optimum sphere diameter expression was determined analytically and was found to be independent of the heat generation rate of the solid spheres. This same quality was found to be the same for the corresponding minimum thermal resistance. It can be concluded that the optimum solid sphere diameter and the minimum thermal resistance were both robust when applied to a porous medium where the LTE assumption was valid. The minimum temperature difference analytical solution compared very well with numerical solutions when air and liquid water properties were used for the fluid phase and wood and silica properties were used for the solid phase. The absolute value of the minimum temperature difference predicted by the ANSYS Fluent 14 was about half the value predicted by the derived analytical model. Because the minimum thermal resistance was directly proportional to the minimum temperature difference, the same conclusion could be drawn, namely that the absolute value of the minimum thermal resistance predicted by ANSYS Fluent 14 would be about half the value predicted by the analytical model.

## 7.3. RECOMMENDATIONS

All the optimisations of the circulating fluidised combustor that were done in the study were focused at one variable at a time. This could be extended by conducting a multivariable optimisation of combustor diameter and air-fuel mass ratio. Also given that the ultimate aim of the study was the generation of heat while reducing carbon dioxide emissions, the co-firing of coal and wood in a combustor could be studied in order to find the optimal blending ratios that result in minimal irreversibilities and low carbon dioxide emissions.

UNIVERSITEIT VAN PRETORIA
UNIVERSITY OF PRETORIA
YUNIBESITHI YA PRETORIA


The modelling of the discarded hot char as a porous medium used for heat recovery could be extended to model turbulent flow through the porous medium, which would be a more realistic scenario.

Given that the circulating fluidised bed combustor was made up of more than the combustor, the thermodynamic analysis and optimisations of other components such as the cyclone separator could also be studied, all in an effort to eventually arrive at an optimised circulating fluidised bed combustor as a whole system.

UNIVERSITEIT VAN PRETORIA
UNIVERSITY OF PRETORIA
YUNIBESITHI YA PRETORIA


# REFERENCES

[1] Moran MJ, Shapiro HN. Fundamentals of engineering thermodynamics. 3rd ed. SI Version. Chichester: John Wiley and Sons Inc; 1998.

[2] Anamalai K, Puri IK. Advanced thermodynamics engineering. Florida: CRC Press Inc; 2002.

[3] Bejan A. Advanced engineering thermodynamics. New York: John Wiley and Sons Inc; 1988.

[4] Bejan A. Entropy generation minimization: the method of thermodynamic optimization of finite-size systems and finite-time processes. Florida: CRC Press Inc; 1996.

[5] Chen W, Chen C, Hung C, Shen C, Hsu H. A comparison of gasification phenomena among raw biomass, torrefied biomass and coal in an entrained-flow reactor. *Applied Energy* 2013; Vol. 112: pp. 421-430.

[6] Tran K, Luo X, Seisenbaeva G, Jirjis R. Stump torrefaction for bioenergy application. *Applied Energy* 2013; Vol. 112: pp. 539-546.

[7] Zhang J, Zhao Z, Zhang G, Xi Z, Zhao F, Dong L, Xu G. Pilot study on jetting pre-oxidation fluidized bed gasification adapting to caking coal. *Applied Energy* 2013; Vol. 110: pp. 276-284.

[8] Louis JJJ, Kok JBW, Klein SA. Modeling and measurements of a 16-kW turbulent nonadiabatic syngas diffusion flame in a cooled cylindrical combustion chamber. *Combustion and Flame* 2001; Vol. 125: pp. 1012-1031.

[9] Li J, Zhong B. Experimental investigation on heat loss and combustion in methane/oxygen micro-tube combustor. *Applied Thermal Engineering* 2008; Vol. 28: pp. 707-716.

UNIVERSITEIT VAN PRETORIA
UNIVERSITY OF PRETORIA
YUNIBESITHI YA PRETORIA



[10] Sivadas HS, Caton JA. Effects of exhaust gas recirculation on exergy destruction due to isobaric combustion for a range of conditions and fuels. *International Journal of Energy Research* 2008; Vol. 32: pp. 896-910.

[11] Mago PJ, Srinivasan KK, Chamra LM, Somayaji C. An examination of exergy destruction in organic Rankine cycles. *International Journal of Energy Research* 2008; Vol. 32: pp. 926-938.

[12] Anheden M, Svedberg G. Exergy analysis of chemical-looping combustion systems. *Energy Conversion and Management* 1998; Vol. 39 (16-18): pp. 1967-1980.

[13] Jin H, Ishida M. A new type of coal gas fuelled chemical-looping combustion. *Fuel*; Vol. 83: pp. 2411-2417.

[14] Saidi MH, Allaf Yazdi MR. Exergy model of a vortex tube system with experimental results. *Energy* 1999; Vol. 24: pp. 625-632.

[15] Rosen MA, Scott DS. Entropy production and exergy destruction: Part I - Hierarchy of Earth's major constituencies. *International Journal of Hydrogen Energy* 2003; Vol. 28: pp. 1307-1313.

[16] Liang SY, Wong TN, Nathan GK. Study on refrigerant circuitry of condenser coils with exergy destruction analysis. *Applied Thermal Engineering* 2000; Vol. 20: pp. 559-577.

[17] Tsatsaronis G, Park M. On avoidable and unavoidable exergy destructions and investments costs in thermal systems. *Energy Conversion and Management* 2002; Vol. 43: pp. 1259-1270.

[18] Kelly S, Tsatsaronis G, Morosuk T. Advanced exergetic analysis: approaches for splitting the exergy destruction into endogenous and exogenous parts. *Energy* 2009; Vol. 34: pp. 384-391.

UNIVERSITEIT VAN PRETORIA
UNIVERSITY OF PRETORIA
YUNIBESITHI YA PRETORIA



[19] Elfasakhany A, Tao L, Espenas B, Larfeldt, Bai XS. Pulverised wood combustion in a vertical furnace: experimental and computational analyses. *Applied Energy* 2013; Vol. 112: pp. 454-464.

[20] Ziebik A, Stanek W. Influence of blast-furnace process thermal parameters on energy and exergy characteristics and exergy losses. *International Journal of Energy Research* 2006; Vol. 30: pp. 203-219.

[21] Ziebik A, Stanek W. Energy and exergy system analysis of thermal improvements of blast-furnace plants. *International Journal of Energy Research* 2006; Vol. 30: pp. 101-114.

[22] Nur Izyan Z, Shuhaimi M. Exergy analysis for fuel reduction strategies in crude distillation unit. *Energy* 2014; Vol. 66: pp. 891-897.

[23] Gupta AVSSKS, Reddy BV. Effect of pressure on thermal aspects in the riser column of a pressurized circulating fluidized bed. *International Journal of Energy Research* 2006; Vol. 30: pp. 149-162.

[24] Cihan A, Hacihafizoglu O, Kahveci K. Energy-exergy analysis and modenization suggestions for a combined-cycle power plant. *International Journal of Energy Research* 2006; Vol. 30: pp. 115-126.

[25] Ghazikhani M, Hatami M, Ganji DD, Gorji-Bandpy M, Behravan A, Shahi G. Exergy recovery from the exhaust cooling in a DI diesel engine for BSFC reduction purposes. *Energy* 2014; Vol. 65: pp. 44-51.

[26] Chintala V, Subramanian KA. Assessment of maximum available work of a hydrogen fuelled compression ignition engine using exergy analysis. *Energy* 2014; Vol. 67: pp. 162-175.

UNIVERSITEIT VAN PRETORIA
UNIVERSITY OF PRETORIA
YUNIBESITHI YA PRETORIA



[27] Jafarmadar S. Multidimensional modelling of the effect of EGR (exhaust gas recirculation) mass fraction on exergy terms in an indirect injection diesel engine. *Energy* 2014; Vol. 66: pp. 305-313.

[28] Kunii D, Levenspiel O. Fluidization Engineering. Stoneham: Massachusetts, 1991.

[29] Gupta AVSSKS, Reddy BV. Effect of pressure on thermal aspects in the riser column of a pressurized circulating fluidized bed. *International Journal of Energy Research* 2006; Vol. 30: pp. 149-162.

[30] Han L, Wang Q, Luo Z, Rong N, Deng G. $H_2$ rich gas production via pressurized fluidized bed gasification of sawdust with in situ $CO_2$ capture. *Applied Energy* 2013; Vol. 109: pp. 36-43.

[31] Aisyah L, Ashman PJ, Kwong CW. Performance of coal fly-ah based oxygen carrier for the chemical looping combustion of synthesis gas. *Applied Energy* 2013; Vol. 109: pp. 44-50.

[32] Ting TW, Hung YM, Guo N. Entropy generation of nanofluid flow with streamwise conduction in microchannels. *Energy* 2014; Vol. 64: pp. 979-990.

[33] Le Roux WG, Bello-Ochende T, Meyer JP. Optimum performance of a small-scale open and direct solar thermal Brayton cycle at various environmental conditions and constraints. *Energy* 2012; Vol. 46 (1): pp. 42-50.

[34] Mwesigye A, Bello-Ochende T, Meyer JP. Numerical investigation of entropy generation in a parabolic through receiver at different concentration ratios. *Energy* 2013; Vol. 53: pp. 114-127.

[35] Le Roux WG, Bello-Ochende T, Meyer JP. Operating conditions of an open and direct solar thermal Bryaton cycle with optimised cavity receiver and recuperator. *Energy* 2011; Vol. 36 (10): pp. 6027-6-36.

UNIVERSITEIT VAN PRETORIA
UNIVERSITY OF PRETORIA
YUNIBESITHI YA PRETORIA



[36] Hua J, Wu M, Kumar K. Numerical simulation of the combustion of hydrogen-air mixture in micro-scaled chambers. Part I: Fundamental study. *Chemical Engineering Science* 2005; Vol. 60: pp. 3497-3506.

[37] Norton DG, Vlachos DG. Combustion characteristics and flame stability at the microscale: a CFD study of premixed methane/air mixtures. *Chemical Engineering Science* 2003; Vol. 58: pp. 4871-4882.

[38] Feng L, Liu Z, Li Y. Numerical study of methane and air combustion inside a small tube with an axial temperature gradient at the wall. *Applied Thermal Engineering* 2010; Vol. 30: pp. 2804-2807.

[39] Alazmi B, Vafai K. Constant wall heat flux boundary conditions in porous media under local thermal non-equilibrium conditions. *International Journal of Heat and Mass Transfer* 2002; Vol. 45: pp. 3071-3087.

[40] Nield DA, Kuznetsov AV, Xiong M. Effect of local thermal non-equilibrium on thermally developing forced convection in a porous medium. *International Journal of Heat and Mass Transfer* 2002; Vol. 45: pp. 4949-4955.

[41] Tao Y-X, Gray DM. Validation of local thermal equilibrium in unsaturated porous media with simultaneous flow and freezing. *International Communication in Heat and Mass Transfer* 1993; Vol. 20: pp. 323-332.

[42] Kuwahara F, Yang S, Ando K, Nakayama A. Exact solutions for a thermal nonequilibrium model of fluid saturated porous media based on an effective porosity. *Journal of Heat Transfer* 2011; Vol. 133.

[43] Amiri A, Vafai K. Analysis of dispersion effects and non-thermal equilibrium, non-Darcian, variable porosity incompressible flow through porous media. *International Journal of Heat and Mass Transfer* 1994; Vol. 37(6): pp. 939-954.

UNIVERSITEIT VAN PRETORIA
UNIVERSITY OF PRETORIA
YUNIBESITHI YA PRETORIA



[44] Nield DA, Kuznetsov AV. Local thermal nonequilibrium effects in forced convection in a porous medium channel: a conjugate problem. *International Journal of Heat and Mass Transfer* 1999; Vol. 42: pp. 3245-3252.

[45] Jiang P, Ren Z, Wang B. Numerical simulation of forced convection heat transfer in porous plate channels using thermal equilibrium and nonthermal equilibrium models. *Numerical Heat Transfer*, Part A 1999; Vol. 35: pp. 99-113.

[46] Kim SJ, Kim D, Lee DY. On the local thermal equilibrium in microchannel heat sinks. *International Journal of Heat and Mass Transfer* 2000; Vol. 43: pp. 1735-1748.

[47] Shivakumara IS, Lee J, Vajravelu K, Mamatha AL. Effects of thermal nonequilibrium and non-uniform temperature gradients on the onset of convection in a heterogeneous porous medium. *International Communication in Heat and Mass Transfer* 2011; Vol. 38: pp. 906-910.

[48] Kim SJ, Jang SP. Effects of the Darcy number, the Prandtl number, and the Reynolds number on local thermal non-equilibrium. *International Journal of Heat and Mass Transfer* 2002; Vol. 45: pp. 3885-3896.

[49] Yang K, Vafai K. Restrictions on the validity of the thermal conditions at the porous-fluid interface: an exact solution. *Journal of Heat Transfer* 2001; Vol. 33.

[50] Haddad OM, Al-Nimr MA, Al-Khateeb AN. Validation of the local thermal equilibrium assumption in natural convection from a vertical plate embedded in porous medium: non-Darcian model. *International Journal of Heat and Mass Transfer* 2004; Vol. 47: pp. 2037-2042.

[51] Lloyd MG, Razani A, Kim KJ. Formulation and numerical solution of non-local thermal equilibrium equations for multiple gas/solid porous metal hydride reactors. *Journal of Heat Transfer* 2001; Vol. 123: pp. 520-526.

UNIVERSITEIT VAN PRETORIA
UNIVERSITY OF PRETORIA
YUNIBESITHI YA PRETORIA



[52] Kuznetsov AV, Vafai K. Analytical comparison and criteria for heat and mass transfer models in metal hydride packed beds. *International Journal of Heat and Mass Transfer* 1995; Vol. 38 (15): pp. 2873-2884.

[53] Reddy BVK, Narasimhan A. Heat generation effects in natural convection inside a porous annulus. *International Communications in Heat and Mass Transfer* 2010; Vol. 37: pp. 607-610.

[54] Whitaker S. Improved constraints for the principle of local thermal equilibrium. *Industrial Engineering Chemical Resources* 1991; Vol. 30 (5).

[55] Boomsma K, Poulikakos D. On the effective thermal conductivity of a three-dimensionally structured fluid-saturated metal foam. *International Journal of Heat and Mass Transfer* 2001; Vol. 44: pp. 827-836.

[56] Jeng T, Tzeng S, Hung Y. An analytical study of local thermal equilibrium in porous heat sinks using fin theory. *International Journal of Heat and Mass Transfer* 2006; Vol. 49: pp. 1907-1914.

[57] Kou H, Huang D. Fully developed laminar mixed convection through a vertical annular duct filled with porous media. *International Communication in Heat and Mass Transfer* 1997; Vol. 24 (1): pp. 99-110.

[58] Lage JL. The implications of the thermal equilibrium assumption for surrounding-driven steady conduction within a saturated porous medium layer. *International Journal of Heat and Mass Transfer* 1999; Vol. 42: pp. 477-485.

[59] Teng H, Zhao TS. An extension of Darcy's law to non-stokes flow in porous media. *Chemical Engineering Science* 2000; Vol. 55: pp. 2727-2735.

[60] Bello-Ochende T, Meyer JP, Ighalo FU. Combined numerical optimization and constructal theory for the design of microchannel heat sinks. *Numerical Heat Transfer, Part*

UNIVERSITEIT VAN PRETORIA
UNIVERSITY OF PRETORIA
YUNIBESITHI YA PRETORIA



*A: Applications: An International Journal of Computation and Methodology* 2010; Vol. 58 (11): pp. 882-899.

[61] Bello-Ochende T, Meyer JP, Bejan A. Constructal mult-scale pin fins. *International Journal of Heat and Mass Transfer* 2010; Vol. 53 (13-14): pp. 2773-2779.

[62] Lorente S, Bejan A. Heterogeneous porous media as multiscale structures for maximum flow access. *Journal of Applied Physics* 2006; Vol. 100.

[63] Ordonez JC, Bejan A, Cherry RS. Designed porous media: optimally nonuniform flow structures connecting one point with more points. *International Journal of Thermal Sciences* 2003; Vol. 42: pp. 857-870.

[64] Combelles L, Lorente S, Anderson R, Bejan A. Tree-shaped fluid flow and heat storage in a conducting solid. *Journal of Applied Physics* 2012; Vol. 111.

[65] Cho K, Lee J, Kim M, Bejan A. Vascular design of constructal structures with low flow resistance and nonuniformity. *International Journal of Thermal Sciences* 2010; Vol. 49: pp. 2309-2318.

[66] Wei D, Lu X, Lu Z, Gu J. Performance analysis and optimization of organic Rankine cycle (ORC) for waste heat recovery. *Energy Conversion and Management* 2007; Vol. 48: pp. 1113-1119.

[67] Tillman DA, Rossi AJ, Kitto WD. Wood combustion: principles, processes and economics. New York: Academic Press Inc; 1981.

[68] ANSYS FLUENT Release 14.0. Theory Guide. ANSYS Inc.: Southpointe, 2011.

[69] Eisenschitz RK. Matrix algebra for physicists. London: Heinemann Educational Books Ltd; 1966.

[70] Kraus AD. Matrices for engineers. Washington: Hemisphere Publishing Corporation; 1987.

UNIVERSITEIT VAN PRETORIA
UNIVERSITY OF PRETORIA
YUNIBESITHI YA PRETORIA



[71] Browne ET. Introduction to the theory of determinants and matrices. Chapel Hill: The University of North Carolina Press; 1958.

[72] Duffy DG. Advanced engineering mathematics with Matlab. 2nd ed. Florida: CRC Press LLC; 2003.

[73] Baloyi J, Bello-Ochende T, Meyer JP. "The analysis of exergy destruction of a wood fired adiabatic combustor". International Conference on Applied Energy. Pretoria, South Africa, 2013.

[74] Aghbalou F, Badia F, Illa J. Exergetic optimization of solar collector and thermal energy storage system. *International Journal of Heat and Mass Transfer* 2006; Vol. 49: pp. 1255-1263.

[75] Kousksou T, Strub F, Castaing Lasvignottes J, Jamil A, Bedecarrats JP. Second law analysis of latent thermal storage for solar system. *Solar Energy Materials & Solar Cells* 2007; Vol. 91: pp. 1275-1281.

[76] Li Y, He Y, Wang Z, Xu C, Wang W. Exergy analysis of two phase change materials storage for solar thermal power with finite-time thermodynamics. *Renewable Energy* 2012; Vol. 39: pp. 447-454.

[77] Jegadheeswaran S, Pohekar SD, Kousksou T. Exergy based performance evaluation of latent heat thermal storage system: a review. *Renewable and Sustainable Energy Reviews* 2010; Vol. 14: pp. 2580-2595.

[78] Brandvoll O, Bolland O. "Inherent CO_2 capture using chemical looping combustion in a natural gas fired power cycle". Proceedings of ASME TURBO EXPO: Amsterdam, The Netherlands, 2002.

[79] Srinivas T, Gupta AVSSKS, Reddy BV, Nag PK. Parametric analysis of a coal based combined cycle power plant. *International Journal of Energy Research* 2006; Vol. 30: pp. 19-36.

[80] Bapat SM, Majali VS, Ravindranath G. Exergetic evaluation and comparison of quintuple effect evaporation units in Indian sugar industries. *International Journal of Energy Research* 2013; Vol. 37: pp. 1415-1427.

[81] Ghazikhani M, Hatami M, Safari B, Ganji DD. Experimental investigation of performance improving and emissions reducing in a two stroke SI engine by using ethanol additives. *Propulsion and Power Research* 2013; Vol. 2(4): pp. 276-283.

[82] Ghazikhani M, Hatami M, Safari B. The effect of alcoholic fuel additives on exergy parameters and emissions in a two stroke gasoline engine. *Arabic Journal of Science and Engineering* 2014; Vol. 39: pp. 2117-2125.

[83] Hua J, Wu M, Kumar K. Numerical simulation of the combustion of hydrogen-air mixture in micro-scaled chambers. Part II: CFD analysis for a micro-combustor. *Chemical Engineering Science* 2005; Vol. 60: pp. 3507-3515.

[84] Baloyi J, Bello-Ochende T, Meyer JP. Thermodynamic optimisation and computational analysis of irreversibilites in a small-scale wood-fired circulating fluidised bed adiabatic combustor. *Energy* 2014; Vol. 70: pp. 653-663.

[85] Le Roux WG, Bello-Ochende T, Meyer JP. Optimum performance of a small-scale open and direct solar thermal Brayton cycle at various environmental conditions and constraints. *Energy* 2012; Vol. 46 (1): pp. 42-50.

[86] Mwesigye A, Bello-Ochende T, Meyer JP. Numerical investigation of entropy generation in a parabolic through receiver at different concentration ratios. *Energy* 2013; Vol. 53: pp. 114-127.

UNIVERSITEIT VAN PRETORIA
UNIVERSITY OF PRETORIA
YUNIBESITHI YA PRETORIA



[87] Le Roux WG, Bello-Ochende T, Meyer JP. Operating conditions of an open and direct solar thermal Brayton cycle with optimised cavity receiver and recuperator. *Energy* 2011; Vol. 36 (10): pp. 6027-6036.

[88] Baloyi J, Bello-Ochende T, Meyer JP. "The analysis of exergy destruction of a wood fired adiabatic combustor". International Conference on Applied Energy. Pretoria, South Africa, 2013.

[89] White FM. Viscous fluid flow. 3rd ed., International Edition. McGraw-Hill: Singapore, 2006.

[90] Nield DA, Bejan A. Convection in porous media. 3rd ed., Springer: New York, 2006, pp. 7.

[91] Bhattacharjee S, Grosshandler WL. The formation of wall jet near a high temperature wall under microgravity environment, *ASME HTD 96*, 1988, pp. 711-716.

[92] Petrescu S. Comments on the optimal spacing of parallel plates cooled by forced convection. *International Journal of Heat and Mass Transfer* 1994, Vol. 37: pp. 1283.

[93] ANSYS FLUENT Release 16.2. Theory Guide. ANSYS Inc.: Southpointe, 2011.

[94] Ziviani D, Beyene A, Venturini M. Advances and challenges in ORC systems modeling for low grade thermal energy recovery. *Applied Energy* 2014; Vol. 121: pp. 79-95.

[95] Toffolo A, Lazzaretto A, Manente G, Paci M. A multi-criteria approach for the optimal selection of working fluid and design parameters in organic Rankine cycle systems. *Applied Energy* 2014; Vol. 121: pp. 219-232.

[96] Zhang J, Liu P, Zhou Z, Ma L, Li Z, Ni W. A mixed-integer nonlinear programming approach to the optimal design of heat network in a polygeneration energy system. *Applied Energy* 2014; Vol. 114: pp. 146-154.

UNIVERSITEIT VAN PRETORIA
UNIVERSITY OF PRETORIA
YUNIBESITHI YA PRETORIA



[97] Li Y, Wang X, Ding Y. An optimal design methodology for large-scale gas liquefaction. *Applied Energy* 2012; Vol. 99: pp. 484-490.

[98] Lian ZT, Chua KJ, Chou SK. A thermodynamic analysis of biomass energy for trigeneration. *Applied Energy* 2010; Vol. 87: pp. 84-95.

[99] Qian Y, Liu J, Huang Z, Kraslawski A, Cui J, Huang Y. Conceptual design and system analysis of a poly-generation system for power and olefin production from natural gas. *Applied Energy* 2009; Vol. 86: pp. 2088-2095.

[100] Blanco-Marigorta AM, Suarez-Medina J, Vera-Castellano A. Exergetic analysis of a biodiesel production process from Jatropha curcas. *Applied Energy* 2013; Vol. 101: pp. 218-225.

[101] Kohl T, Teles M, Melin K, Laukkanen T, Jarvinen M, Park SW, Guidici R. Exergoeconomic assessment of CHP-intergrated biomass upgrading. *Applied Energy* 2015; Vol. 156: pp. 290-305.

[102] Li S, Jin H, Gao L, Zhang X. Exergy analysis and the energy saving mechanism for coal to synthetic/substitute natural gas and power cogeneration system without and with CO2 capture. *Applied Energy* 2014; Vol. 130: pp. 552-561.

[103] McTigue JD, White AJ, Markides CN. Parametric studies and optimisation of pumped thermal electricity storage. *Applied Energy* 2015; Vol. 137: pp. 800-811.

[104] Arjmandi HR, Amani E. A numerical investigation of the entropy generation in and thermodynamic optimization of a combustion chamber. *Energy* 2015; Vol. 81: pp. 706-718.

[105] Baklacoiglu T, Turan O, Aydin H. Dynamic modelling of exergy efficiency of turboprop engine components using hybrid genetic algorithm-artificial neural networks. *Energy* 2015; Vol. 86: pp. 709-721.

UNIVERSITEIT VAN PRETORIA
UNIVERSITY OF PRETORIA
YUNIBESITHI YA PRETORIA



[106] Blanco-Marigorta AM, Masi M, Manfrida G. Exergo-environmental analysis of a reverse osmosis desalination plant in Gran Canaria. *Energy* 2014; Vol. 76: pp. 223-232.

[107] Safari M, Reza M, Sheikhi H. Large eddy simulation-based analysis of entropy generation in a turbulent nonpremixed flame. *Energy* 2014; Vol. 78: pp. 451-457.

[108] Nguyen T, Fulop TG, Breuhaus P, Elmegaard B. Life performance of oil and gas platforms: site intergration and themodynamic evaluation. *Energy* 2014; Vol. 73: pp. 282-301.

[109] Ramakrishnan S, Edwards CF. Maximum-efficiency architectures for steady-flow combustion engines, I: Attractor trajectory optimization approach. *Energy* 2014; Vol. 72: pp. 44-57.

[110] Ramakrishnan S, Edwards CF. Maximum-efficiency architectures for steady-flow combustion engines, II: Work-regenerative gas turbine engines. *Energy* 2014; Vol. 72: pp. 58-68.

[111] Hagi H, Le Moullec Y, Nemer M, Bouallou C. Performance assessment of first generation oxy-coal power plants through an exergy-based process integration methodology. *Energy* 2014; Vol. 69: pp. 272-284.

[112] Feng Y, Zhang Y, Li B, Yang J, Shi Y. Sensitivity analysis and thermoeconomic comparison of ORCs (organic Rankine cycles) for low temperature waste heat recovery. *Energy* 2015; Vol. 82: pp. 664-677.

[113] Tapasvi D, Kempegowda RS, Tran K, Sreiberg Ø, Grønli M. A simulation study on the torrefied biomass gasification. *Energy Conversion and Managemen*t 2015; Vol. 90: pp. 446-457.

UNIVERSITEIT VAN PRETORIA
UNIVERSITY OF PRETORIA
YUNIBESITHI YA PRETORIA



[114] Li C, Gillum C, Toupin K, Donaldson B. Biomass boiler energy conversion system analysis with the aid of exergy-based methods. *Energy Conversion and Management* 2015; Vol. 103: pp. 665-673.

UNIVERSITEIT VAN PRETORIA
UNIVERSITY OF PRETORIA
YUNIBESITHI YA PRETORIA



# APPENDICES

## APPENDIX A: CHEMICAL FORMULA CALCULATION

The empirical chemical formula for the chosen fuel of pitch pine is derived from ultimate analysis data as found in Tillman [67]. Table A-1 shows the weight fractions of the elements that constitute the fuel in Column 2, the molecular weight in Column 3 and the computed gram-moles in Column 4.

The gram-moles in Column 4 are computed by dividing the weight fraction by the molecular weight.

**Table A- 1: Empirical chemical formula calculation**

| Element | Weight (%) | Molecular weight | Gram-moles |
|---|---|---|---|
| Carbon (C) | 59 | 12 | 4.9 |
| Hydrogen (H) | 7.2 | 1 | 7.2 |
| Oxygen (O) | 32.7 | 16 | 2.0 |
| Nitrogen (N) | -- | 14 | 0 |
| Sulphur (S) | -- | 32 | 0 |
| Ash | -- | N/A | 0 |

The calculated empirical formula is constructed by using the computed value in Column 4 of Table A-1, and is expressed by Eq. A-1:

$$C_{4.9}H_{7.2}O_{2.0} \qquad \textbf{(A-1)}$$

UNIVERSITEIT VAN PRETORIA
UNIVERSITY OF PRETORIA
YUNIBESITHI YA PRETORIA



## APPENDIX B: STOICHIOMETRIC COEFFICIENT CALCULATIONS

The stoichiometric coefficient calculation is for a seven combustion product gaseous species mixture. The seven combustion product species that were considered were $H_2O$, $CO_2$, $N_2$, CO, C<s>, $H_2$ and OH.

The balanced equation of a combustion process that is either complete or incomplete, burning pitch pine as represented by Eq. (A-1) is given by Eq. (B-1):

$$C_{4.9}H_{7.2}O_2 + (z)n_1(3.76N_2 + O_2) \rightarrow n_2H_2O + n_3CO_2 + n_4N_2 + n_5CO + n_6C < s > + n_7CH_4 + n_8H_2 \quad \textbf{(B-1)}$$

where:

$n_1, n_2, ...., n_8$ are stoichiometric coefficients.

$z$ is the excess or deficit multiple of the theoretical amount of air.

The number 3.76 is the ratio of the molar fraction of molecular nitrogen to that of molecular oxygen found in the air. The stoichiometric coefficient $n_1$ is the same as for the balanced Equation (B-1) for a complete combustion process with theoretical amount of air, as represented by Eq. (B-2):

$$C_{4.9}H_{7.2}O_2 + 5.7(3.76N_2 + O_2) \rightarrow 3.6H_2O + 4.9CO_2 + 21.4N_2 \quad \textbf{(B-2)}$$

Therefore, for any combustion process, burning pitch pine using air, whether complete or incomplete, the combustion will always have $n_1 = 5.7$.

The molar fractions of the seven combustion product species as they are related to the stoichiometric coefficients are expressed by Eq. (B-3):

$$x_j = \frac{n_j}{\sum_{i=2}^{8} n_i} \quad \textbf{(B-3)}$$

For j=2, 3, 4, 5, 6, 7, 8.

UNIVERSITEIT VAN PRETORIA
UNIVERSITY OF PRETORIA
YUNIBESITHI YA PRETORIA



Eq. (B-3) can be expanded to give a set of seven homogeneous equations. However, given that homogeneous equations have an infinite number of solutions [67-70], a solution was found whereby the value of one of the stoichiometric coefficients of the combustion product species was set to a known value. Given the assumption made that nitrogen does not get involved in the combustion process, the stoichiometric coefficient for molecular nitrogen of 21.4 found in Eq. (B-2) was chosen to be that known value. Therefore, in Eq. (B-1) $n_4 = 21.4$ . The equation for each combustion product species stoichiometric coefficient is derived separately below from Eq. (B-3).

For $n_2$:

$$n_2 = \frac{x_2}{1-x_2}\sum_{i=3}^{8} n_i \qquad \textbf{(B-4)}$$

For $n_3$:

$$n_3 = \frac{x_3}{1-x_3}\left(n_2 + \sum_{i=4}^{8} n_i\right) \qquad \textbf{(B-5)}$$

Substituting Eq. (B-4) into Eq. (B-5) and grouping like terms together give:

$$n_3 = \frac{x_3}{1-x_2-x_3}\sum_{i=4}^{8} n_i \qquad \textbf{(B-6)}$$

For $n_4$:

$$n_4 = \frac{x_4}{1-x_4}\left(n_2 + n_3 + \sum_{i=5}^{8} n_i\right) \qquad \textbf{(B-7)}$$

Substituting Eq. (B-4) and Eq. (B-6) into Eq. (B-7) and grouping like terms together give:

$$n_4 = \frac{K}{1-K}\sum_{i=5}^{8} n_i \qquad \textbf{(B-8)}$$

where:

$$K = \frac{x_2 x_3 x_4}{(1-x_2-x_3)(1-x_2)} + \frac{x_2 x_4}{1-x_2} + \frac{x_3 x_4}{1-x_2-x_3} + x_4 \qquad \textbf{(B-9)}$$

For $n_5$:

$$n_5 = \frac{x_5}{1-x_5}\left(\sum_{i=2}^{4} n_i + \sum_{j=6}^{8} n_j\right) \qquad \textbf{(B-10)}$$

UNIVERSITEIT VAN PRETORIA
UNIVERSITY OF PRETORIA
YUNIBESITHI YA PRETORIA



Substituting Eq. (B-4), Eq. (B-6) and Eq. (B-8) into Eq. (B-10) and grouping like terms together give:

$$n_5 = \frac{G}{(1-G-K)}\sum_{i==6}^{8} n_i \qquad \textbf{(B-11)}$$

where:

$$G = \frac{x_3 x_5}{(1-x_2)(1-x_2-x_3)} + \frac{x_5}{1-x_2} \qquad \textbf{(B-12)}$$

For $n_6$:

$$n_6 = \frac{x_6}{1-x_6}\left(\sum_{i=2}^{5} n_i + n_7 + n_8\right) \qquad \textbf{(B-13)}$$

Substituting Eq. (B-4), Eq. (B-6), Eq. (B-8) and Eq. (B-11) into Eq. (B-13) and grouping like terms together give:

$$n_6 = \frac{M}{1-M}(n_7 + n_8) \qquad \textbf{(B-14)}$$

where:

$$M = \left\{ \begin{array}{l} \dfrac{JKG}{(1-K)(1-K-G)} + \dfrac{JK}{1-K} + \dfrac{JG}{1-K-G} + J + \dfrac{x_2 x_6}{(1-x_2)}\dfrac{KG}{(1-K)(1-K-G)} \\ + \dfrac{x_2 x_6}{(1-x_2)(1-K)} + \dfrac{x_2 x_6}{(1-x_2)(1-K-G)} + \dfrac{x_2 x_6}{1-x_2} + \dfrac{x_6 KG}{(1-K)(1-K-G)} + \dfrac{x_6 K}{1-K} \\ + \dfrac{x_6 G}{1-K-G} + x_6\dfrac{LKG}{(1-K)(1-K-G)} + \dfrac{LK}{1-K} + L + \dfrac{LG}{1-K-G} \end{array} \right\} \qquad \textbf{(B-15)}$$

where:

$$J = \frac{x_2 x_3 x_6}{(1-x_2)(1-x_2-x_3)} \qquad \textbf{(B-16)}$$

$$L = \frac{x_3 x_6}{1-x_2-x_3} \qquad \textbf{(B-17)}$$

For $n_7$:

$$n_7 = \frac{x_7}{1-x_7}\left(\sum_{i=2}^{6} n_i + n_8\right) \qquad \textbf{(B-18)}$$

Substituting Eq. (B-4), Eq. (B-6), Eq. (B-8), Eq. (B-11) and Eq. (B-15) into Eq. (B-18) and grouping like terms together give:

$$n_7 = \frac{P}{1-P} n_8 \qquad \textbf{(B-19)}$$

UNIVERSITEIT VAN PRETORIA
UNIVERSITY OF PRETORIA
YUNIBESITHI YA PRETORIA



where:

$$P=\left\{\begin{aligned}
&\frac{NKGM}{(1-M)(1-K-G)(1-K)}+\frac{NKG}{(1-K-G)(1-K)}+\frac{NKM}{(1-M)(1-K)}+\frac{NK}{1-K}\\
&+\frac{NGM}{(1-K-G)(1-M)}+\frac{NG}{(1-K-G)}+\frac{NM}{1-M}+N+\frac{x_2x_7KGM}{(1-M)(1-x_2)(1-K)(1-K-G)}\\
&+\frac{x_2x_7KG}{(1-x_2)(1-K)(1-K-G)}+\frac{x_2x_7KM}{(1-x_2)(1-M)(1-K)(1-K-G)}+\frac{x_2x_7K}{(1-x_2)(1-K)(1-K-G)}\\
&+\frac{x_2x_7KM}{(1-M)(1-x_2)(1-K)}+\frac{x_2x_7K}{(1-x_2)(1-K)}+\frac{x_2x_7GM}{(1-M)(1-x_2)(1-K-G)}+\frac{x_2x_7G}{(1-x_2)(1-K-G)}\\
&+\frac{x_2x_7M}{(1-x_2)(1-M)}+\frac{x_2x_7}{1-x_2}+\frac{x_3x_7KGM}{(1-x_2-x_3)(1-K)(1-K-G)(1-M)}+\frac{x_3x_7KG}{(1-x_2-x_3)(1-K)(1-K-G)}\\
&+\frac{x_3x_7KM}{(1-x_2-x_3)(1-K)(1-M)}+\frac{x_3x_7K}{(1-x_2-x_3)(1-K)}+\frac{x_3x_7GM}{(1-x_2-x_3)(1-K-G)(1-M)}\\
&+\frac{x_3x_7G}{(1-x_2-x3)(1-K-G)}+\frac{x_3x_7M}{(1-x_2-x_3)(1-M)}+\frac{x_3x_7}{1-x_2-x_3}+\frac{x_7KGM}{(1-M)(1-K)(1-K-G)}\\
&+\frac{x_7KG}{(1-K)(1-K-G)}+\frac{x_7KM}{(1-M)(1-K)}+\frac{x_7K}{1-K}+\frac{x_7GM}{(1-M)(1-K-G)}+\frac{x_7G}{1-K-G}+\frac{x_7M}{1-M}+x_7
\end{aligned}\right\} \quad \textbf{(B-20)}$$

and where:

$$N=\frac{x_2x_3x_7}{(1-x_2)(1-x_2-x_3)} \quad \textbf{(B-21)}$$

For $n_8$:

$$n_8=\frac{x_8}{1-x_8}\sum_{i=2}^{7}n_i \quad \textbf{(B-22)}$$

Substituting Eq. (B-4), Eq. (B-6), Eq. (B-8), Eq. (B-11), Eq. (B-15) and Eq. (B-19) into Eq. (B-22) and grouping like terms together give:

$$n_8=\frac{(1-K-G)(1-M)}{K}n_4-n_7 \quad \textbf{(B-23)}$$

Because $n_4$ is known, Eq. (B-23) can be substituted into Eq. (B-19) to express $n_7$ in terms of $n_4$ to give:

$$n_7=(1-K-G)(1-M)\frac{P}{K}n_4 \quad \textbf{(B-24)}$$

UNIVERSITEIT VAN PRETORIA
UNIVERSITY OF PRETORIA
YUNIBESITHI YA PRETORIA



# APPENDIX C: WALL HEAT FLUX FILLED CONTOUR PLOTS FOR CHAPTER 5

The filled contour plots of temperature on a section through the geometry of the combustor were created for the two cases at conditions when they achieved their minima entropy generation rate, and were plotted in Figure C-1 and Figure C-2.

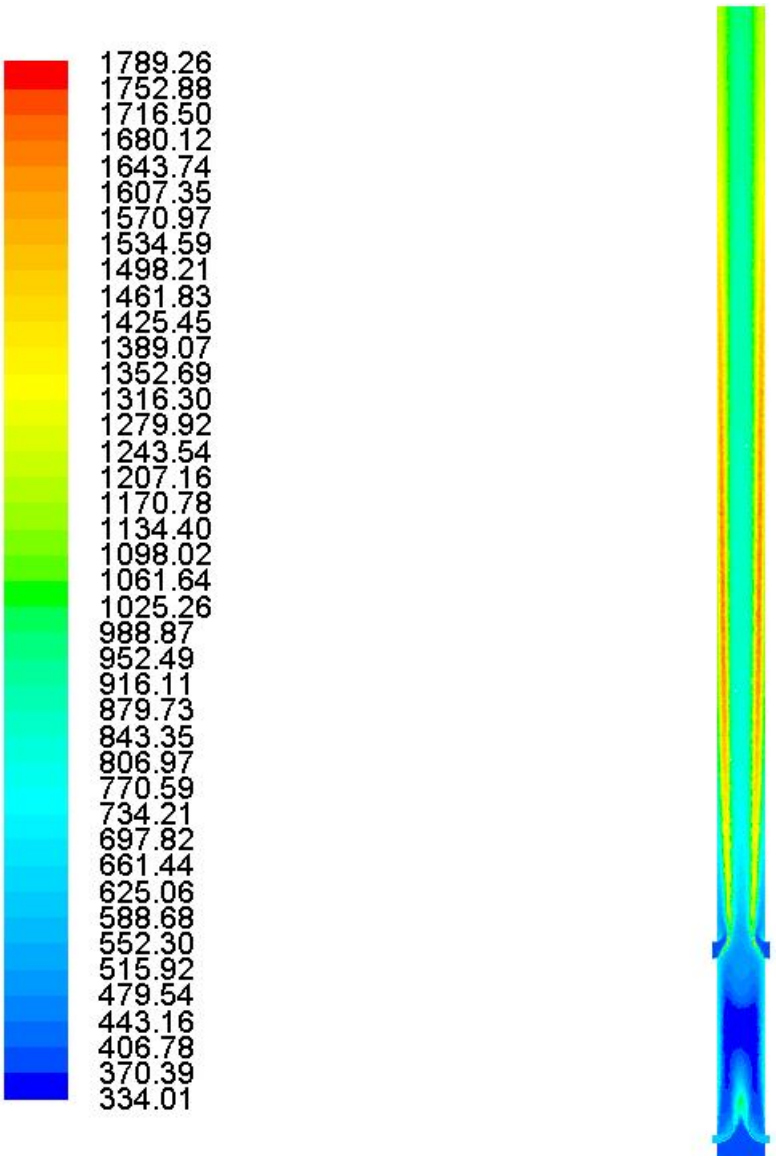


**Figure C-1: Section plot of filled temperature contours (Kelvins) for Case 1 with AF of 4.8.**

UNIVERSITEIT VAN PRETORIA
UNIVERSITY OF PRETORIA
YUNIBESITHI YA PRETORIA



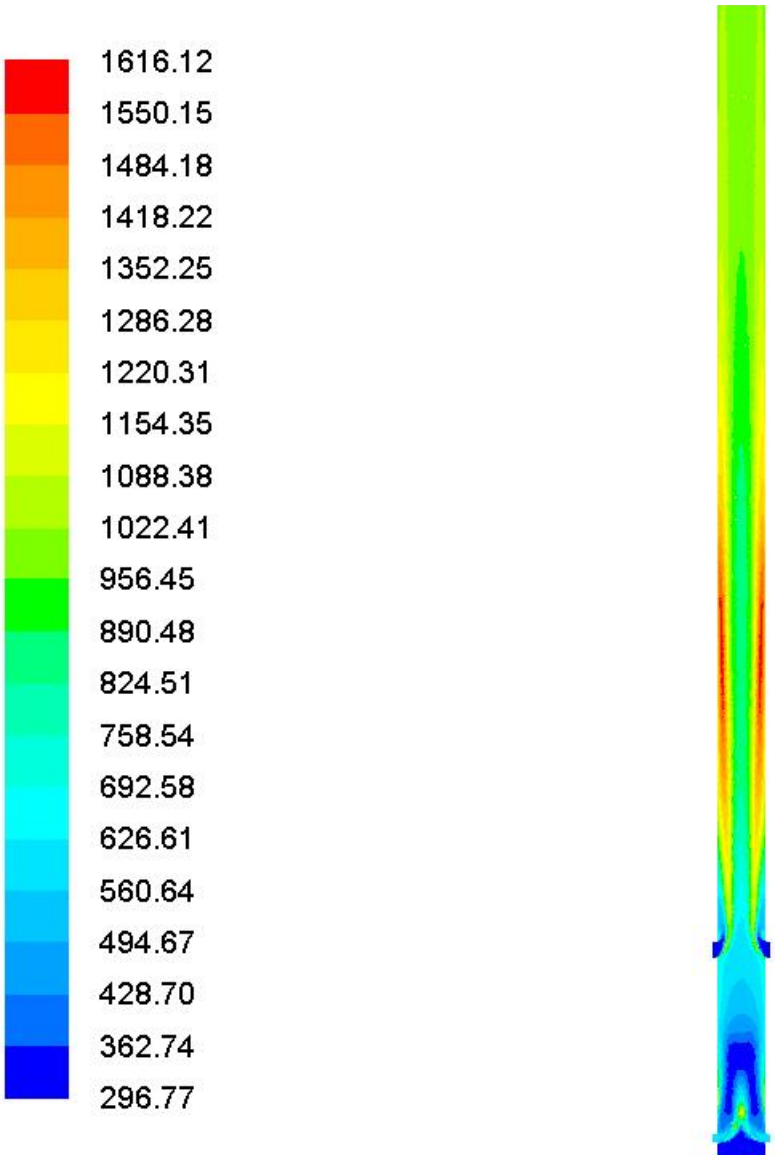


**Figure C-2: Section plot of filled temperature contours (Kelvins) for Case 2 with AF of 4.9.**

Filled contour plots of temperature on a section through the geometry of the combustor were also created for the two cases for the condition when combustion occurred with a theoretical amount of air, and are shown in Figure C-3 and Figure C-4.

UNIVERSITEIT VAN PRETORIA
UNIVERSITY OF PRETORIA
YUNIBESITHI YA PRETORIA



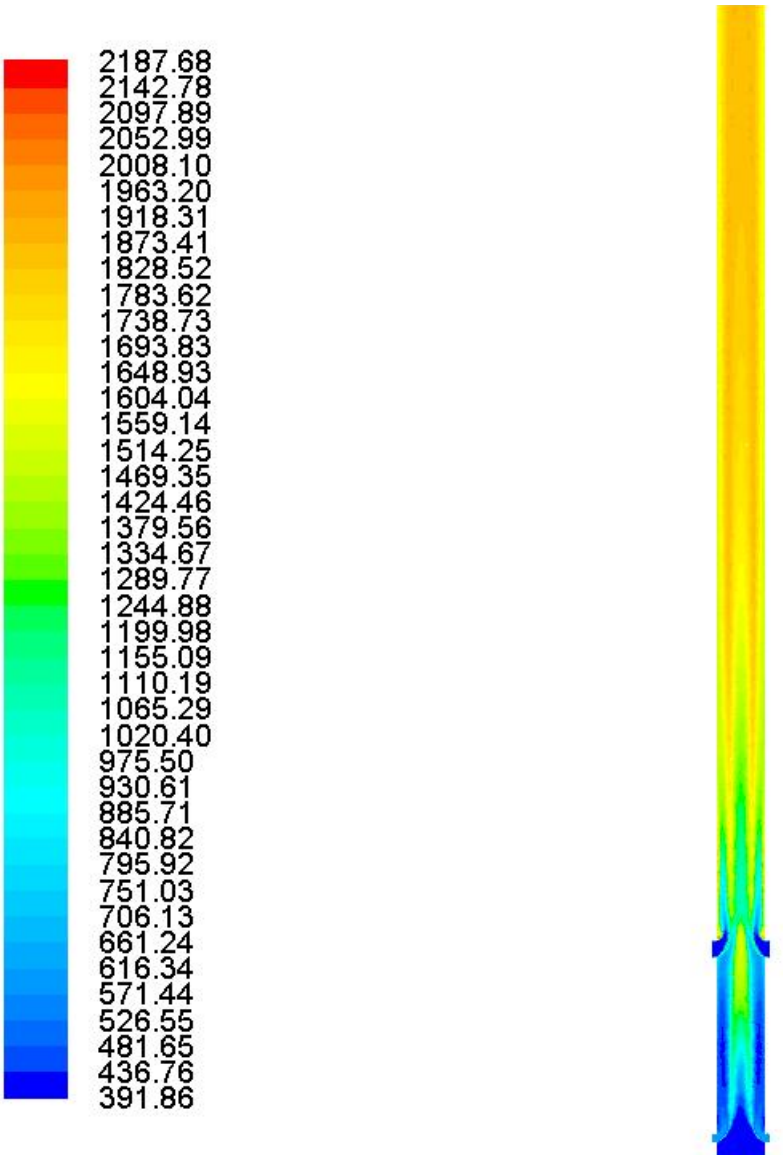


**Figure C-3: Section plot of filled temperature contours (Kelvins) for Case 1 with AF of 8.02.**

UNIVERSITEIT VAN PRETORIA
UNIVERSITY OF PRETORIA
YUNIBESITHI YA PRETORIA



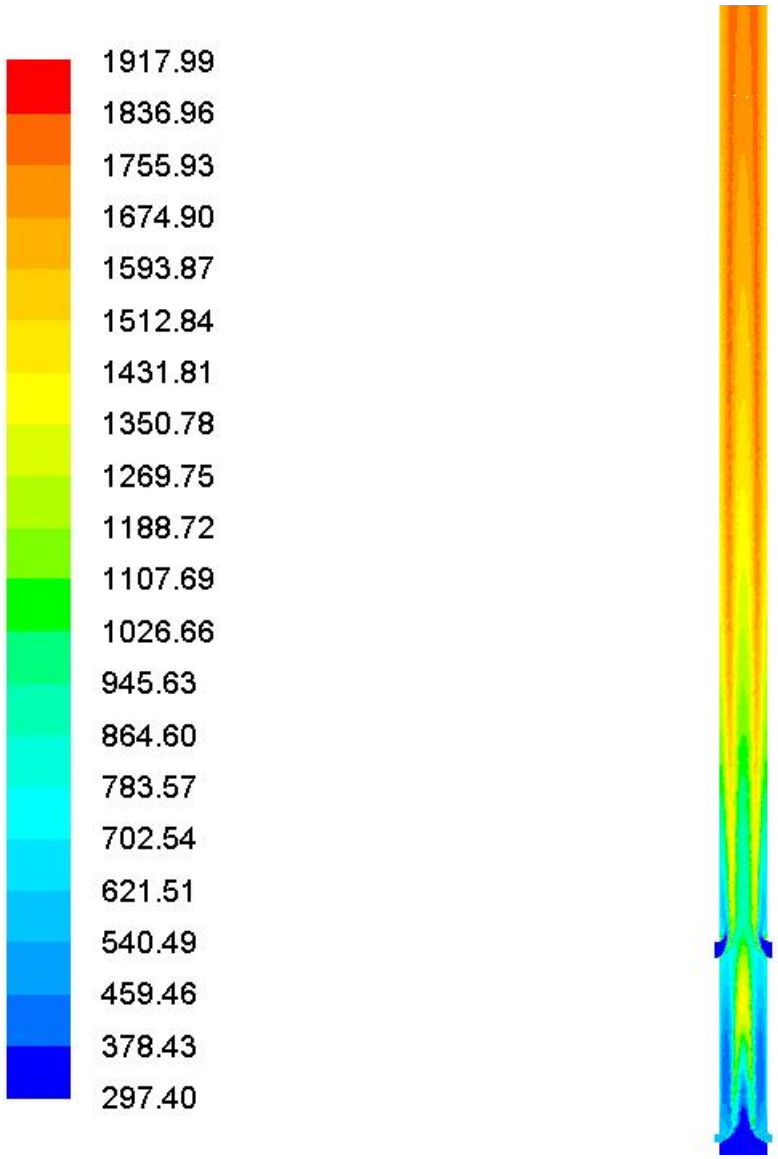


**Figure C-4: Section plot of filled temperature contours (Kelvins) for Case 2 with AF of 8.02.**

The filled contour plots of temperature on a section through the geometry of the combustor and the cylinder wall were created for Case 3 at condition when it achieved the minimum entropy generation rate, and were plotted in Figure C-5 and Figure C-6 respectively.

UNIVERSITEIT VAN PRETORIA
UNIVERSITY OF PRETORIA
YUNIBESITHI YA PRETORIA



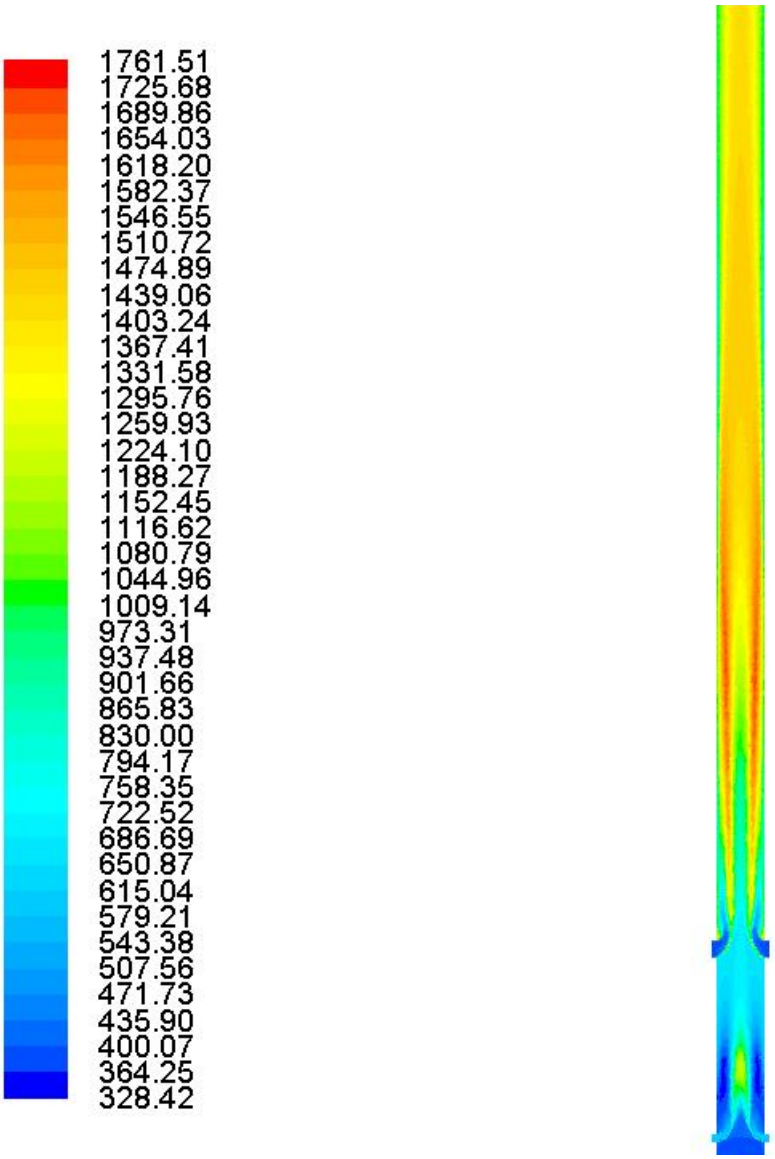


**Figure C-5: Section plot of filled temperature contours (Kelvins) for Case 3 with AF of 6.0.**

UNIVERSITEIT VAN PRETORIA
UNIVERSITY OF PRETORIA
YUNIBESITHI YA PRETORIA



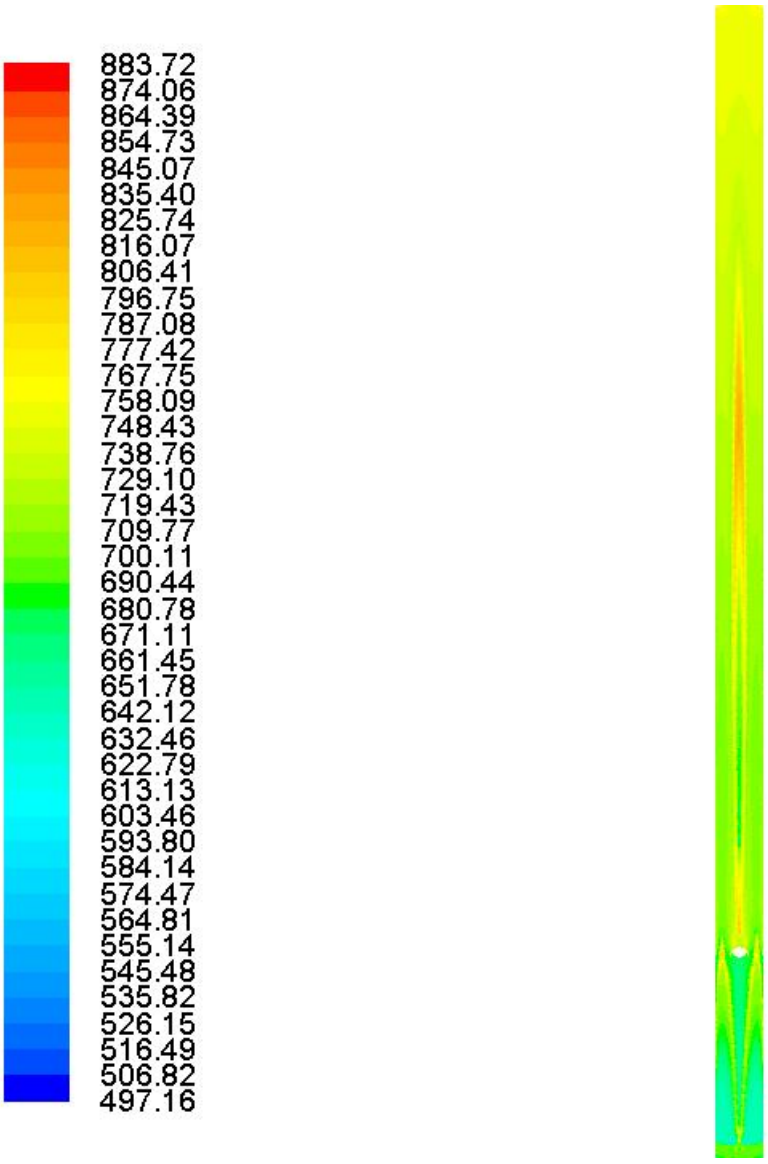


**Figure C-6: Wall plot of filled temperature contours (Kelvins) for Case 3 with AF of 6.0.**

The filled contour plots of temperature on a section through the geometry of the combustor and the cylinder wall were created for Case 3 at condition when combustion occurred with a theoretical amount of air, and were plotted in Figure C-7 and Figure C-8 respectively.

UNIVERSITEIT VAN PRETORIA
UNIVERSITY OF PRETORIA
YUNIBESITHI YA PRETORIA



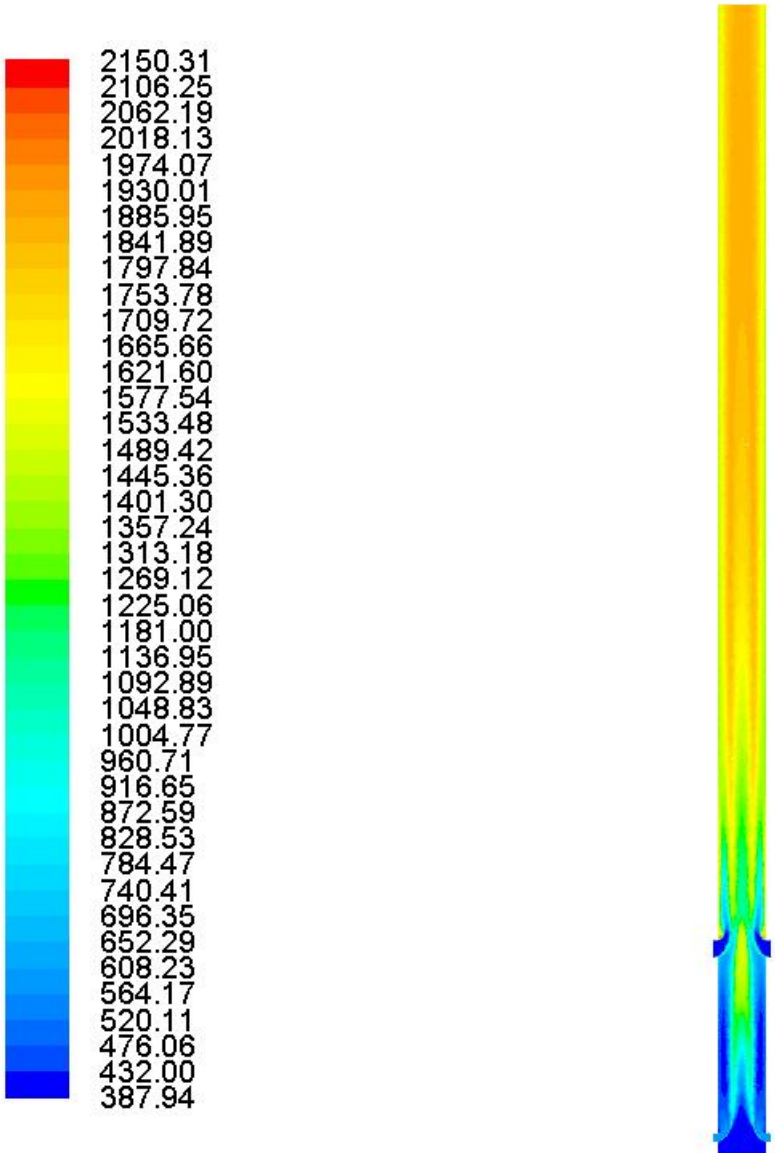


**Figure C-7: Section plot of filled temperature contours (Kelvins) for Case 3 with AF of 8.02.**

UNIVERSITEIT VAN PRETORIA
UNIVERSITY OF PRETORIA
YUNIBESITHI YA PRETORIA



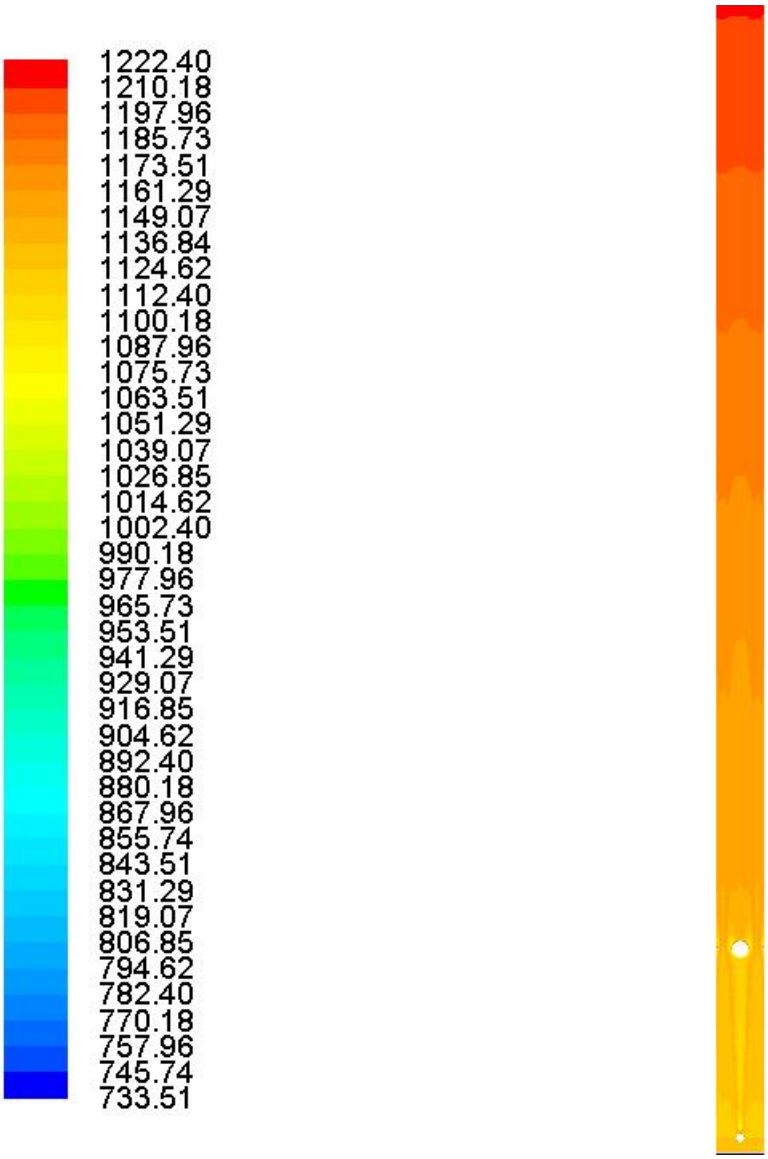


**Figure C-8: Wall plot of filled temperature contours (Kelvins) for Case 3 with AF of 8.02.**